Development of A Rheological Measurement Technique to Study Diffusion in Molten Polystyrene

Wissam Nakhle

A Thesis

In the Department

of

Mechanical, Industrial and Aerospace Engineering

Presented in Partial Fulfillment of the Requirements

For the Degree of

Doctor of Philosophy (Mechanical Engineering) at

Concordia University

Montreal, Quebec, Canada

September 2018

CONCORDIA UNIVERSITY

SCHOOL OF GRADUATE STUDIES

This is to certify that the thesis prepared

By: Wissam Nakhle

Entitled: Development of a Rheological Measurement Technique to Study Diffusion in Molten Polystyrene

and submitted in partial fulfillment of the requirements for the degree of
Doctor Of Philosophy (Mechanical Engineering)

complies with the regulations of the University and meets the accepted standards with respect to originality and quality.

Signed by the final examining committee:

_____ Chair
Dr. Samuel S. Li

_____ External Examiner
Dr. Jeffery Giacomin

_____ External to Program
Dr. Catherine Mulligan

_____ Examiner
Dr. Ali Dolatabadi

_____ Examiner
Dr. Martin D. Pugh

_____ Thesis Supervisor
Dr. Paula Wood-Adams

Approved by
Dr. Ali Dolatabadi, Graduate Program Director

Monday, October 22, 2018 _____
Dr. Amir Asif, Dean
Gina Cody School of Engineering and Computer Science

ABSTRACT

Development Of A Rheological Measurement Technique To Study Diffusion In Molten Polystyrene

Wissam Nakhle, Ph.D.

Concordia University, 2018

Diffusion through polymers impacts a wide range of existing applications, and could create new applications for polymers. Diffusion in polymer melts has gained considerable interest, and its industrial importance has triggered the need for faster measurement techniques. Rheological measurements characterize the behavior of polymeric materials, and are an effective tool to study various aspects of diffusion and interdiffusion in molten polymers. The rheological behavior in the molten state of high density polyethylene exposed to carbon dioxide has been probed under small amplitude oscillatory shear, but relatively few papers have been published on this topic. Results show that SAOS accelerates diffusion, but only a limited number of cases have been reported. This observation provides evidence that SAOS accelerates diffusion, and defines new research directions. This study aims at developing a robust experimental technique and accurate analytical and numerical methods to probe diffusion and interdiffusion in molten polymers. Both approaches can be applied to parallel disk rheometry data, to determine fundamental properties governing the diffusion process in polymer melts. Diffusion of small solvent molecules through molten polystyrene, as well as interdiffusion across a binary polystyrene interface, are studied here. We found that applying SAOS accelerates diffusion, even thought there is no large scale net convection of fluid. At constant temperature, the diffusion coefficient is independent of the oscillation frequency, and at temperatures closer to the glass transition temperature, applying SAOS further accelerates the diffusion.

Acknowledgment

First and foremost, I would like to express my deepest appreciation to my supervisor, Dr. Paula Wood-Adams for her guidance, advice and support during my research. She always encouraged me to learn more and think better.

I would like to thank all of the administrative staff of Mechanical and Industrial Engineering, especially Leslie Hosein, Maureen Thuringer and Arlene Zimmerman. I would also like to thank Daniel Page, and Mazen Samara for their technical assistance.

My special thanks to my lovely, amazing family and all of my friends especially, who always supported and encouraged me.

Dedicated to

My Mom Camelia and My Dad Bahij

Contributions of Authors

1. Wissam Nakhle, and Paula Wood-Adams, "Solvent Diffusion in Molten Polystyrene under Small Amplitude Oscillatory Shear", *Polymer*, vol. 132, pp. 59-68, 2017.

[**Chapter 3 of this thesis**]

- The experimental work of this article was performed by the author Wissam Nakhle as a part of this PhD dissertation. This research is supported by NSERC and Concordia University. The original idea for working on diffusion in polystyrene rings was proposed by Paula Wood-Adams who supervised this work during the entire research. The first draft of the article was written by Wissam Nakhle which was revised and modified by Paula Wood-Adams before submission. Paula Wood-Adams supervised this work during the entire research.

2. Wissam Nakhle, and Paula M. Wood-Adams, "A general method for obtaining diffusion coefficients by inversion of measured torque from diffusion experiments under small amplitude oscillatory shear", *Rheologica Acta*, 2018. https://doi.org/10.1007/s00397-018-1093-9

[**Chapter 4 of this thesis**]

- The experimental work of this article was performed by the author Wissam Nakhle as a part of this PhD dissertation. This research is supported by NSERC and Concordia University. The idea of numerically resolving the torque-time data was discussed with Paula Wood-Adams. The first draft of the article was written by Wissam Nakhle which was revised and modified by the other authors before submission. Paula Wood-Adams supervised this work during the entire research.

3. Wissam Nakhle, and Paula M. Wood-Adams, “Effect of Temperature on Solvent Diffusion in Molten Polystyrene under Small Amplitude Oscillatory Shear”, *Journal of Rheology*, 2018 (under review).

[**Chapter 5 of this thesis**]

- The experimental work of this article was performed by the author Wissam Nakhle as a part of this PhD dissertation. This research is supported by NSERC and Concordia University. Exploring the effect of temperature and SAOS was all performed at Concordia University. The first draft of the article was written by Wissam Nakhle which was revised and modified by Paula Wood-Adams before submission. Paula Wood-Adams supervised this work during the entire research.

4. Wissam Nakhle, Paula M. Wood-Adams, and Marie-Claude Heuzey, “Interdiffusion Dynamics at the Interface between two Polystyrenes with Different Molecular Weight Probed by a Rheological Tool”. Department of Chemical Engineering, Concordia University, Ecole Polytechnique Montreal.

[**Chapter 6 of this thesis**]

- The experimental work of this article was performed by the author Wissam Nakhle as a part of this PhD dissertation. This research is supported by NSERC and Concordia University. The idea of measuring interdiffusion in a binary polystyrene-polystyrene composite disk phase was first discussed with Paula Wood-Adams. The first draft of the article was written by Wissam Nakhle which was revised and modified by the other authors before submission. Paula Wood-Adams and Marie-Claude Heuzey (Ecole Polytechnique) supervised this work during the entire research.

TABLE OF CONTENTS

LIST OF FIGURES

LIST OF TABLES

ABBREVIATIONS AND SYMBOLS

SAOS	Small Amplitude Oscillatory Shear
HDPE	High Density Poly-Ethylene
LVE	Linear Visco-Elastic
TR	Tikhonov Regularization
RP	Regularization Parameter
TCB	1,2,4-Trichlorobenzene
MWD	Molecular Weight Distribution
M_w	Weight Average Molecular Weight
M_n	Number Average Molecular Weight
T_g	Glass Transition Temperature
T_m	Melting Temperature
η^*	Complex Viscosity
G'	Storage Modulus
$G^{"}$	Loss Modulus
τ	Shear Stress
T_0	Torque Amplitude
γ_0	Strain Amplitude
ω	Frequency
D	Diffusion coefficient
a	Inner radius
b	Outer radius

CHAPTER 1

INTRODUCTION

1.1. OVERVIEW

Diffusion in polymers has been the subject of experiments for over three decades, using various experimental techniques such as rheology [1], fluorescence [2, 3] and light scattering [4]. Diffusion of small molecules (i.e., the addition of solvents) through polymers has significant importance in different scientific and engineering fields such as medicine, the textile industry, and packaging in the food industry. As a result, a better knowledge of the polymer's morphology and structure [5], and of the diffusion properties is gained.

Diffusion experiments are often conducted under conditions [6] that are also quasi-satisfied by the analytical mathematical solution available. Recently, considerable efforts was expended in numerical analysis of the diffusion equation, and in developing efficient computer programs to numerically solve it. While it is not necessary to establish a mathematical solution first, it is often harder to appreciate what the simpler numerical method has to offer. A large number of mathematical solutions are available, but their application to practical problems may present difficulties, in cases where diffusion is complicated by anisotropy or swelling. Analytical methods are often restricted to simple geometries, and apply strictly to linear forms of the diffusion equation.

Solvent diffusion in molten polymers, is important in the design of many polymer processing operations. It is often difficult to measure diffusion coefficients at elevated temperatures, and limited data at low temperatures must be extrapolated. There is strong worldwide interest to provide a complete framework, and to realize more details about the fundamentals of the diffusion process, to generalize the governing laws, and to find fast and reliable measurement techniques.

1.2. OBJECTIVES

The main objectives of this study are now presented according to the sequence of chapters in this thesis.

➢ To develop a rotational rheometry-based technique to measure and study solvent diffusion through molten polystyrene. This technique relies on equilibrium flow and LVE properties in SAOS. (1st stage presented in Chapter 3). To determine the diffusion coefficient from Small Amplitude Oscillatory Shear flow and Linear Viscoelastic properties. To determine whether applying SAOS accelerates diffusion and to describe the frequency dependence of diffusion, and the experimental conditions leading to higher diffusion coefficients. (Presented in Chapter 3).

➢ To numerically resolve the torque-viscosity integral, and to solve the problem of inverting torque-time SAOS diffusion data using Tikhonov regularization. Local viscosity profiles are recovered from SAOS torque data during diffusion using a numerical algorithm, and the diffusion coefficient is determined for a wide range of diffusion systems. (Presented in Chapter 4).

➢ To determine the effect of temperature on 1,2,4-TCB diffusion in molten polystyrene. This study investigates this accelerated diffusion kinetics due to SAOS flow over a wider range of temperature. (Presented in Chapter 5). We also investigate interdiffusion at a polymer-polymer interface using this rheological technique. We present novel data on the diffusion of TCB in molten polystyrene and the interdiffusion between two polystyrenes (Presented in Chapter 6).

1.3. THESIS ORGANIZATION

This thesis has seven chapters which are briefly described here. The first chapter provides a brief introduction to diffusion in molten polymers and an overview of current challenges. The objectives of the thesis are also presented in this chapter.

Chapter 2 includes a comprehensive review on experimental diffusion measurements including rheology and gravimetry. The choice of solvent-polymer system, and of experimental procedures and conditions are discussed with a focus on rotational rheometry. The advantages/disadvantages of the various experimental methods available for measuring diffusion coefficients in polymeric systems are discussed. The thermodynamics and mathematics of diffusion are also discussed, and in the last section of Chapter 2 a review of diffusion models and numerical methods is presented.

In Chapter 3 we provide a validated method for rheological studies of diffusion in molten polymers, focusing on the characterization of solvent diffusion. The method combines, experimental measurements in SAOS, a Fickian diffusion model, the free volume model and the theory of linear viscoelasticity. The experimental procedure for rheological and gravimetric measurements of diffusion is discussed, and in the last section rheological and sorption diffusion data is presented at a single temperature.

Chapter 4 starts with a brief introduction to inverse problems and their numerical solutions, and then focuses on the numerical regularization technique (i.e., Tikhonov Regularization). The application of the flattest slope method to deterministically locate the most promising value of the regularization parameter is also discussed.

Chapter 5 includes a fundamental study of the effect of temperature on diffusion in the TCB/PS system in order to generalize the diffusion kinetics under SAOS. Temperature has a significant impact on the magnitude of this effect, and the combined temperature-oscillation effect on diffusion is characterized in this chapter. Chapter 5 investigates this accelerated diffusion kinetics due to SAOS flow as a function of temperature, and confirms that the diffusion rate is increased by oscillatory motion.

Polymer-polymer interdiffusion is discussed in Chapter 6. The effects of polydispersity and entanglements, and the effect of SAOS are explored to characterize the interface behavior and the composition profile. In Chapter 6, a novel analytical approach based on the Flory-Huggins and mean field theories is explained. The numerical regularization method is also applied for the PS/PS system with different molecular weights and dispersity index. Chapter 7 summarizes the conclusions and contributions.

---

1. Chapter 3 is published as: Wissam Nakhle, Paula M. Wood-Adams, "Solvent diffusion in molten polystyrene under small amplitude oscillatory shear", Polymer: vol. 132, pp. 59 – 68, 2017.

2. Chapter 4 is published as: Wissam Nakhle, Paula M. Wood-Adams, "A general method for obtaining diffusion coefficients by inversion of measured torque from diffusion experiments under small amplitude oscillatory shear", Rheologica Acta, (2018). https://doi.org/10.1007/s00397-018-1093-9.

3. Chapter 5 is under review with Journal of Rheology: Wissam Nakhle, Paula M. Wood-Adams, "Effect of Temperature on Solvent Diffusion in Molten Polystyrene under Small Amplitude Oscillatory Shear".

4. Chapter 6 will be published shortly: Wissam Nakhle, Paula M. Wood-Adams and Marie-Claude Heuzey, "Interdiffusion Dynamics at the Interface between two Polystyrenes with Different Molecular Weight Probed by a Rheological Tool".

Two conference papers have also been published based on this work, which are not presented in this thesis as chapters, but mentioned here:

A. Diffusion in Polymer Melts under SAOS, The 17th International Congress on Rheology (ICR2016), Aug 2016, Kyoto, Japan.

B. SAOS in Solvent-polymer Diffusion, The 89th annual meeting of the society of rheology, Oct 2017, Denver, CO, United States.

CHAPTER 2

2.1. CHARACTERIZATION METHODS

One of the first direct measurements of time-dependent concentration profiles at the interface between two partially miscible polymers, was obtained using an ion beam technique [5 - 7]. Diffusion of chain molecules in a molten polymeric matrix has been studied using photo and fluorescent labelling [2 - 4], using deuteration [5] combined with SANS or ion scattering techniques [6, 7]. Despite many limitations in capturing diffusion in polymers, experimental characterization of diffusion is still required to accurately describe all its features. In the following section, advances and limitations in the experimental characterization of diffusion in polymers are summarized.

In molecular probing, small molecules introduced into a host polymer are used as probe to investigate diffusion dynamics in polymers [2 - 4]. Molecular probing is commonly combined with fluorescence correlation spectroscopy [2 - 4], which detects fluorescent light emitted by probe molecules within a finite volume element, and correlates intensity fluctuations to diffusion properties [2]. In the last decade, dynamic rheological measurements [1] have been commonly used to characterize diffusion, and have shown to be suitable to study diffusion.

A relatively large number of experimental attempts related to various applications of diffusion are presented in previous literature [1 - 9] to study the diffusion of penetrant molecules through polymeric materials. Diffusion through polymers depends on several factors [10, 11] including solubility and diffusivity of the solvent, the polymer's morphology, and the degree of plasticization. A fewer number of scientific attempts related to diffusion at higher temperatures in the molten state have been previously presented [5 - 7]. Low-temperature data is often extrapolated to estimate the diffusivity at higher temperatures, due to the lack of available experimental methods in this temperature range. Diffusion is often limited by the choice of diffusion system and operating conditions, such as temperature.

2.1.1. Measurement Techniques

Molecular probing and spectroscopy require different light absorbance levels [2]. They may also require heavy probes that affect diffusion. Industrial processes often involve both flow and diffusion, whereas probe molecules diffuse into quiescent polymers, and are more suitable to study diffusion problems in the absence of flow [2]. Fluorescence Correlation Spectroscopy correlates the intensity of light measured at a time t and its intensity measured at an incremental time τ, using statistical methods to detect non-randomness in the data [2 - 4] (Figure 2.1). The resulting autocorrelation function can then be fitted with the diffusion autocorrelation function for molecules with three translational degrees of freedom, to measure the diffusion coefficient (Figure 2.2).

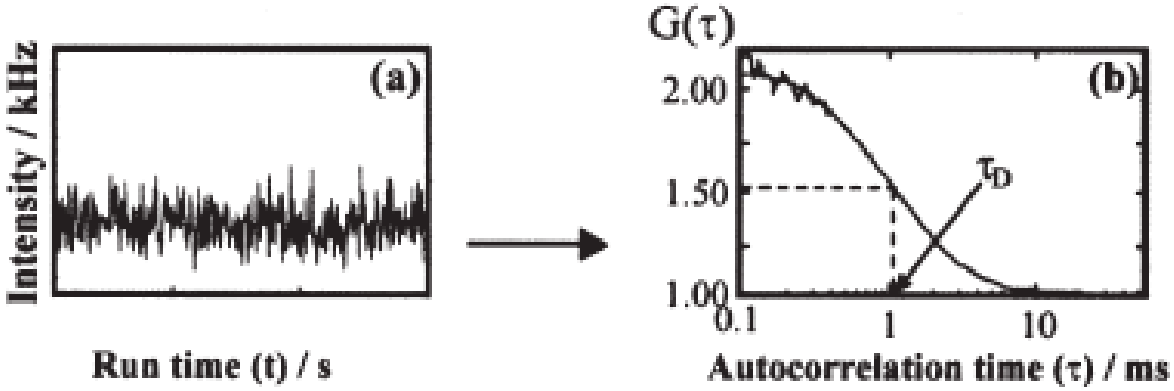

Figure 2.1. Light intensity & Autocorrelation time in FCS measurements [2].

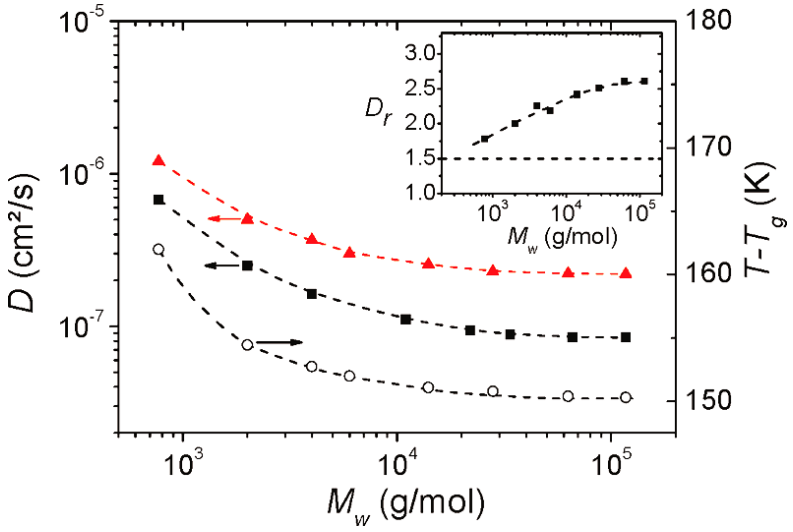

Figure 2.2. Diffusion Coefficient as a function of molecular weight from FCS measurements [2].

One of the first direct measurements of time-dependent concentration profiles at the interface between two polymers, was obtained using an ion beam technique [5, 6]. A Helium beam strikes the sample and penetrates through the interface to trigger a nuclear reaction [5, 6]. The reaction emits energetic particles, and the energy spectrum is used to determine the concentration profile as a function of depth (Figure 2.3).

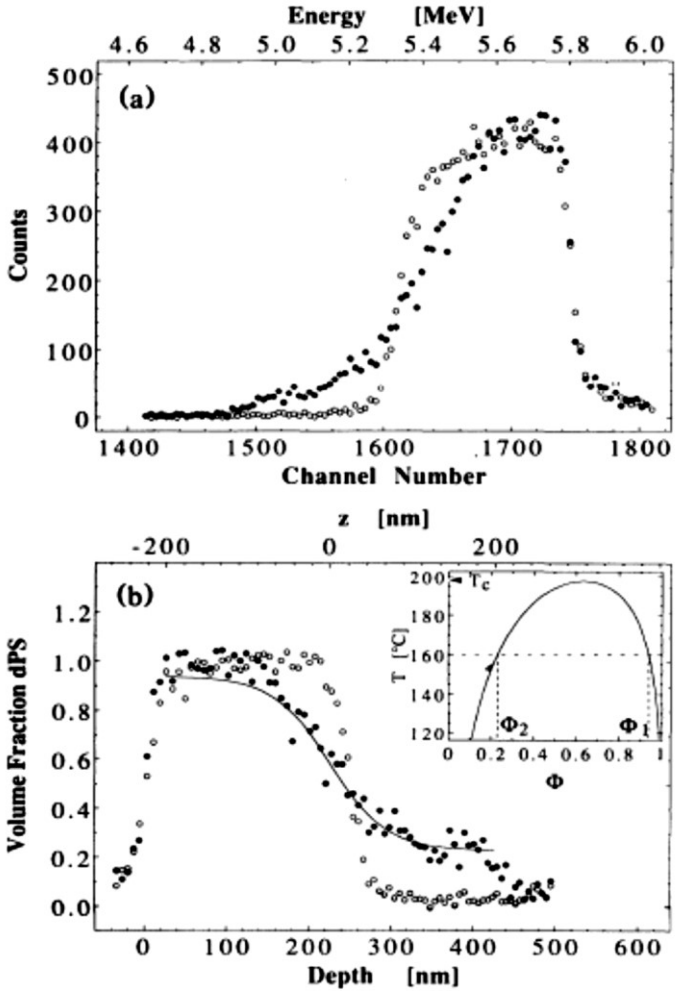

Figure 2.3. (a) Energy Spectra emitted from interdiffusion of deuterated and protonated polystyrene. (b) Concentration-depth profile for unannealed (light symbols) and annealed at 160 °C (dark symbols). The solid curve is fit from the Flory-Huggins model to the annealed system [7].

The diffusion coefficient can also be determined using rheometry by monitoring changes in rheological properties [1].

Further, recent findings have shown that SAOS accelerates diffusion of CO_2 in HDPE, and significantly affects the diffusion process [12] (Figure 2.4). The rheology of molten high density polyethylene exposed to carbon dioxide has been probed under SAOS. Results show that SAOS accelerates diffusion of CO_2 in HDPE, but only a limited number of cases have been reported [12]. The scope includes a study of the effect of frequency and SAOS on diffusion. The diffusion of small solvents through polymers, and interdiffusion between partially miscible polymers are also covered.

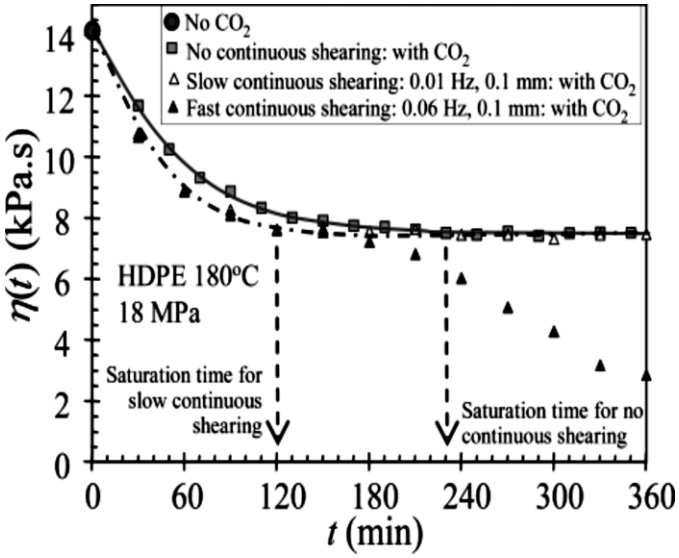

Figure 2.4. Effect of oscillatory shearing on the viscosity decrease during absorption of CO_2. The viscosity was measured at a shear rate of 0.63 s^{-1} [12]. (Lines show trends only, not model predictions.)

Photolabeled polystyrene with different molecular weight, terminated with dichloroxylylene and characterized by Gel Permeation Chromatography (GPC), has been used to study interdiffusion [13, 14]. The diffusion coefficient was measured by a holographic grating technique [13]. A lower beam is diffracted, and the diffracted light is detected by a photomultiplier [13]. A data processor stores the diffraction intensity, which is then used to determine the diffusion coefficient in polystyrene matrices with different molecular weight.

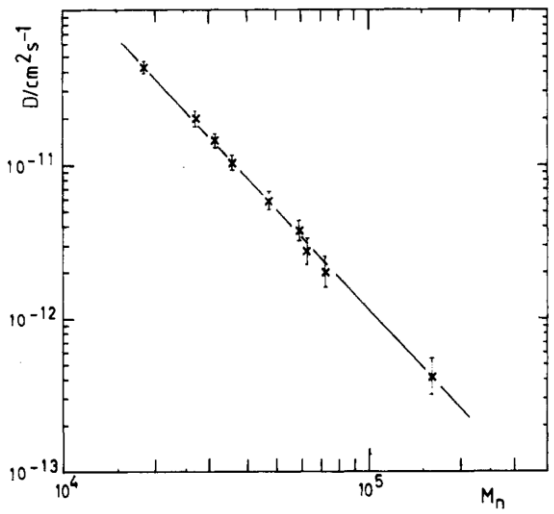

Figure 2.5. Diffusion coefficients of labeled PS chains in a high molecular weight matrix at 217°C [13].

Beside with FTIR-FCS techniques, a variety of methods are available for measuring diffusion coefficients of small penetrants into polymers. Gravimetric techniques [8, 9] that directly follow mass changes with time are frequently used for investigating the sorption kinetics.

2.1.2. Gravimetric Techniques

Gravimetric techniques directly follow mass changes with time, and are frequently used to investigate sorption kinetics [8, 9]. A thin polymer sample is placed in a diffusant-rich medium that is maintained at a constant temperature. Sorption kinetics are obtained by recording the sample weight as function of time. In sorption studies, rectangular samples are commonly immersed in a large solvent bath. This is the case of double-sided diffusion through a plane sheet of thickness 2L, whose surfaces at $x = \pm L$, are maintained at a constant concentration [8, 9]. It is assumed that the solvent enters through the faces and only a negligible amount through the edges, that the region $-L < x < L$ is initially free of solvent, and that the surfaces are maintained at a constant concentration (Figure 2.6).

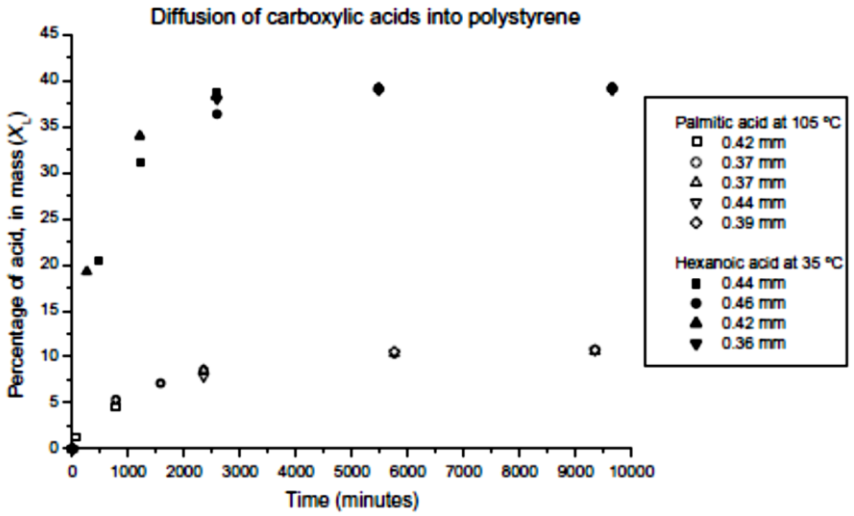

Figure 2.6. Percentage of mass increase with time for polystyrene with different thickness in acids [8].

Sorption measurements involve weighing the solvent uptake using a high accuracy electronic balance, this technique has been the source of the great majority of solvent-polymer diffusion data [8, 9] (Figure 2.7). The polymer is immersed in a solvent bath, the change in mass of the polymer sample is measured with time, and Fick's second law is applied to determine the diffusion coefficient. The use of a one dimensional Fick's law in sorption measurements requires a thin sample, and a temperature below the solvent boiling point to avoid evaporation [8, 9].

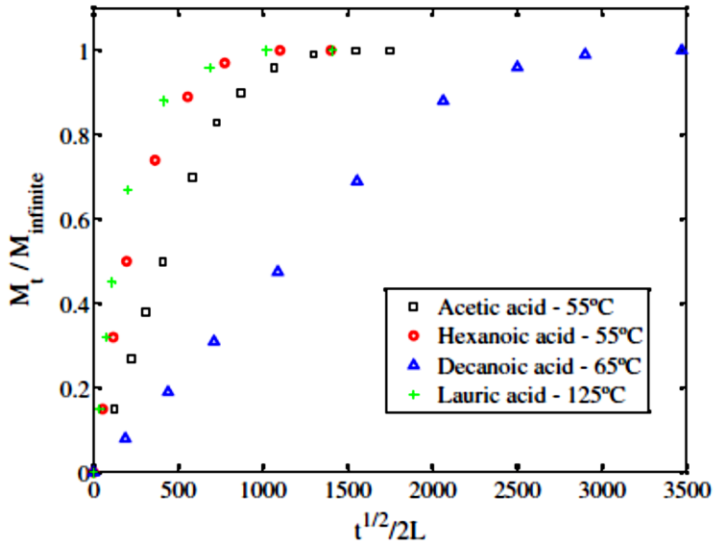

Figure 2.7. Sorption plots for linear carboxylic acids in polystyrene at different temperatures [9].

The solubility and the diffusivity of CO_2 into the molten state polymers has been studied using a Magnetic Suspension Balance (MSB) [15]. Figure 2.8 illustrates the experimental setup. The resolution and the accuracy of the balance are 10 μg (±0.002%) [15]. A polymer sample about 0.5 g in weight was set in an aluminum basket which was attached to the magnetic suspension [15]. The chamber was heated to the specified temperature and kept under vacuum for 30 minutes. Then, CO_2 was introduced into the chamber. The data of the electronic microbalance readouts, are then retrieved on-line by a computer.

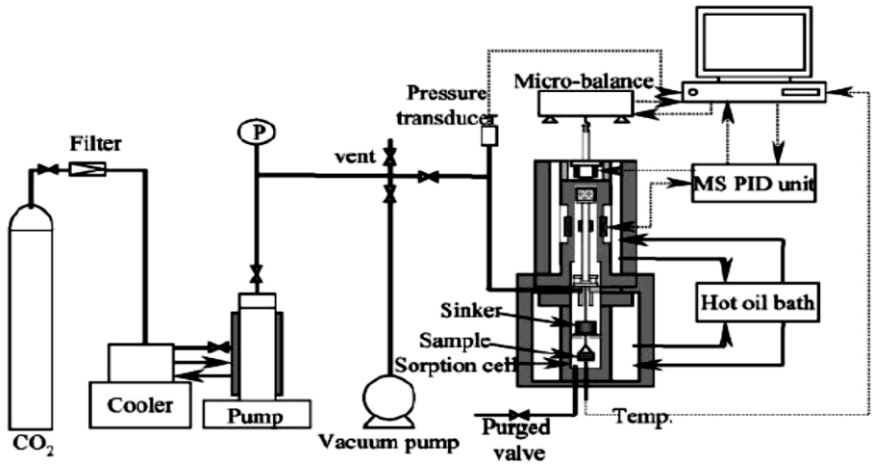

Figure 2.8. Experimental Magnetic Suspension Balance (MSB) setup for CO_2 diffusivity and solubility measurements [15].

The gain in weight of the PS sample is measured as a function of time, and the amount of solvent which has diffused at time t is given as function of the equilibrium solubility M_∞, which may be practically impossible to measure due to polymer dissolution [9]. Sorption measurements may also be affected by polymer dissolution, which may result in a weight loss. Sorption measurements yield valuable information about the diffusion process, without having to carry out difficult measurements [8, 9]. The sorption method may capture the diffusion mechanism to a reasonable extent, but diffusion coefficients can be determined with better accuracy from a number of other methods, including the rheological approach. Results from sorption measurements are used in this thesis to validate diffusion coefficients obtained from rheological measurements.

2.1.3. The Rheological Method

A fundamental difference between Newtonian fluids and Hookean solids is their response to an applied deformation [10, 11]. The behavior of non-Newtonian fluids such as molten polymers deviates from that of Newtonian fluids and elastic solids, and both constitutive equations fail to predict their response [11]. Polymers exhibit both viscous and elastic behaviors, and when subjected to shear flow their behavior depends on several factors [10]. Viscoelastic properties of polymers are a function of deformation, time, and other kinematic parameters that affect the flow (See Appendix A2.1 and A2.2).

Oscillatory shear measurements using a rotational rheometer is one of the most widely used techniques to determine viscoelastic properties of polymers [10, 11]. Oscillatory shear measurements are almost always carried out in a cone-and-plate or a parallel-plate torsional rheometer. In small-amplitude oscillatory shear experiments, a sample is exposed to a sinusoidal strain of small amplitude. Deformation occurs within the linear viscoelastic limit, and rheological properties are independent of the size of the deformation [11]. Linear viscoelasticity is exhibited by molten polymers in SAOS, when molecules of a polymeric material are hardly disturbed from their equilibrium configuration and entanglement state [10, 11]. When subjected to diffusion, the complex viscosity becomes dependent on the kinematic parameters of diffusion as well (See Appendix A2.1).

In the study of diffusion of CO_2 in HDPE, SAOS flow at a frequency of 0.01 Hz and a strain amplitude of 0.1 mm significantly accelerates the diffusion process (See Figure 2.4); this observation is made by comparing the saturation time of samples with and without continuous oscillatory shear [12]. It was also found that further increasing the frequency to 0.06 Hz did not enhance the diffusion process, and did not shorten the saturation time [12]. This study emphasizes the effects of pressure and concentration on changes in rheological properties. While pressure alone increases viscosity, the combined effect of pressure and CO_2 concentration was found to decrease viscosity [12]. This decrease in viscosity is attributed to the plasticizing effect of CO_2 having the larger impact on the viscosity of HDPE, and implies that viscosity measurements could be used to determine

the diffusion coefficient in molten polymers, with reasonable accuracy [12]. In this study of diffusion, the direct measurement of the diffusion coefficient is difficult and subject to considerable uncertainty, because the high-pressure sliding plate rheometer used does not allow for an independent control of pressure and concentration [12]. Further, the rheometer used can only operate at the saturation concentration, and experimental results are obtained when HDPE samples are saturated with CO_2 [12].

Diffusion-reaction systems are governed by two processes, diffusion and chemical reactions, and their reaction rate depends on both diffusive and reactive properties [18]. Diffusion-limited systems are systems in which products of chemical reactions form much faster than the rate of transport of reactants, and chemical reactions are limited by the rate of diffusion rather than the reaction rate [18]. In another study on diffusion-reaction of epoxy and polybutylene terephthalate under SAOS, samples blended in a mixer were compared with planar samples in which epoxy is sandwiched between two PBT plates [18]. No clear increase in reaction rates (See Figure 2.9) was observed for samples blended in a mixer, but the reaction rates for planar sandwiched samples increased with angular frequency [18]. Chemical reactions in samples blended in a mixer, are not diffusion-limited and are controlled by the reaction rate rather than the rate of diffusion, thus the reaction between PBT and epoxy was not affected by small-amplitude oscillatory shear [18].

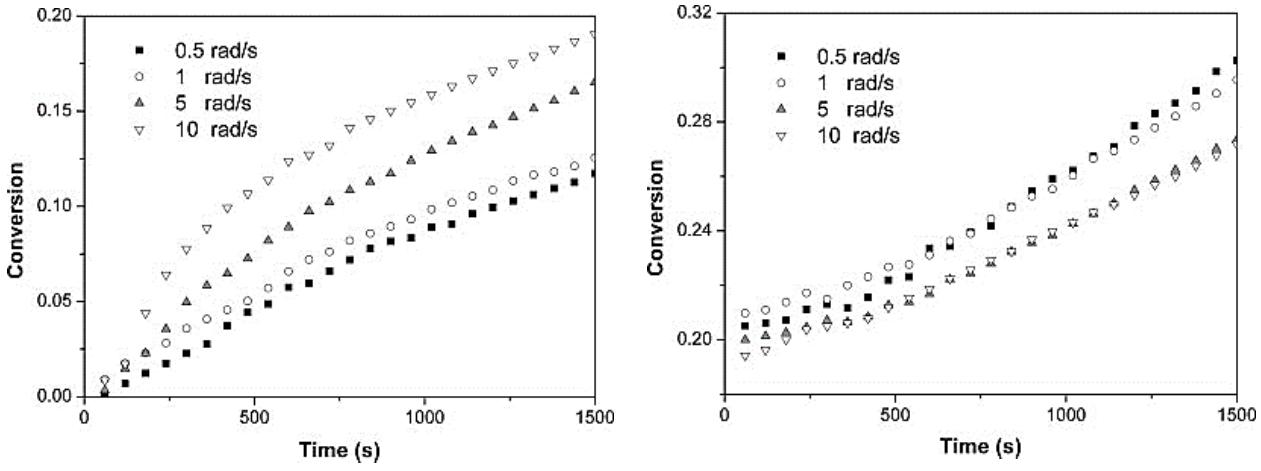

Figure 2.9. Plot of reaction conversion at various angular frequencies (at 240 °C); (a) for sandwich samples. (b) for blended samples [18].

Epoxy reacts with the carboxyl acid end group of PBT, and by comparing the carboxyl acid content before and during the experiment, the reaction rate can be determined [18]. The end group determination method monitors the carboxyl acid content to obtain the reaction rate, by measuring pH-values of the mixture before and during the experiment [18]. When experimental results from the rheological method are compared with results from the end group determination method, the agreement supports the use of the rheological method to study diffusion-reaction systems [18].

Another rheological approach allowing the quantification of diffusion at polymer/polymer interfaces and the measurement of the self-diffusion coefficient of polymer melts using rheological tools has been previously used [16]. The technique consists of measuring the dynamic moduli as a function of time for a multilayer sandwich-like assembly as shown in Figure 2.10. The technique was tested on a polystyrene/polystyrene system sheared in oscillatory mode under small amplitudes of deformation for different times of welding.

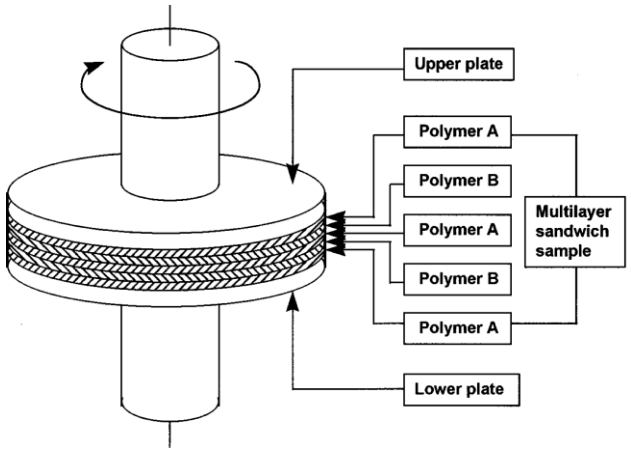

Figure 2.10. Multilayer polystyrene sample setup for rheological testing [16].

A free volume approach of the diffusion of organic molecules in polymers above their glass transition temperature has also been previously addressed [17]. They have shown [17] that the diffusion of small molecules, like plasticizers, above Tg, can be described by Fick's classical law [17]. The experiments were carried out on a parallel plate geometry rheometer, as shown in Figure 2.11.

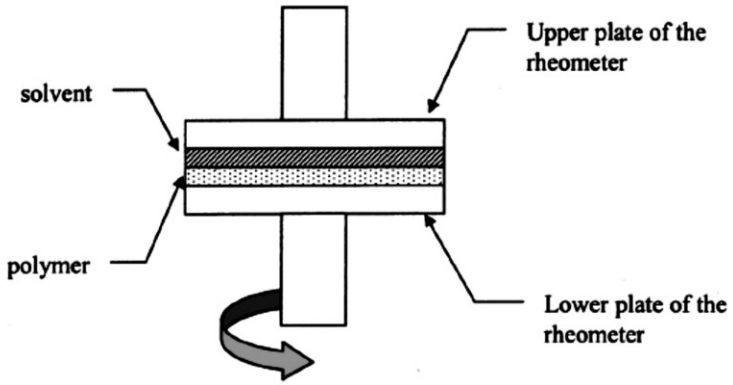

Figure 2.11. Sample setup for rheological testing of DOP in EVA [17].

The last decade has seen extensive efforts in the use of rheology as a tool to probe diffusion in polymers, and results in key rheological studies show that SAOS significantly affects diffusion in reactive and non-reactive polymeric systems [5-7, 18-20]. Despite advances made in the experimental characterization of diffusion, there is no clear theoretical framework that defines the mechanism of diffusion in polymer melts under SAOS. From torque measurements during solvent diffusion, fundamental parameters such as the concentration profile and the diffusion coefficient can be determined. SAOS is ideal for probing diffusion because of its sensitivity to changes in the microstructure, and can be used to study the effect of molecular weight, frequency and other relevant parameters. SAOS measurements are thus suitable to investigate various aspects of diffusion and interdiffusion in molten polymers.

For a specified frequency within the linear viscoelastic limit, the measured torque for neat polymers retains a constant value as a function of time. Torque measurements carried out during diffusion, are a function of time and are used to measure and study diffusion. The torque measured in this case reflects the translational diffusivity of the solvent. Measurements of rotational diffusion are usually difficult, and require extremely sensitive atomic resolution techniques, such as Nuclear Magnetic Resonance.

2.2. DIFFUSION THERMODYNAMICS

Polymeric systems can exhibit pseudo-Fickian, Fickian, anomalous, and case II diffusion [19]. In anomalous and case II diffusion, the solvent diffusion rate is faster than the polymer relaxation rate, and the interface moves at constant speed in the direction of the concentration gradient. The Flory-Huggins theory [19 - 21] has also been used to describe interdiffusion and the slow evolution of an initial sharp interface separating two molten polymers. The type of diffusion behavior is therefore strongly dependent on both host polymer and diffusing species, and on the experimental temperature. In the case of solvent diffusing in a polymer well above its glass transition temperature the behavior is Fickian and the only parameter necessary is the diffusion coefficient.

According to the free volume theory [22], diffusion occurs in the portion of free volume available in the host polymer [22]. The free volume theory also accounts for the contribution of the diffusing polymer to the increase in free volume (See Appendix A2.3). Diffusion is an irreversible mass transport process that occurs in the accessible free volume [22]. The number of ways atoms or molecules can rearrange defines the entropy of mixing [19 - 21]. Diffusion is accompanied by heat addition or removal, due to the endothermic repulsions and the exothermic attractions, which defines the enthalpy of mixing [19 - 21]. In the study of diffusion of CO_2 in HDPE, The relationship between the viscosity of HDPE and the concentration of CO_2 contains two parameters, one is a characteristic of the available free volume in HDPE and the other accounts for the contribution of CO_2 to the increase of free volume in the system [12]. A model based on the free-volume theory has been used to determine this relationship for the CO_2/HDPE system [12].

2.2.1. Fujita-Kishimoto: Free Volume Theory

The free volume theory (See Appendix A2.3) accounts for the contribution of solvent to the increase in free volume, and describes the effect of solvent concentration on the complex viscosity of a molten polymer. Free volume parameters A and B reflect the fractional free volume in the pure polymer, and the solvent's contribution to the increase

in free volume [22]. The free volume theory serves as a method for describing polymer–solvent systems, it is commonly used to correlate the effect of solvent concentration on viscoelastic behavior, and it has been shown to produce good predictions for melt, rubbery and glassy polymer-solvent systems as well as being convenient for use in understanding diffusion. Fujita and Kishimoto [22] derived an equation analogous to the Williams – Landel – Ferry (WLF) [24] and Arrhenius equations, to determine the concentration-viscosity relationship. In the study of diffusion of CO_2 in HDPE, the Fujita Kishimoto model with two parameters is used [12] (See Figure 2.12). Free volume models [22, 23] describe well the effect of concentration on the viscosity of melts, provided the polymer is not saturated. The horizontal shift factor a_C describes the effect of solvent concentration on the melt viscosity, and the vertical shift factor b_C is a correction factor that describes changes in polymer density [10].

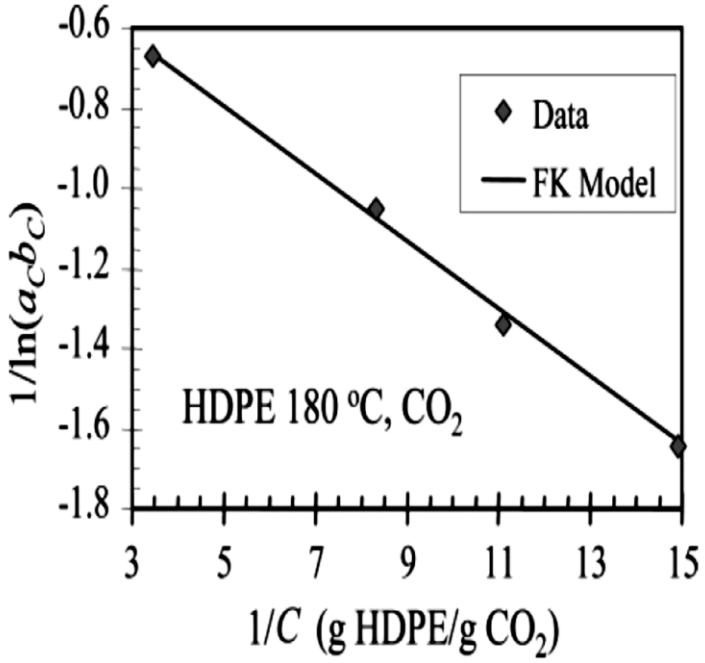

Figure 2.12. Effect of concentration on the concentration shift factor for CO_2. The line is the best fit of the Fujita-Kishimoto model, with A =2.67 and B=0.22 [12].

2.2.2. Flory-Huggins: Solution Theory

During diffusion, expansion and compression forces arise and polymer chains experience configuration changes [25 - 27]. Diffusion depends on interactions between diffusant molecules and polymer chains. Fick's laws do not account for these interactions, and are only valid when diffusing molecules are sufficiently small [25]. In the absence of significant interactions, the time for structural rearrangements of polymeric chains is short [23]. Non-Fickian diffusion is best explained in terms of chemical thermodynamics (See Appendix A2.4.), which indicates that the fundamental driving force for diffusion is the chemical potential gradient of each component in the system [21]. Diffusion is essentially due to the existence of chemical potential differences and reflects the time for structural rearrangement [25 - 27].

Various aspects of diffusion can be characterized by monitoring the interface width and mass. The mass uptake and interface width increase with the square root of time for a Fickian diffusion, but the diffusion type exponent for interdiffusion in partially miscible polymers is expected to be smaller [25 - 27]. This is a result of the reduced entropy or accessible free volume, and the increased heat of mixing or interaction energy, during interdiffusion in partially miscible polymers [19, 21]. The interface width is determined from the local concentration profile, but the mass uptake depends on the average concentration and is much less sensitive to the local structure [25 - 27].

The Flory-Huggins theory provides a framework for understanding the thermodynamics of polymer melts [21]. It describes the competition between entropy and enthalpy of mixing, and defines the available Gibbs free energy of mixing [21]. This Gibbs energy determines the evolution of an initial sharp interface separating two molten polymers, and to what extent initially separate systems of different composition mix [25 - 27]. When the diffusion type and free volume parameters are known, it is possible to determine the Flory-Huggins interaction parameter for Non-Fickian interdiffusion, the front velocity for Anomalous and Case II diffusion, and the diffusion coefficient for all cases.

2.3. DIFFUSION MODELS: SOLVENTS

Solvent diffusion in polymeric systems can be of Fickian, Anomalous, or Case II diffusion type. Fickian diffusion is observed in polymer melts well above their glass transition temperature, and Case II and anomalous diffusion is observed in glassy polymers [28]. The solvent diffusion rate for Fickian diffusion is slower than the polymer relaxation rate, its concentration decreases exponentially, and a large penetration gradient is observed. This is shown on the 0.9 and 0.99 curves in figure 2.13, which represent Fickian diffusion, and an exponentially decaying concentration profile (zero front velocity).

Solvent diffusion close to or below the glass transition induces significant polymer swelling, and results in a special diffusion, known as Case II diffusion. In Anomalous and Case II diffusion, the solvent diffusion rate is faster than the polymer relaxation rate. Case II and anomalous diffusion requires Fick's second law to be modified to describe adequately the solvent penetration [28, 29]. In anomalous and Case II diffusion, the solvent front moves into the polymer at a constant velocity [28] (See Figure 2.13). This is shown on the 0.01 and 0.1 curves in figure 2.13, which represent a concentration front moving at constant velocity. Measurement of the diffusion coefficient in a glassy polymer is complicated by the slow mechanical response of the polymer chains.

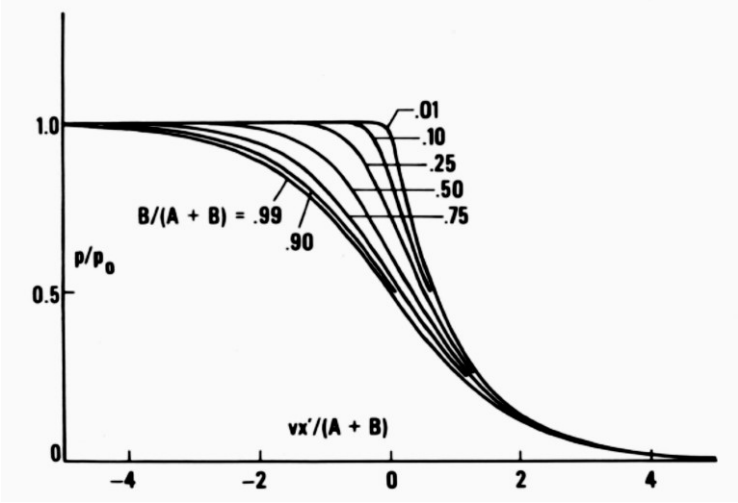

Figure 2.13. Pressure (or concentration) profiles with constant front velocity versus depth, as a function of the diffusion coefficient: 0.99 and 0.9 curves represent higher diffusion coefficients and a more Fickian Behavior; 0.01 and 0.1 curves are typical of Glassy diffusion [29].

2.4. INTERDIFFUSION MODELS: POLYMERS

Polymer-polymer diffusion is usually described using the mean-field theory and a free energy mixing function (See Appendix A2.4). The volume of the system does not change during interdiffusion, and this free energy function describes chain interaction and entropy, based on a Flory-Huggins approach [25 - 27]. Each polymer rearranges and repels unfamiliar chains across the interface, the two polymers do not freely and completely mix, and the diffusion mechanism is different from free (or Fickian) diffusion. In the case of Non-Fickian solvent-polymer diffusion and polymer-polymer interdiffusion, the diffusion flux is a non-linear function of the chemical potential, and the concentration profile is obtained by solving a non-Fickian diffusion equation [25 - 27] (See Figure 2.14).

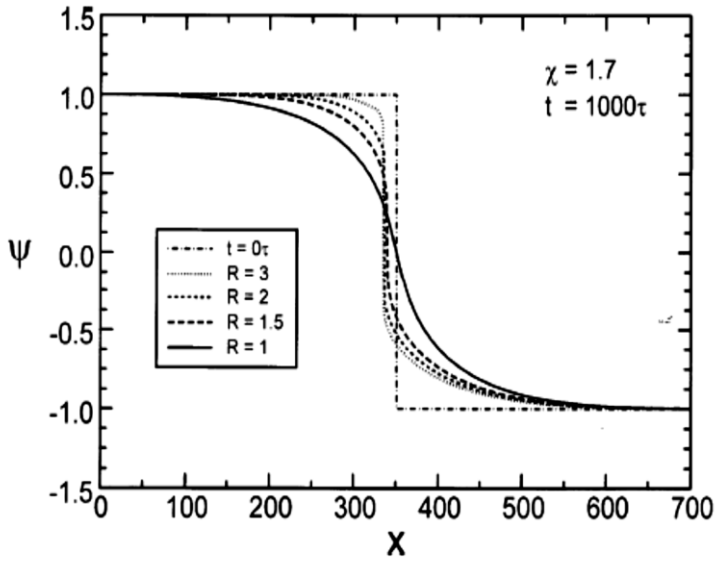

Figure 2.14. Concentration profiles for Non-Fickian interdiffusion between two partially miscible polymers versus depth, as a function of the molecular weight ratio between the two: R = 1 curves represent the case of Fickian diffusion, R = 2 and R = 3 curves are typical of polymeric interdiffusion [25].

CHAPTER 3

Solvent Diffusion in Molten Polystyrene Under Small Amplitude Oscillatory Shear

ABSTRACT

Diffusion of 1, 2, 4-trichlorobenzene through polystyrene in the melt state is studied using a rotational rheometer under small amplitude oscillatory shear (SAOS), and the diffusion coefficient D is measured at various oscillation frequencies, ω_0. The effect of solvent concentration C on the polymer complex viscosity η^* is described using the Fujita-Kishimoto free volume relationship. Free volume parameters A and B are determined separately to diffusion measurements, from melt viscosities of neat and homogeneous solvent-polymer mixtures, and a single parameter fitting is then used to determine the diffusion coefficient. Oscillatory shearing leads to a faster diffusion. This observation is made by comparing the diffusion coefficient of samples subjected to intermittent-type oscillations and those subjected to continuous SAOS. The study clearly confirms that such SAOS measurements can be used to determine the diffusion coefficient with reasonable accuracy as compared to sorption measurements, and shows that the diffusion rate is increased by oscillatory motion.

3.1. INTRODUCTION

Over the last decade, understanding diffusion through molten polymers has been essential to advances in polymer technologies such as coating [30], foaming [31], and plastic welding [32]. In polymers, diffusion is complicated by free volume limitations [33], multiple relaxation time scales [34, 35], and often limited by partial miscibility [36]. Solvent diffusion can be captured in polymer solutions using a variety of sorption techniques [37] and drying-based techniques coupled with spectroscopic quantification of concentration [33, 38], which are limited by vitrification or crystallization and there is a

real lack of experimental data [33]. The quantitative study of solvent diffusion is also complicated by other processes such as polymer swell and dissolution which are typically occurring along with solvent diffusion [39].

Diffusion of chain molecules in a molten polymeric matrix has been studied using photo and fluorescent labelling [40, 41], using deuteration combined with SANS [42] or ion scattering techniques [43] and by rheometry using a sandwich configuration [34]. The importance of further experimental study of diffusion of both polymer chains and particles in molten polymer nanocomposites has recently been clearly elucidated [44]. These techniques are versatile, but require sophisticated equipment and are limited to particular systems. Mass uptake measurements [37] are simple and accurate, and can be used to measure the diffusion coefficient of solvents or gases in molten polymers. Rheometry is another potential technique for studying diffusion [45] that has not been fully exploited. Here we develop and validate a simple and versatile rheometry-based technique for measuring diffusion of solvents in polymer melts and concentrated solutions.

Mass uptake measurements which provide the evolution of the mass of a specimen during sorption require the application of a model to infer the diffusion coefficient. In general, the mass uptake in molten polymers follows a power law dependency on time [45], with an exponent of ½. In this case, the polymer's relaxation rate is fast compared to the solvent diffusion rate, and classic Fickian diffusion occurs. An experimental complication with this technique is dissolution of the polymer which is confounded with the impact of sorption on the overall specimen mass.

Small amplitude oscillatory shear (SAOS) measurements are widely used to determine linear viscoelastic properties of a material, and are extremely sensitive to compositional or structural changes in the material. SAOS measurements in the linear viscoelastic region are only frequency-dependent, which makes them suitable to examine irreversible processes such as diffusion [44]. If rheometry is applied to measure diffusion coefficients then models of the diffusion process and of SAOS flow, as well as the dependency of the LVE properties on composition, are all required.

Fickian diffusion [45] of small molecules in polymers is often observed well above the glass transition temperature of the polymer. In this case, the polymer relaxation rate is faster than the solvent diffusion rate, its concentration decreases exponentially and a large penetration gradient is observed. However, there are cases where diffusion is non-Fickian [46]. It may be useful to characterize this behavior using a type of Deborah number: the ratio of the relaxation time to the diffusion time. When this number is much larger than unity, diffusing molecules move into an almost elastic polymer, this is a typical case of diffusion of small molecules into a glassy polymer. When the Deborah number is much less than unity, relaxation is fast, and the diffusion mechanism is of Fickian type. The mass uptake profile in polymer-penetrant and polymer-polymer systems varies as a power law function of time of the form:

$$\frac{M_t}{M_\infty} = K \cdot t^n \quad \textbf{(1)}$$

where M_t and M_∞ are the mass uptakes at times t and at saturation respectively. Here, K is a constant which depends on the diffusion system and temperature and n is an exponent related to the transport mechanism [45, 47] defining the diffusion type.

The effect of material composition on the LVE properties can be modeled in different ways ranging from tube model based molecular theories [48, 49] to the free volume theory [50]. These models generally involve a set of parameters that must be fit from experimental measurements of homogeneous systems. The free volume theory involves two fitting parameters and is most accurate in the region of high polymer concentration. These parameters can be determined from LVE data of the neat polymer melt and concentrated solutions.

In SAOS flow [51], the deformation is sufficiently small that polymer chains are hardly disturbed from their equilibrium state and linear viscoelasticity is exhibited. The response is measured in terms of torque, which remains constant during time sweep measurements at constant frequency on homogeneous samples. Solvents plasticize molten polymers, which causes the measured torque to decrease as solvent diffuses into the polymer in the outward radial direction. The SAOS torque curve is thus dependent on the diffusion kinetics and the concentration profile. The diffusion model [45], the free

volume theory [49], and the theory of linear viscoelasticity [50] are then used to determine the diffusion coefficient from the torque curve. Recent findings suggest that SAOS accelerates diffusion [52, 53] but only a limited number of cases have been reported. It is well known that polymeric chains under SAOS in the LVE region are hardly disturbed from their equilibrium state and therefore physical factors that lead to a faster diffusion are unclear. The main objective is to determine the diffusion coefficient from time-dependent rheological measurements, and to explain if and why SAOS accelerates diffusion in polymer melts.

In a study of diffusion of carbon dioxide in high density polyethylene [51, 52], Park and Dealy show that subjecting the sample to SAOS at a frequency of 0.01Hz significantly accelerates the diffusion process as compared to the quiescent case. It was also found that further increasing the frequency to 0.06Hz did not enhance the diffusion process. The authors used the free volume theory to describe the viscosity of the polymer-CO_2 solution with two parameters: one is a characteristic of the available free volume in the polymer and the other accounts for the increase of free volume in the system due to CO_2 [51]. In another study on the diffusion of epoxy and its reaction with polybutylene terephthalate (PBT) under SAOS [54], samples blended in a mixer were compared with planar samples in which epoxy is sandwiched between two PBT plates. The reaction rates for planar samples increased with frequency while those of homogeneous samples did not, indicating that epoxy diffusion is limiting the reaction rate in the planar samples and that the rate of diffusion increases with frequency [54].

In the Park and Dealy study, a High Pressure Sliding Plate (HSPR) rheometer with a rectilinear flow geometry is used. In that case the flow direction is x, the velocity-gradient direction is z and the diffusion occurs in x and y. In the Xie and Zhou study, a rotational rheometer with parallel-plate geometry is used but the specimens are in the form of sandwiches. Here the flow direction is θ, the velocity-gradient direction is z and the diffusion direction is z. In comparison to these two studies, our experiments are performed on a rotational rheometer with concentric specimens. Therefore the flow is in the θ direction, the velocity-gradient direction is z and the diffusion direction is r.

There exists no satisfactory explanation for the observed effect of SAOS and oscillation frequency on diffusion. In this work we provide a validated method for rheological studies of diffusion in molten polymers, focusing on the characterization of solvent diffusion. The method combines, experimental measurements in SAOS, a Fickian diffusion model, the free volume model and the theory of linear viscoelasticity.

3.2. THEORETICAL CONSIDERATIONS: DIFFUSION DYNAMICS

Polymeric systems can exhibit pseudo-Fickian, Fickian, anomalous, and case II diffusion [45]. In anomalous and case II diffusion, the solvent diffusion rate is faster than the polymer relaxation rate, and the interface moves at constant speed in the direction of the concentration gradient. The Flory-Huggins [39, 55, 61] theory has been used to describe interdiffusion [39, 55, 61], and the slow evolution of an initial sharp interface separating two molten polymers [57, 58]. The type of diffusion behavior is therefore strongly dependent on both host polymer and diffusing species, and on the experimental temperature. In the case of solvent diffusing in a polymer well above its glass transition temperature the behaviour is Fickian and the only parameter necessary is the diffusion coefficient. Here we consider Fickian diffusion described by Fick's second law (eq. 2).

$$\frac{\partial \mathbf{C}}{\partial \mathbf{t}} = \mathbf{D} \cdot \boldsymbol{\nabla}^{\mathbf{2}}\mathbf{C} \qquad \textbf{(2)}$$

3.2.1. Diffusion Dynamics in Rheometry

Parallel disk rheometers measure torque [58], which is the integral or sum of moments generated by circumferential stresses at a given time. In the absence of a composition gradient and in the LVE region, the magnitude of the circumferential stress is known and linear. The integral equation relating measured torque and shear stress in SAOS can be solved, and expressed in terms of complex viscosity (eq. 3). In the presence of a composition gradient, the torque integral cannot be explicitly solved (eq. 4).

Under SAOS at constant frequency [59] the complex viscosity of a pure polymer (Figure 1a) is time-independent and the torque amplitude is constant (eq. 3).

$$\mathbf{T(\omega_0, 0)} = \left[\frac{\pi\omega_0\theta_0 R^4}{2H}\right] |\eta^*(\omega_0, 0)| \neq \mathbf{f(t)} \quad \textbf{(3)}$$

Here T (ω_0, 0) is the torque amplitude, θ_0 is the angular displacement, ω_0 is the frequency, H is the gap size, $\eta^*(\omega_0, 0)$ is the complex viscosity of the polymer, and R is the disc radius.

On the other hand, the torque in constant frequency SAOS measurements carried out on a concentric binary specimen (Figure 3.1(b)) is time-dependent and reflects the diffusion process (eq. 4).

$$\mathbf{T(\omega_0, t)} = \left[\frac{2\pi\omega_0\theta_0}{H}\right] \int_a^b [|\eta^*(\omega_0, C)| \cdot r^3] dr = \mathbf{f(t)} \quad \textbf{(4)}$$

Here T (t, ω_0) is the time-dependent torque amplitude, a is the inner radius, b is the outer radius, and $\eta^*(\omega_0, C)$ is the concentration-dependent complex viscosity. We note that eq. 4 shows that the design of our specimen geometry is such that the solvent diffusion in the outward radial direction will have a much more significant impact on the torque than polymer dissolution in the center of the ring.

(a) (b)

Figure 3.1. Schematics of samples used in rheological characterization of: (a) Neat polystyrene; (b) Solvent diffusion. The inner radius is variable, and two different geometries are studied.

Free volume models describe well the effect of concentration on the viscosity of melts, provided the polymer is not saturated [49], and if the volume of the mixture is additive [52]. The horizontal shift factor a_C describes the effect of solvent concentration on the melt viscosity, and the vertical shift factor b_C is a correction factor that describes changes in polymer density [52]. In this case, the pure polymer density is constant, and the vertical correction factor b_C can be determined (eq. 5):

$$\boldsymbol{\rho(0) \equiv \frac{C}{b_C(C)}} \quad \textbf{(5)}$$

In practice, shift factors are determined by a simultaneous shift vertically ($a_C \cdot b_C$) and horizontally (a_C) on the complex viscosity of homogeneous solvent-polymer samples at different concentrations, and the response of the pure polymer [51]. Consistency is verified using (eq. 5) with a constant density for the pure polymer (±0.6%).

The free volume theory accounts for the contribution of solvent to the increase in free volume, and describes the effect of solvent concentration on the complex viscosity of a molten polymer (eq. 6). Free volume parameters A and B reflect the fractional free volume in the pure polymer, and the solvent's contribution to the increase in its free volume [49].

$$\boldsymbol{a_C(C) \cdot b_C(C) = \frac{\eta^*(\omega,\ C)}{\eta^*(\omega,\ 0)} = e^{-\frac{1}{[A]+[B]\cdot\frac{1}{C}}}} \quad \textbf{(6)}$$

In combination with eq. (4), the free volume theory allows us to define a relationship between concentration, and measured torque eq. (7).

$$\boldsymbol{\frac{T(t)}{T(0)} = \frac{4}{R^4} \cdot \int_a^b \left[e^{-\frac{1}{A+B\cdot\frac{1}{C(r,t)}}} \right] \cdot r^3 \cdot dr} \quad \textbf{(7)}$$

where **A, B** are the free volume parameters. The Fickian diffusion model can then be incorporated by assuming that: (i) a finite amount of solvent is initially distributed uniformly through a thin cylinder of radius a, and (ii) there is no flow of diffusant leaving the system. We start with Fick's 2nd law (eq. 8), in a semi-infinite medium with the following boundary and initial conditions (eq. 9):

$$\boldsymbol{\frac{1}{r} \cdot \frac{\partial}{\partial r}\left(r \cdot \frac{\partial C}{\partial r}\right) = \frac{1}{D} \cdot \frac{\partial C}{\partial t}} \quad \textbf{(8)}$$

$$\boldsymbol{C = C_0 \quad \text{at} \quad 0 < r < a, \quad t = 0}$$

$$\boldsymbol{C = 0 \quad \text{at} \quad a < r < \infty, \quad t = 0}$$

$$\boldsymbol{C = 0 \quad \text{at} \quad r = \infty, \quad t \geq 0} \quad \textbf{(9)}$$

The solution [60] to this problem is:

$$\boldsymbol{\frac{C_{(r,t)}}{C_0} = \frac{1}{2Dt} \cdot e^{-\frac{r^2}{4Dt}} \cdot \int_0^a e^{-\frac{\acute{r}^2}{4Dt}} \cdot I_0\left(\frac{r\acute{r}}{2Dt}\right) \cdot \acute{r} d\acute{r}} \quad \textbf{(10)}$$

where **D** is the diffusion coefficient, and $\mathbf{I_0}$ is the modified Bessel function of 1st kind and of order 0.

This solution has been obtained by Crank [59], and whether it is applicable to this diffusion problem depends on the exact experimental conditions. This solution is realized in practice in the experiment in which the PS rings contain a small volume of solvent relative to the sample volume. In other words, the concentration tends to zero at the outer rim. This means that concentration changes do not reach the outer rim during the time of the experiment. We note that our approach is similar to the model used in and the analysis of Park and Dealy [52].

In some instances of our experiments, small concentration changes reach the outer rim, and the boundary condition that the concentration tends to zero as x approaches the outer rim must be replaced by the condition that there is no flow of diffusing substance through the outer rim necessitating a different solution than eq. 10. This time refers to the late diffusion stages, and limits the applicability of the analytical solution (eq. 10). Applying conservation of mass for Fickian diffusion shows that this critical time for violating the outer boundary condition, can be estimated from the geometric factor k (k=b/a), and the diffusion time scale or the time required for the measured torque to become quasi-constant.

3.2.2. Diffusion Dynamics in Sorption Experiments

In the sorption studies, rectangular samples are immersed in an infinite solvent bath [37]. This is the case of double-sided diffusion through a plane sheet of thickness 2L, whose surfaces at x = ± L, are maintained at a constant concentration. It is assumed that the solvent enters through the faces and a negligible amount through the edges [37], that the region $-L < x < L$ is initially free of solvent, and that the surfaces are maintained at a constant concentration. The amount of diffusing substance [59] which has entered the sheet at time t is given by:

$$\frac{\mathbf{M(t)}}{\mathbf{M_\infty}} = \mathbf{1} - \frac{\mathbf{8}}{\boldsymbol{\pi}^{\mathbf{2}}} \sum_{\mathbf{n=0}}^{\infty} \left\{ \frac{\mathbf{1}}{(\mathbf{2n+1})^{\mathbf{2}}} \right\} \cdot \mathbf{e}^{\left[-\frac{\mathbf{Dt}}{\mathbf{4L^2}}\right] \cdot \boldsymbol{\pi}^{\mathbf{2}} \cdot (\mathbf{2n+1})^{\mathbf{2}}} \qquad \textbf{(11)}$$

where **D** is the diffusion coefficient. The values of D determined from eq. (11) using the sorption data, are used to validate values of D obtained from eq. (7) and eq. (10) using the rheological method.

3.3. EXPERIMENTAL METHODS

3.3.1. Materials and Sample Preparation

A commercial grade polystyrene (M_w = 350 kg/mol, M_w / M_n = 2) was purchased from Sigma - Aldrich **(**product 441147). The solvent, 1, 2, 4-trichlorobenzene (Acros Organics product 296104) was used as diffusant because of its high boiling point (214ºC). Neat polymer pellets are dried in a vacuum oven at 110°C for 48h, to remove moisture. Polymer disks (1.2mm thick and 25mm diameter) and flat rings (1.2mm thick with an outer diameter of 25mm and an inner diameter of 6.25 or 12.5mm) are prepared by compression molding under identical molding conditions. We refer to the geometry of the rings using the ratio of outer-to-inner radius, k. Square specimens for sorption tests (45 x 45mm x 1.2mm) are also prepared by compression molding.

3.3.2. Rheological Measurements

All small-amplitude oscillatory shear measurements are done at 190°C under nitrogen atmosphere, at a gap of 1.1mm using an Anton-Paar MCR500 rheometer equipped with parallel plate geometry (25mm diameter). For small strains, viscoelastic properties are independent of the strain amplitude, and a strain sweep is used to identify this linear region. When the experiment time is unusually long as is the case for diffusion studies, thermal degradation becomes an important factor. Long-time sweeps in the LVE region were used to confirm the stability of the neat polymer under these conditions. A frequency sweep is then used to determine LVE properties of the neat polymer and homogeneous solvent-polymer mixtures, at various mixing concentrations. To study diffusion using rheometry, we use polymer specimens in the shape of flat rings. The ring is loaded into the rheometer and the solvent is dispensed into the center hole. Time sweeps at a constant frequency are performed and the torque is measured as a function of

time, with a strain amplitude of 4%. Although these measurements lie in the linear viscoelastic region, there are indications in the literature that SAOS may still affect the diffusion process [45, 51].

To clarify the effect of SAOS on diffusion both continuous and intermittent-type oscillation experiments are performed. In the continuous-type experiments shown in Figure 3.2, the sample is subjected to oscillatory flow during the entire test time. In the intermittent-type oscillation experiments in Figure 3.2, oscillations are applied for 2 minutes followed by rest stages where no flow is applied. Rest stages of 2000, 4000 and 10000s were studied.

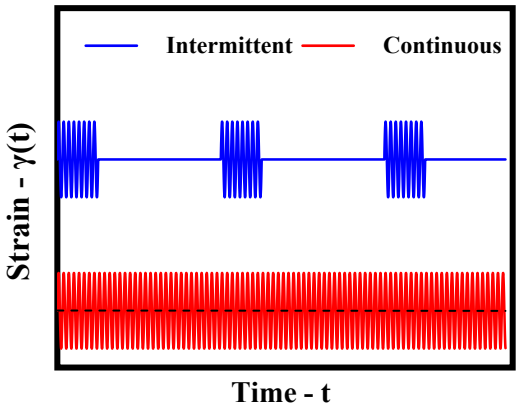

Figure 3.2. Schematic illustration of strain histories in intermittent-type oscillation experiments compared with continuous-type oscillation experiments.

3.3.3. Sample Geometry in Rheometric Diffusion Studies

In diffusion measurements, a PS ring with the solvent dispensed at the center, is squeezed between the bottom and top plate of the rheometer. The excess is then trimmed at the outer radius, so that there is no net change in the radial position of the outer boundary (b=12.5mm). Consequently, the interface position at the inner radius moves toward the centre due to squeezing as follows:

$$\mathbf{a(H,k)} = \mathbf{a_i} \cdot \left[\left(\frac{-Hk+H+k+1}{2}\right)\right] \qquad \mathbf{H} = \frac{\mathbf{h_i}}{\mathbf{h_{test}}} \quad , \quad \mathbf{k} = \frac{\mathbf{b}}{\mathbf{a_i}} \qquad \textbf{(12)}$$

Here, **a(H, k)** is the inner radius after squeezing, $\mathbf{a_i}$ is the initial inner radius, **k** is the ratio of outer-to-inner radius, and H is the squeeze ratio.

Table 3.1. Effect of squeezing on sample geometry and interface position in diffusion measurements

a_i (mm)	k	a(H, k) – mm	Displacement - %
3.125	4	2.75	12
6.25	2	5.94	5

The values of a(H, k) for the two geometries studied experimentally, and with H=1.1 (h_i=1.2mm and h_{test}=1.1mm) are shown in Table 3.1. The volumetric thermal expansion coefficient of polystyrene [62] is on the order of 4×10^{-4} 1/C, and the inner radius at 190°C is displaced due to thermal expansion, but by less than 0.1%. Thermal expansion results in negligible changes in the inner radius in comparison to squeezing. Therefore we consider only the squeezing effect and the correction factor applied to the interface boundary at the inner radius is 12% and 5% for k = 4 and k = 2 respectively.

3.3.4. Sorption Measurements

The square specimen is immersed in a beaker containing the preheated solvent which is placed in an oil bath to control the temperature at 190°C. The system shown in Figure 3.3 is placed under a fume hood, and the beaker, is sealed with an open-ended watch glass to control solvent evaporation. An abundant amount of solvent is used to insure continuous exposure of the polymer. After 15s of immersion, the specimen is removed from the beaker using a hook system, cleaned with absorbent paper and weighed on an analytical balance, before being placed back in the beaker. At 190°C, diffusion for this solvent-polymer system is rapid and saturation is achieved in less than 5 minutes. Solvent diffusion is accompanied by PS dissolution into the solvent. In order to assess measurements reliability, some samples were immersed for longer time periods and for all cases, the experimental error based on 9 different samples was less than 3%.

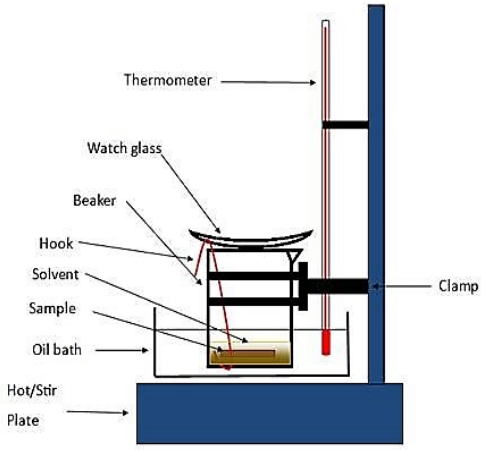

Figure 3.3. Schematic illustration of the mass uptake measuring system.

3.4. RESULTS AND DISCUSSION

3.4.1. Linear Viscoelastic Characterization: Homogeneous Systems

The dynamic moduli (Figure 3.4) show typical behavior with a cross-over frequency at 4.5s^{-1} and a clear rubbery plateau. The relaxation spectrum H (λ) is calculated from this oscillatory storage and loss modulus data at 190°C, using a nonlinear Tikhonov regularization method and a software developed by the Freiburg Materials Research Center [58]. The weighted relaxation spectrum, λ·H(λ), is plotted against relaxation times λ in Figure 3.4.(b), and a characteristic peak at 1.8s is observed.

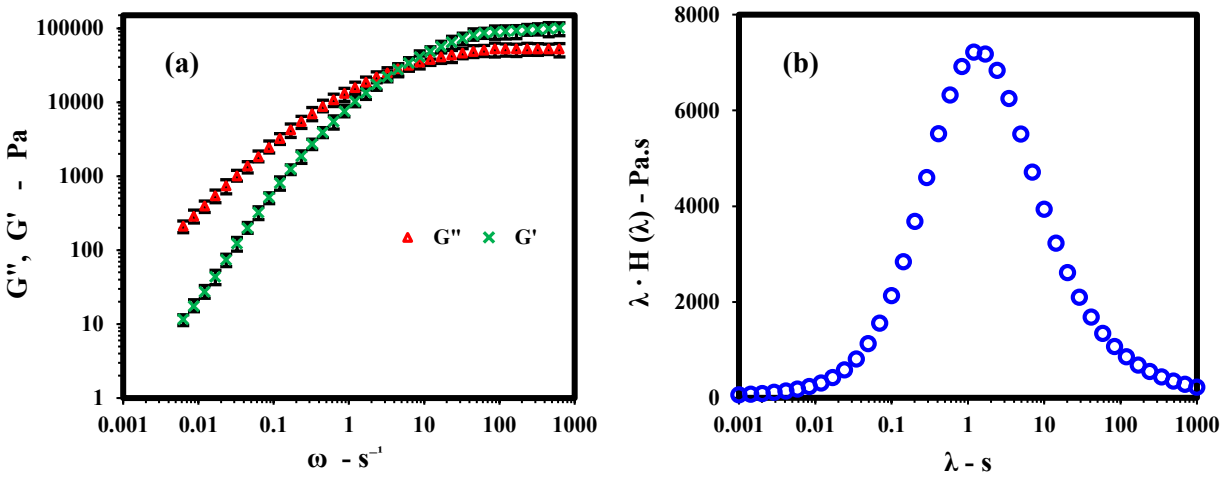

Figure 3.4. A frequency sweep test with a shear amplitude γ = 4% at 190°C. (a) Storage modulus (G') and loss modulus (G") as a function of frequency for neat PS; (b) weighted relaxation spectrum of neat PS. Error bars represent the standard deviation of 9 measurements.

In the Appendices, the complex viscosity of homogeneous polymer solutions at several concentrations are shown, from which the concentration shift factors (a_C and b_C) are determined (Figure A3.1). The applicability of the free volume theory to these results is shown in Figure 3.4., from which free volume parameters are determined. According to eq. (5), a plot of 1 / ln [(a_C (C) · b_C (C)] versus [1 / C] should be a straight line with slope B and intercept A (Figure 3.5). It is clear that the free volume theory and the Fujita-Kishimoto free volume model [49], can describe the effect of solvent concentration on the complex viscosity of PS - TCB solutions in the concentration range of interest.

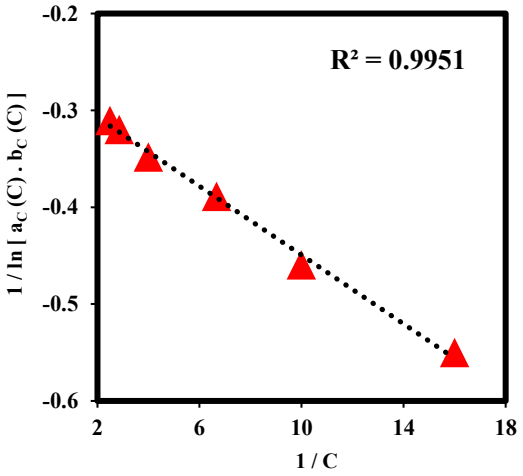

Figure 3.5. Applicability of the free volume theory at 190°C. The free volume parameters, were determined to be A = 0.2717 and B = 0.0178, for solutions ranging from 60wt% to 93.75wt% polymer (See Figure A3.1).

3.4.2. Sorption Measurements

Figure 3.5 shows experimental sorption results as a function of time, as well as the best fit of eq. (11) with the corresponding diffusion coefficient. The main challenge in studying diffusion is to evaluate the diffusion coefficient [37]. In sorption experiments, the gain in weight of a rectangular PS film is measured as a function of time. Eq. (11) well describes this process, provided the film does not dissolve [46]. Dissolution of PS at 190°C may be one of the limiting factors in the accuracy of the sorption method for determining the diffusion coefficient. However, the high temperature also results in a high diffusion rate meaning that reliable measurements are still possible at short times where the impact of dissolution is minimized. Eq. (11) represents the mass uptake for

sorption in a thin film, where M_∞ is the equilibrium solubility, which may be practically impossible to measure due to dissolution of the polymer.

A least-squared-error fitting of eq. (11) is applied to experimental sorption data and the diffusion coefficient is determined as single fitting parameter. Our fitting approach is applied to sequential subsets of the original data (Figure 3.6(a)), to determine an estimate for the diffusion coefficient which is least affected by polymer dissolution. In Figure 3.6(a) we can see that data after 60s of immersion are somewhat affected by polymer dissolution, at an even longer time dissolution overcomes sorption and a weight loss is observed (see Figure A3.2 in the Appendices). We therefore apply the fit to all data up to 60s and obtain an average value of D = 2.167 · 10-4 mm2/s. This result is used to validate diffusion coefficients from rheological measurements.

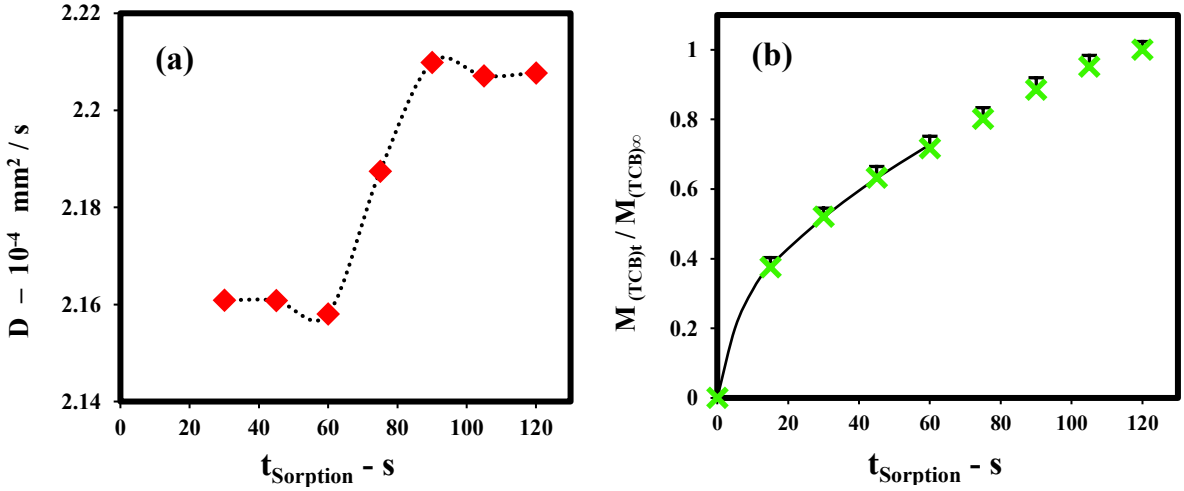

Figure 3.6. Mass uptake measurements at 190°C. (a) Sensitivity of the inferred diffusion coefficient to the experimental sorption time; (b) Sorption plot for the TCB|PS system. Symbols represent average of 9 experiments. Curve represents eq. (11) with a diffusion coefficient of $2.167 \cdot 10^{-4}$ mm^2/s.

3.4.3. Diffusion Measurements in SAOS

Figure 3.7 shows plots of the torque, $T(\omega_0, t)$, at five different frequencies ω_0, for specimens of geometry k = 4 (Figure 3.7(a)) and k = 2 (Figure 3.7(b)). The solvent which is initially confined within the polymer ring, diffuses outwards, resulting in a decreasing torque over time. The effect of diffusion is more pronounced in the early stages of the experiment, and the system later reaches a state where the torque becomes independent of

time. The key feature of this plot is the time required for the torque to become constant to ±2%. This time, 16 hours (~ 60 000s) for a ring with outer-to-inner radius ratio k = 4, and 8hours (~ 30 000s) for k = 2, is characteristic of the diffusion time scale.

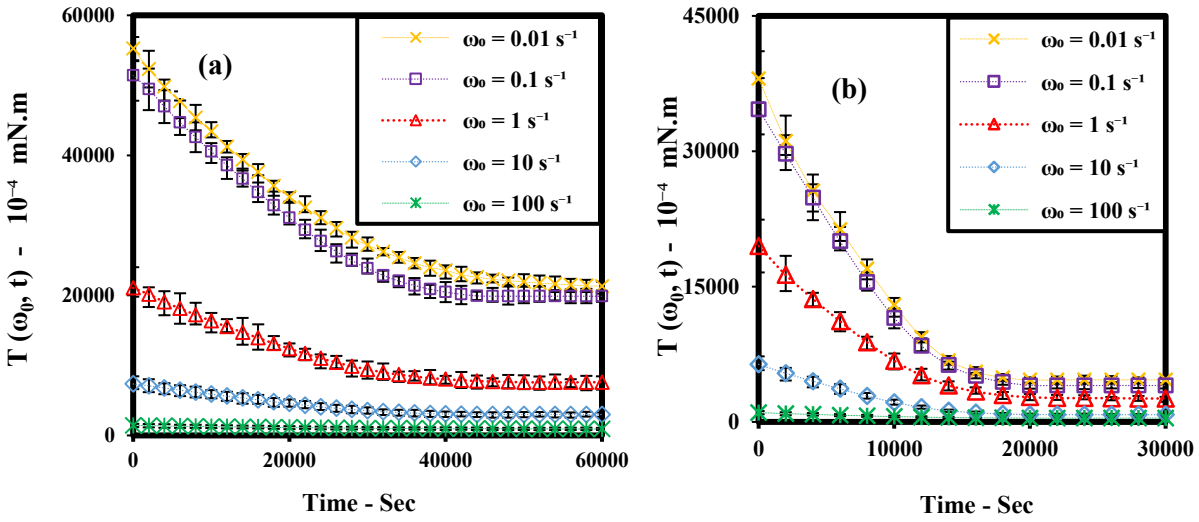

Figure 3.7. Experimental diffusion measurements at 190°C for 5 frequency decades from 0.01s^{-1} to 100s^{-1}: torque T (ω_0, t) as a function of frequency for (a) k = 4; (b) k = 2. Error bars represent the standard deviation of 6 measurements.

In Figure 3.7, measured torque is normalized by the torque at time t = 0, as T (ω_0, t) / T (ω_0, 0). This torque T (ω_0, 0) reflects the response of pure PS before solvent diffusion. The normalized data in Figure 3.8 are used to determine the diffusion coefficient for this TCB-PS system at 190°C, from both geometries (k = 4 and k = 2). In this figure we can see that except for ω_0=100 s^{-1}, diffusion appears to be unaffected by frequency. Shearing at 100s^{-1} results in a higher dissipation rate then shearing at lower frequencies of 1 s^{-1}, which implies that the diffusion system may have been affected by viscous heating for ω_0=100 s^{-1}, so it is not possible to make a clear determination at this frequency. Using velocity, shear area and perimeter, density and viscosity of polystyrene at 190°C, we can estimate the Reynolds number (10^{-3} for 100 s^{-1}, 10^{-5} for 1 s^{-1}) Using an SAOS velocity of 0.05 m/s (determined from strain amplitude 5%, frequency 100 s^{-1} and plate gap 0.001m), density (1040 kg/m^3), thermal conductivity (0.1 W/m.K) and viscosity (1kPa.s) of polystyrene at 190°C [55], we can estimate viscous dissipation and obtain a maximum temperature rise of 1K [55].

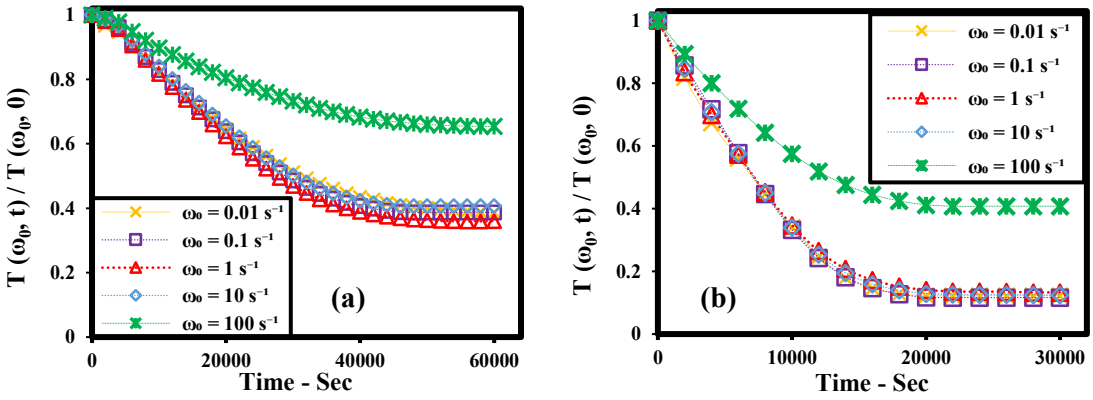

Figure 3.8. Normalized Torque at 190°C, measured as a function of time, for (a) k = 4; (b) k = 2.

In order to explore the effect of SAOS on the diffusion rate reported in literature [12, 52], we study diffusion under intermittent oscillations. As shown in Figure 3.9 (a)-(d), samples continuously sheared produce the steepest decrease in measured torque, compared with samples undergoing only short intermittent oscillation and long rest periods.

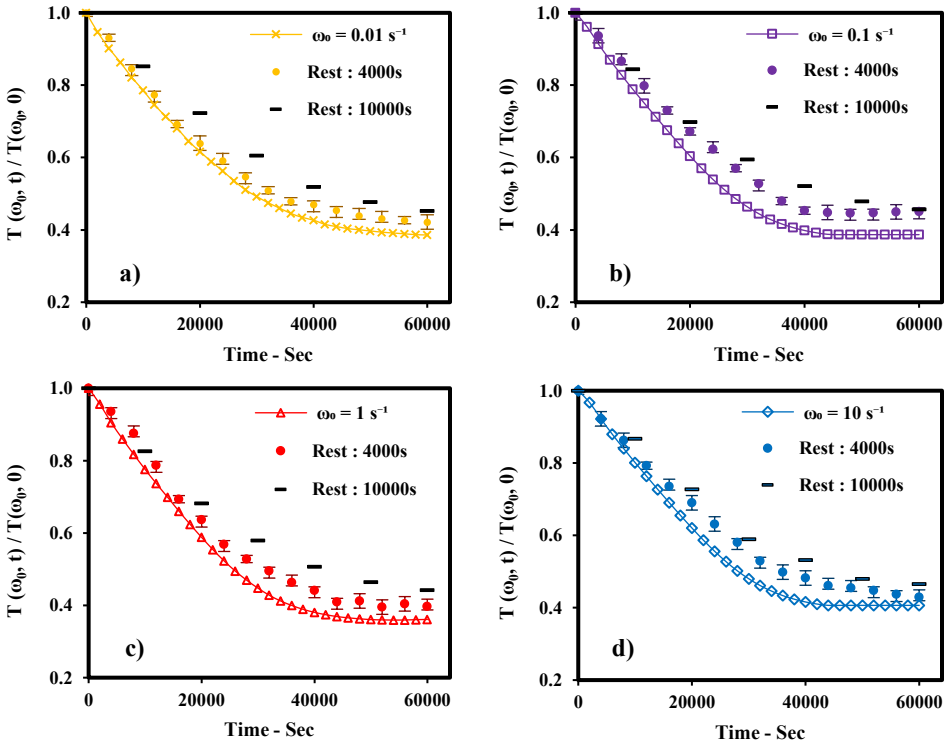

Figure 3.9. Normalized Torque at 190°C, for samples continuously sheared, compared with samples undergoing periods of intermittent oscillations and long rest periods, for k = 4, at 190°C and ω_0 = (a) 0.01 s^{-1}; (b) 0.1 s^{-1}; (c) 1 s^{-1}; (d) 10 s^{-1}.

3.4.4. Inferring Diffusion Coefficients From Rheological Data

Using eq. 10, a least-squared-error fitting of eq. 7 is applied to experimental torque data. A gradient-based iterative search method is used [59], with the diffusion coefficient as single adjustable parameter, where the inner radius, a, is given by eq. 12. This equation incorporates the effects of initial sample squeezing. The free volume parameters (A and B) in eq. 7 are determined from a separate experiment (See Figure 3.5). The fit is applied to torque data in the early experimental times; up to half the time it takes for the torque to become constant. In Figure 3.10 for k = 4, we see that the torque is constant after 40000s and we therefore apply the fit to all data up to 20000s, to obtain a value of D in the range of ~3 x 10^{-4} mm^2/s. We have done the fitting in this way because the concentration profile from eq. (10) is less accurate at long times as the boundary condition applied at the outer rim is no longer valid. Continuous-type oscillation diffusion data for k = 4 (for $1s^{-1}$ and $100s^{-1}$) and their corresponding fits are shown in Figure 3.10. Equivalent data for k = 2 are presented in the supporting information.

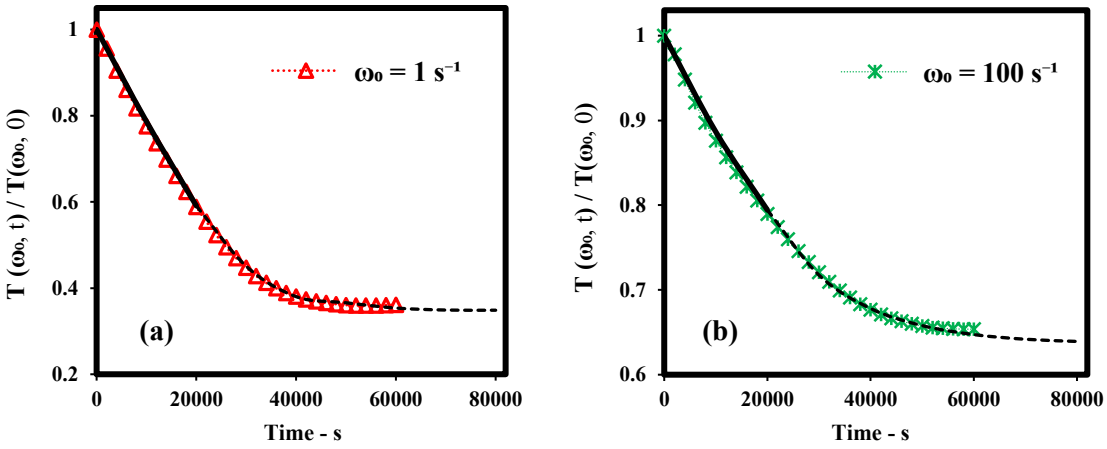

Figure 3.10. Measured torque during diffusion for k = 4, at 190°C. Lines represent the best fit with the dashed lines illustrating the extrapolation of the fit. (a) $\omega_0 = 1s^{-1}$, D = 3.32 ± 0.012 (10^{-4} mm^2 / s); (b) 100 s^{-1}, D = 3.019 ± 0.025 (10^{-4} mm^2 / s).

For each frequency, diffusion coefficients are determined from the non-linear model-fitting procedure explained above which neglects polymer swelling. Swelling results in a migrated interface, and has an impact on our inferred diffusion coefficients. The effect of swelling is small when small amounts of TCB (0.125g - 0.15g) are used compared to the

size of the PS samples (2g - 3g) as is the case with our diffusion studies. In our experiments the least effect of swelling is expected when k = 4. In order to estimate the effect of swelling, we perform a set of simulations where we fit diffusion coefficients to our experimental data with smaller values of inner radius as shown in Figure 3.11. We see that even in the case of a reduction in the inner radius by 20% for k = 2, which would represent significant swell, the estimated diffusion coefficient is only increased by 11%. We therefore neglect swell in our estimates of the diffusion coefficient and instead assign this to uncertainty.

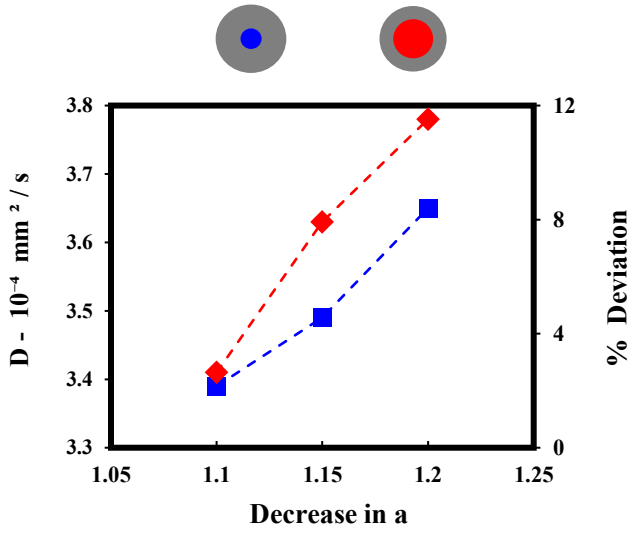

Figure 3.11. Effect of swelling on the uncertainty in diffusion coefficient for k = 4 and k = 2, at 190°C under continuous oscillation at ω_0=1s^{-1}.

At this point we take a look at simulated concentration profiles using eq. (10) with the diffusion coefficient set to D = 3.3 10^{-4} mm² / s. In Figure 3.12, concentration profiles (for k = 4) are plotted at various times throughout the experimental window. At long times, t ≥ 40000s we can see that concentration gradients still exist but the torque is quasi-constant; further indicating that SAOS measurements in this regime are not sensitive to the diffusion process. Additionally we note that our boundary condition at the outer rim becomes inaccurate when a finite concentration gradient at r = b appears at times after 20000s (for k = 4). This time constant can be estimated from data in Figure 3.10, as [40000s / $(1+1/k)^2$] which gives 25000s.

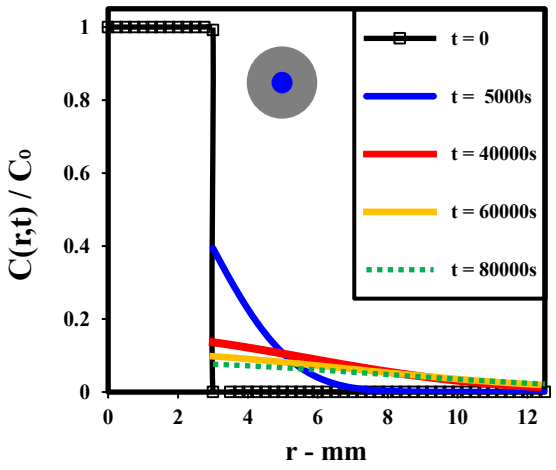

Figure 3.12. Normalized concentration profiles for k = 4, using eq. (10) with D = 3.3 10^{-4} mm²/s

Diffusion coefficients determined from the continuous-type oscillation experiments are shown in Figure 3.13 where we can see that D is independent of sample geometry, and in most cases oscillation frequency. We do see a small change in D at $\omega_0 = 100s^{-1}$ although it is unclear that this observation is physically meaningful. Shearing at $100s^{-1}$ causes the diffusion coefficient to decrease, which implies that the diffusion system may have been affected by the fast shearing but it is not possible to make a clear determination with these data.

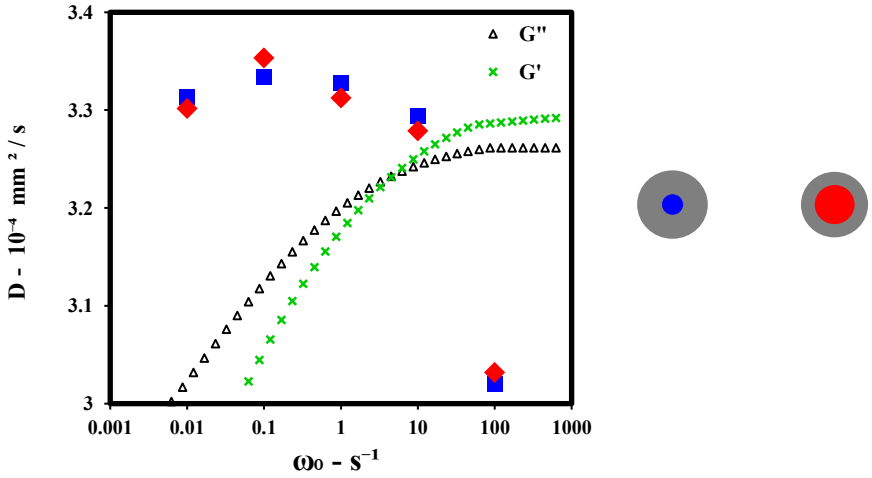

Figure 3.13. Effect of frequency on the diffusion coefficient for k = 4 and k =2, at 190°C under continuous oscillation.

Figure 3.13 shows diffusion coefficients plotted as function of frequency from $0.01s^{-1}$ to $100s^{-1}$ for (i) continuous oscillatory measurements, (ii) intermittent oscillatory measurements with a rest time of 4000s for k = 4 (and 2000s for k = 2), (ii) intermittent oscillatory measurements with a rest time of 10000s (for both k = 4 and k = 2), and (iv) sorption measurements. In Figure 3.14, we see the effect of continuous shearing which accelerates diffusion, relative to the case of intermittent oscillation. The diffusion coefficient under continuous oscillation is ~3.3 x 10^{-4} mm^2/s, while that under intermittent oscillation for rest periods of 10000s is ~2.5 x 10^{-4} mm^2/s. As expected, shorter rest periods of 4000s for k = 4 and 2000s for k = 2, result in a higher diffusion coefficient but is still lower than for the case of continuous oscillation. We note that the sorption experiments provide a diffusion coefficient value of ~2.2 x 10^{-4} mm^2/s. Recall that the sorption D value represents a lower bound of the actual material property due to polymer dissolution as explained previously. From these data we conclude that rheometry can be used to measure the diffusion coefficient for this TCB|PS system at 190°C and in this way we can explore the effect of SAOS on diffusion.

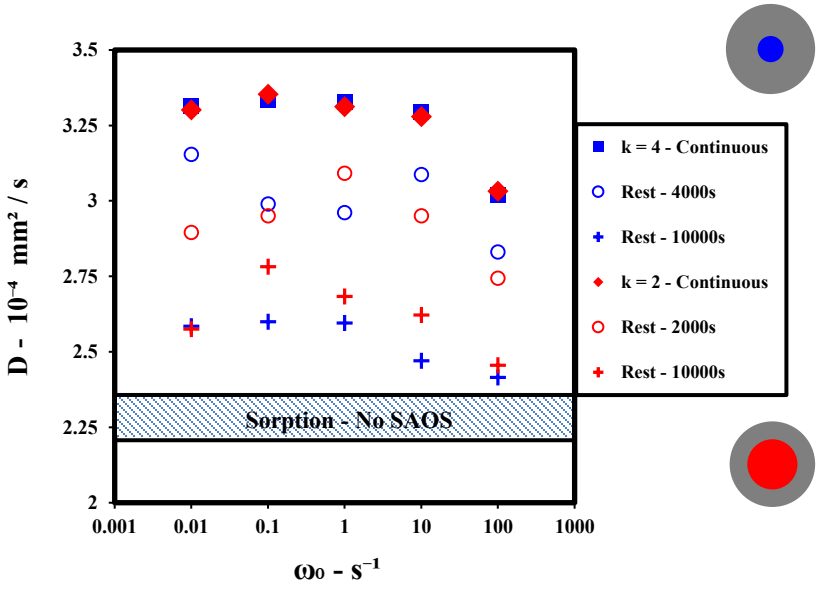

Figure 3.14. Effect of SAOS on the diffusion coefficient at 190°C under continuous oscillation, intermittent oscillation, and from static sorption measurements. Note that the sorption data are presented as a band to illustrate the likely uncertainty due to polymer dissolution.

From results in Figure 3.14, we can the following observations: relative to quiescent diffusion, diffusion under SAOS is always faster, regardless of frequency and resting periods (at least within our experimental window). This occurs even though the flow is oscillatory and there is no net transport of material in one direction. Additionally we note that by definition, the strain amplitude is very small and that the polymer chains are disturbed from their equilibrium state by an infinitesimal amount. We postulate that when reptation occurs in response to this infinitesimal deformation, it provides the opportunity for chains at the interface to convect the smaller TCB molecules in the radial direction. This means that the solvent convection happens over a length scale that is smaller than the size of the polymer chain while the polymer chain remains (approximately) in its original location. We can compare this to the case of mechanical stirring where the entire fluid is convected macroscopically in a single direction: both the solvent molecules and the polymer chains are moved from their original locations by the flow.

3.5. CONCLUSIONS

An experimental technique for determining the diffusion coefficient of solvents in polymer melts from SAOS measurements is developed here. SAOS measurements under intermittent-type oscillations provide values of the diffusion coefficients that are consistent with quiescent diffusion. We found that SAOS accelerates the diffusion of TCB in molten PS at 190°C and that longer rest periods decrease this acceleration effect. Diffusion coefficients measured under continuous oscillation are about 45% higher than those under quiescent diffusion. Additionally, high frequency results indicate that oscillations within the polymer's elastic regime have less impact on diffusion than in the viscous or viscoelastic regimes. This study provides insight into the dynamics of solvent diffusion through amorphous polystyrene in the melt state.

CHAPTER 4

A General Method for Obtaining Diffusion Coefficients by Inversion of Measured Torque From Diffusion Experiments Under Small Amplitude Oscillatory Shear

ABSTRACT

A numerical approach based on Tikhonov regularization is developed to invert torque curves from time dependent SAOS experiments in which diffusion occurs to determine the diffusion coefficient. Diffusion of a solvent into a polymer melt for example causes the measured torque to decrease over time and is thus dependent on diffusion kinetics and the concentration profile. Our numerical approach provides a general method for retrieving local viscosity profiles during diffusion with reasonable accuracy, depending only on the linear viscoelastic constitutive equation and a general power law dependency of the diffusion process on time. This approach also allows us to identify the type of diffusion (Fickian, pseudo-Fickian, anomalous and glassy) and estimate the diffusion coefficient without the a priori identification of a specific diffusion model. Retrieving local viscosity profiles from torque measurements in the presence of a concentration gradient is an ill-posed problem of the second type and requires Tikhonov regularization. The robustness of our approach is demonstrated using a number of virtual experiments, with data sets from Fickian and Non-Fickian theoretical concentration and torque profiles as well as real experimental data.

4.1. INTRODUCTION

The measured torque from parallel plate rheometry in SAOS can simply and directly be converted into shear stress and complex viscosity functions, but only when composition is uniform throughout the sample [65]. This is done using the linear viscoelastic constitutive equation with SAOS kinematics [65, 66]. When a binary sample containing a radial concentration gradient is subjected to SAOS flow, composition is a function of time and geometry [65, 66] and the situation is quite different:[65] complex viscosity varies with radial position. In this work we provide a validated numerical method based on Tikhonov regularization for recovering radial viscosity profiles from the measured torque during diffusion under SAOS, and for estimating the diffusion coefficient [67, 68, 69] with reasonable accuracy.

This class of mathematical problems, type II ill-posed [69], is ill-conditioned, the noise in the experimental data may lead to unreliable results [71, 72]. Given the ill-conditioning of the system, regularization is required in order to select an acceptable solution and provide a reasonable fit to the measured data. By recognizing the ill-posed nature of this recovery problem, Tikhonov regularization is used to reconstruct the solution of a one-dimensional diffusion problem in the radial direction. Tikhonov regularization with an appropriate choice of regularization parameter (λ), is an effective method for solving this class of problems [73]. The effectiveness of Tikhonov regularization as a method of solution, lies in its ability to stabilize the solution and to prevent it from growing unboundedly [72, 73, 74]. A large value of the regularization parameter, leads to smooth material functions at the expense of accurate representation of experimental data, and a small value of the regularization parameter leads to a close match with experimental data but the resulting functions may exhibit excessive fluctuations [75].

This method requires a rigorous route for determining the regularization parameter, which avoids over-regularized or under-regularized solutions. The choice of λ is critical, and a good λ value should minimize errors, and at the same time, give a regularized solution that is as close as possible to the exact solution [75, 76]. Here we adopt the flattest slope method to locate the optimal range [76, 77] for λ. Some of the regularized

solutions of our ill-conditioned problem are less sensitive than others to the choice of λ, and the flattest slope method [75] is used to identify the sensitive and insensitive regions, and to determine the range of optimal λ values.

In the LVE region, the properties of homogeneous samples are only dependent on frequency [65, 72], and the torque integral equation [65] in SAOS can be explicitly solved. In the presence of a composition gradient, the torque integral cannot be resolved (Eq. 1). When diffusion occurs (Figure 4.1), the complex viscosity becomes dependent on the kinematic parameters of diffusion as well.

$$\mathbf{T^C(t) = \beta \cdot \int_a^b [|\,\eta^*(r,t)| \cdot r^3]dr = f(t)} \quad \textbf{(1)}$$

$$\boldsymbol{\beta = \frac{2\pi\omega_0\theta_0}{H}} \quad \textbf{(2)}$$

Eq. 1 then relates the torque and the variable radial complex viscosity. In Eq. 1, T^C (t) is the computed time-dependent torque amplitude, η*(r, t) is the concentration-dependent complex viscosity, b is the outer radius, and a is the inner radius that refers to the radial position of the diffusion interface. In Eq. 2, H is the gap size, θ_0 is the angular displacement, and ω_0 is the oscillation frequency.

The experimental technique [65] involves SAOS torque measurements in a concentric binary specimen as in Figure 4.1 (one material in the center and the second in the outer ring). In practice, we dispense of the solvent at the center of the polystyrene ring after it has been heated to the experimental temperature, which is followed by setting up of the experimental gap and then measurement. This ensures that the solvent is trapped between the two plates of the rheometer. In this way, the interface is as sharp as possible in the experimental start-up, but we recognize that in the short time (less than 5 min.) between dispensing the solvent and beginning the measurement there will already be diffusion.

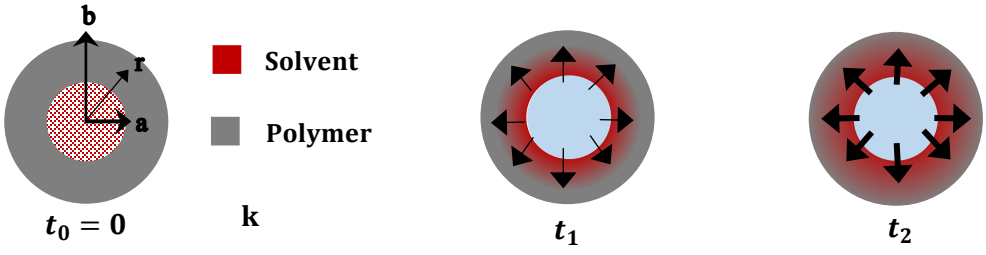

Figure 4.1. Schematic of binary sample geometry considered here in SAOS diffusion measurements, with k as ratio of outer-to-inner radius.

4.2. MATHEMATICAL FORMULATION

Parallel plate rheometry data in SAOS are in the form of a set of measured torque T_i^M at each time i. The superscript M is used to denote the experimentally measured torque, and the superscript C in Eq.1 is used to distinguish the computed torque T_i^C from its experimentally measured counterpart T_i^M. In discretized form, Eq. 1 becomes:

$$\mathbf{T_i^C = \beta \cdot \sum_{j=a}^{b} \eta^*(r_j, t_i) \cdot r_j^3 \cdot \alpha_j \cdot \Delta r} \quad \textbf{(3)}$$

Here α_j are discretization coefficients for the radial position j, which depend on the choice of discretization method, and $\eta^*(r_j, t_i)$ is the set of unknown complex viscosity profiles to be recovered from T_i^M.

Inverse problems are well-conditioned when the noise is identically distributed between time intervals [78]. Reconstructing local viscosity profiles from torque measurements is ill-conditioned, since small variability in the measured torque leads to large perturbations in local viscosity profiles. While well-conditioned inverse problems are formulated as a classical least squares minimization, ill-conditioned problems are instead solved using robust regularization methods that stabilize the solution [72, 73]. Tikhonov regularization minimizes a weighted least squares and uses a regularization parameter to weight the residual and solution norm (Eq. 4). The radial direction is discretized into N uniformly spaced points, and a weighted minimization of the sum of squared differences between T_i^M and T_i^C is applied. Tikhonov regularization finds a weighted least squares solution to an augmented system, using the regularization parameter λ and the regularized torque T_i^R (Eq. 5).

$$\mathbf{Min} \ \left|\sum_{i=0}^{t}\left\{T_i^M - T_i^C - T_i^R\right\}\right|^2 \quad \textbf{(4)}$$

$$\mathbf{Min} \ \left|\sum_{i=0}^{t}\left\{T_i^M - \beta \cdot \left[\sum_{j=a}^{b} \eta^*(r_j, t_i) \cdot r_j^3 \cdot \alpha_j \cdot \Delta r\right] - \lambda \cdot \left[\sum_{j=a}^{b} \eta^*(r_j, t_i)\right]\right\}\right|^2 \quad \textbf{(5)}$$

In Eq. 5 the measured, computed and regularized torques (T^M, T^C, T^R) all have units of torque. T^C is the computed torque and has torque units by definition. The regularization parameter plays the role of a Lagrange multiplier implicitly adding an additional constraint:

$$\left|\eta^{*}_{i,j}\right| > 0 \qquad (6)$$

The Lagrange multiplier is generally the rate of change of the quantity being minimized, as a function of the constraint parameter. This means that the regularization parameter here has units of torque/viscosity, which results in 3rd term in Equation 5 having torque units. Non-negativity and boundedness [73] provide higher quality solutions. After this, the upper and lower bounds of 0 and 1 (no diffusant) are applied by normalizing the viscosity with respect to the initial viscosity.

4.3. TIKHONOV REGULARIZATION

The success of Tikhonov regularization depends on making a good choice of λ, and suffers from a drawback that the the optimal λ is usually not obvious [75, 76]. The optimal value of λ should result in the smallest computed relative error: $| x^{\lambda} - x^{exact} |$ when the exact solution is known, where x is the set of unknown complex viscosity profiles. In general, this best solution is unknown a priori, thus the flattest slope method is used. The flattest slope [75] provides a mathematically rigorous method to determine the optimal range for λ. A plot of (λ, x^{λ}) exhibits two flat portions, which are insensitive to the value of λ (Figure 4.2). An optimal range for λ is expected to fall in the region separating the left and right flat portions of the (λ, x^{λ}) curve. We study the behavior of this curve using simulated data sets from Fickian and Non-Fickian profiles as well as experimental data.

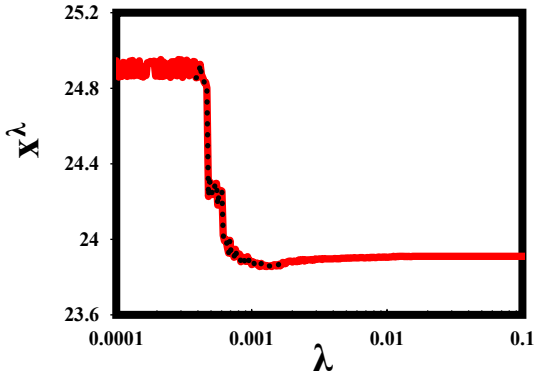

Figure 4.2. Sample plot of (λ, x_{λ}) for the Fickian case (Refer to Fig. 4.3). Diffusion parameters: $D = 3.1 \cdot 10^{-4}$ mm² / s, A = 0.037 and B = 0.24. Simulation parameters: Δt = 1000 s, Δr = 0.05mm, and k = 2. The solid black points represent the sensitive region where the range of optimal λ values lie.

Virtual Experiments

A finite amount of diffusant is initially distributed uniformly through a thin cylinder of radius a, and there is no flow of diffusant leaving the system through the outer rim. The following boundary and initial conditions apply (Eq. 7):

$$\mathbf{C = C_0} \quad \mathbf{at} \quad \mathbf{0 < r < a,} \quad \mathbf{t = 0}$$

$$\mathbf{C = 0} \quad \mathbf{at} \quad \mathbf{a < r < \infty,} \quad \mathbf{t = 0}$$

$$\mathbf{C = 0} \quad \mathbf{at} \quad \mathbf{r = \infty,} \quad \mathbf{t \geq 0} \qquad \mathbf{(7)}$$

Fickian and non-Fickian diffusion equations are then solved to determine theoretical concentration profiles for one-dimensional radial diffusion [79]. Diffusion is of Fickian type [78] when the interface quickly spreads according to the free-diffusion exponent of ½. Fickian diffusion is often observed well above the glass transition temperature. The polymer relaxation rate is faster than the solvent diffusion rate, its concentration decreases exponentially and a large penetration gradient is observed [79]. In solvent-polymer diffusion well above the glass transition, the concentration profile is obtained by solving a Fickian diffusion equation:

$$\frac{\partial \psi_A}{\partial t} = \nabla J_A = -\nabla^2 (D \cdot \psi_A) \qquad \mathbf{(8)}$$

For Non-Fickian diffusion, typical of polymer-polymer interdiffusion, the materials do not interdiffuse freely, and an interface zone separates them [80]. In this case, the interdiffusion exponent is considerably smaller than the Fickian type exponent, the two polymers partially mix and the initial sharp interface slowly broadens [81]. The type of diffusion behavior is strongly dependent on both host polymer and diffusing species [82, 83].

Polymer-polymer diffusion is usually described using the mean-field theory and a free energy mixing function [80]. The volume of the system does not change during interdiffusion, and this free energy function describes chain interaction and entropy, based on a Flory-Huggins approach. Each polymer rearranges and repels unfamiliar chains across the interface, the two polymers do not freely and completely mix, and the diffusion mechanism is different from free (or Fickian) diffusion [81]. In the case of Non-Fickian solvent-polymer diffusion and polymer-polymer interdiffusion, the diffusion flux

is a non-linear function of the chemical potential [80], and the concentration profile is obtained by solving a non-Fickian diffusion equation:

$$\frac{\partial \psi_A}{\partial t} = \nabla \mathbf{J_A} = -\nabla(\Lambda_\psi \cdot \nabla \mu) \quad \textbf{(9)}$$

Here, Λ_ψ is a mutual mobility coefficient that depends on composition, and μ is the chemical potential, which represents local changes in the free energy of this closed system, with respect to changes in composition.

In the first case, we start with Fick's 2nd law (Eq. 10) in a semi-infinite medium, the Fickian concentration profile [20] satisfying Fick's 2nd law and the boundary conditions above is given by Eq. 11:

$$\frac{1}{r} \cdot \frac{\partial}{\partial r}\left(r \cdot \frac{\partial C}{\partial r}\right) = \frac{1}{D} \cdot \frac{\partial C}{\partial t} \quad \textbf{(10)}$$

$$\frac{C_{(r,t)}}{C_0} = \frac{1}{2Dt} \cdot e^{-\frac{r^2}{4Dt}} \cdot \int_0^a e^{-\frac{\acute{r}^2}{4Dt}} \cdot I_0\left(\frac{r\acute{r}}{2Dt}\right) \cdot \acute{r}d\acute{r} \quad \textbf{(11)}$$

where **D** is the diffusion coefficient, and $\mathbf{I_0}$ is the modified Bessel function of 1st kind and of order 0.

In the second case, the composition profile for a two-phase polymer system of similar chemical structure with different molecular weights [84], satisfying conservation of mass and chemical potential [79, 80, 83], as well as the specified boundary conditions is given by Eq. 12:

$$\frac{\partial \psi_A}{\partial t} = \frac{\partial}{\partial x}\left\{\left(\frac{2}{1+R+(R-1)\psi_A}\right) \cdot \left[\left\langle 1 + \frac{1}{R} - \chi_{AB} + \left(\frac{1}{R} - 1\right) \cdot \psi_A + \chi_{AB} \cdot {\psi_A}^2 \right\rangle \cdot \frac{\partial \psi_A}{\partial x} - \frac{\partial^3 \psi_A}{\partial x^3}\right]\right\} \quad \textbf{(12)}$$

Here χ_{AB} is the interaction parameter, R is the molecular weight ratio N_B / N_A, ψ_A is the composition profile, and the factor in front of $\partial\psi_A/\partial x$ is equivalent to the diffusion coefficient [79]. The second term involving $\partial^3\psi_A/\partial x^3$ accounts for an incompatible interface separating two polymers by reducing the gradient steepness [79].

The next step is to relate the concentration profile to the torque. For the Fickian case, this is done by incorporating the Fujita-Kishimoto [84] free volume model (Eq. 13) which describes well the effect of solvent concentration on the viscosity of solutions, provided the polymer is not saturated, and if the volume of the mixture is additive [85]. Free

volume parameters A and B reflect the fractional free volume in the pure polymer, and the contribution of the diffusant to the increase in free volume [84, 86].

$$|\boldsymbol{\eta}^*(\mathbf{r},\ \mathbf{t})| = |\boldsymbol{\eta}_0^*(\mathbf{t_0})| \cdot \mathbf{e}^{-\frac{1}{[\mathbf{A}]+[\mathbf{B}]\cdot\frac{1}{\mathbf{C}_{(\mathbf{r},\mathbf{t})}}}} \quad \textbf{(13)}$$

Here $\eta_0^*(t_0)$ is the initial pure polymer's viscosity, and $C_{(r,t)}$ is the concentration profile obtained from the Fickian case (Eq. 11).

For the non-Fickian case, a non-linear mixing rule [87] is used to describe the effect of composition on the overall viscosity during polymer-polymer interdiffusion (Eq. 12).

$$|\boldsymbol{\eta}^*(\mathbf{r},\ \mathbf{t})| = \left\{\mathbf{w_1}(\mathbf{r},\ \mathbf{t}) \cdot |\boldsymbol{\eta}_1^*|^{(1/3.4)} + [\mathbf{1} - \mathbf{w_1}(\mathbf{r},\ \mathbf{t})] \cdot |\boldsymbol{\eta}_2^*|^{(1/3.4)}\right\}^{3.4} \quad \textbf{(14)}$$

Here η_1^* and η_2^* are the pure polymers viscosities, and $w_{1(r,\,t)}$ is the weight fraction of the inner polymer, which is related using Eq. 14, to the composition profile for the non-Fickian case in Eq. 11.

$$\mathbf{w_1}(\mathbf{r},\ \mathbf{t}) = \frac{\mathbf{C_1}(\mathbf{r},\ \mathbf{t})}{\mathbf{C_1}(\mathbf{r},\ \mathbf{t}) + \mathbf{C_2}(\mathbf{r},\ \mathbf{t})} \quad \textbf{(15)}$$

A relationship between the concentration profile and the torque (Eq. 16), can essentially be obtained from the free-volume theory by substituting Eq. 11 for the Fickian case, or from the mixing rule by substituting Eq. 12 for the non-Fickian case, in the SAOS flow integral (Eq. 1).

$$|\mathbf{T_{Theo}}(\mathbf{t})| = \boldsymbol{\beta} \cdot \left[\int_{\mathbf{a}}^{\mathbf{b}} |\boldsymbol{\eta}^*(\mathbf{r},\ \mathbf{t})| \cdot \mathbf{r^3} \cdot \mathbf{dr}\right] \quad \textbf{(16)}$$

This relationship is used to simulate experimental torque data, the set of measured torque T_i^M is replaced with T_i^{Theo}, and the numerical procedure explained previously is applied.

We next look at simulated Fickian concentration profiles using Eq. 11 with the diffusion coefficient set to $D = 3.1 \cdot 10^{-4}$ mm² / s. In Figure 4.3(a), concentration profiles (for k = b / a = 2, with b = 12.5mm) are plotted using a time step of 1000s with a radial step size of 0.05mm. A random additive noise [71, 77] ranging from 1% to 4% is applied to all concentration profiles. Figure 4.3(b) shows viscosity profiles obtained using concentration profiles in Figure 4.3(a), and the free volume theory Eq. 13, with A = 0.037 and B = 0.24. We have chosen these values as they are appropriate for trichlorobenzene

diffusing in molten polystyrene at 190°C which we have previously studied experimentally [60]. We can also see in Figure 4.3(c), the resulting theoretical torque, using viscosity profiles in Figure 4.3(b) and Eq. 16. The inversion procedure is applied on this set of theoretical torque data, which provides means to evaluate our approach, since the exact solution is known in this case. In the Appendices, we present a second simulated Fickian case with the diffusion coefficient set to $D = 1.1 \cdot 10^{-3}$ mm² / s. A plot of (λ, x^{λ}) and (λ, e_r^{λ}) for this case is shown in Figure A4.1. Regularized and exact viscosity profiles are shown in Figure A4.2, and the corresponding normalized interface width is plotted as a function of time in Figure A4.3.

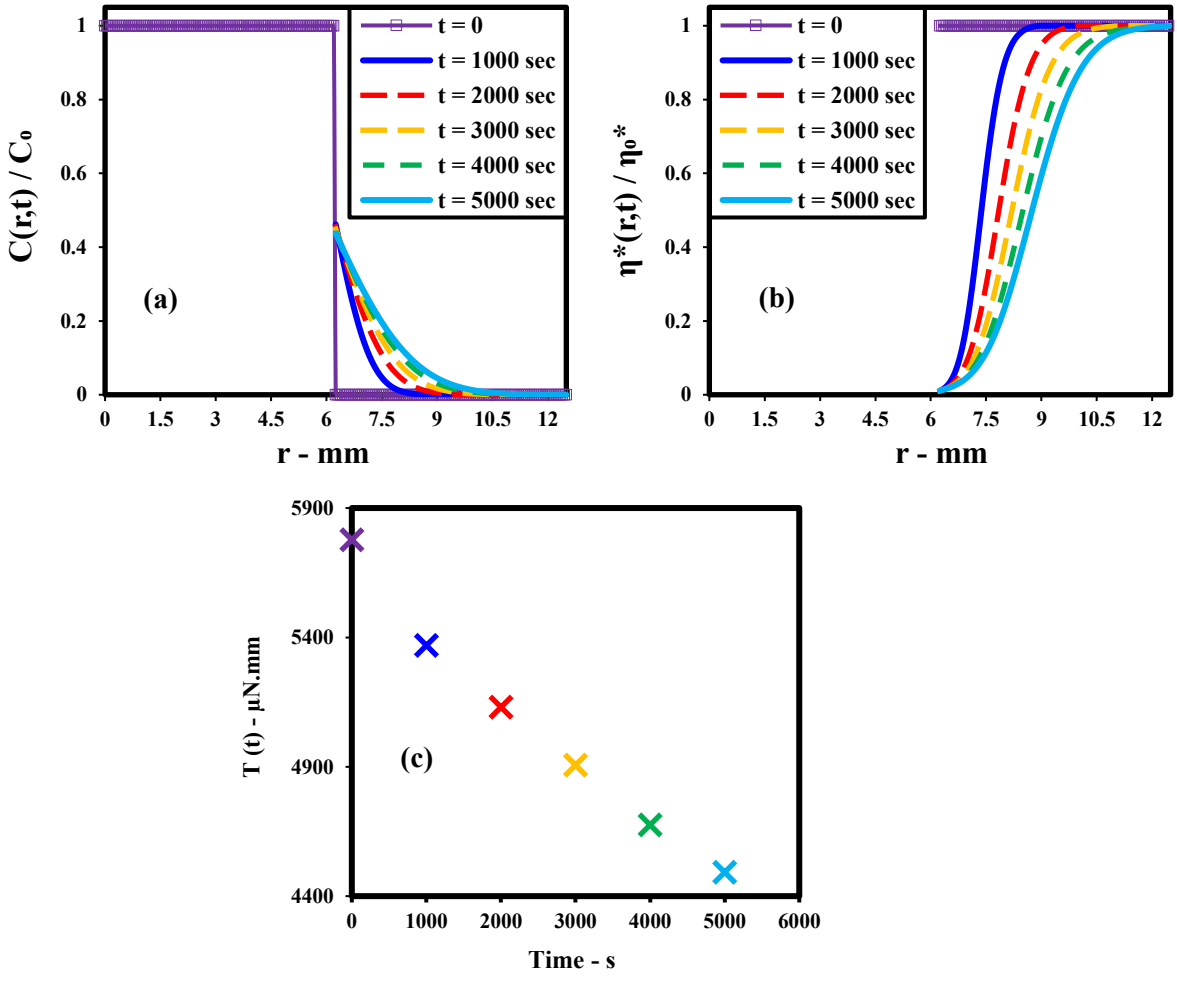

Figure 4.3. Simulated Fickian data with $D = 3.1 \cdot 10^{-4}$ mm² / s, $\Delta t = 1000$s, $\Delta r = 0.05$mm, and k = 2. (a) Concentration profile (Eq. 11); (b) Viscosity profile (Eq. 13); (c) Torque Profile (Eq. 16).

Next we consider the non-Fickian case where the factor in front of $\partial\psi_A/\partial x$ in Eq. (12) describes the diffusion coefficient, with an N^{-2} dependence in accordance with the reputation [86] model (Eq. 17):

$$\boldsymbol{D} \cong \frac{\boldsymbol{R}}{\boldsymbol{N_B^2/m_0}} \qquad \textbf{(17)}$$

Here R is the molecular weight ratio N_B / N_A, and m_0 is the monomer molecular weight [85]. In Figure 4.3(a), non-Fickian concentration profiles using Eq. 12 (with k = b / a = 2, R = 4, and χ_{AB} = 1) are plotted for a time step of 20000s. Figure 4.3(b) shows viscosity profiles obtained using the composition profiles and the non-linear mixing rule [87] (Eq. 14) with η_1^*=500 Pa.s and η_2^*=50 000 Pa.s. Figure 4.3(c) shows the resulting theoretical torque as a function of time using Eq. 16, for this non-Fickian case.

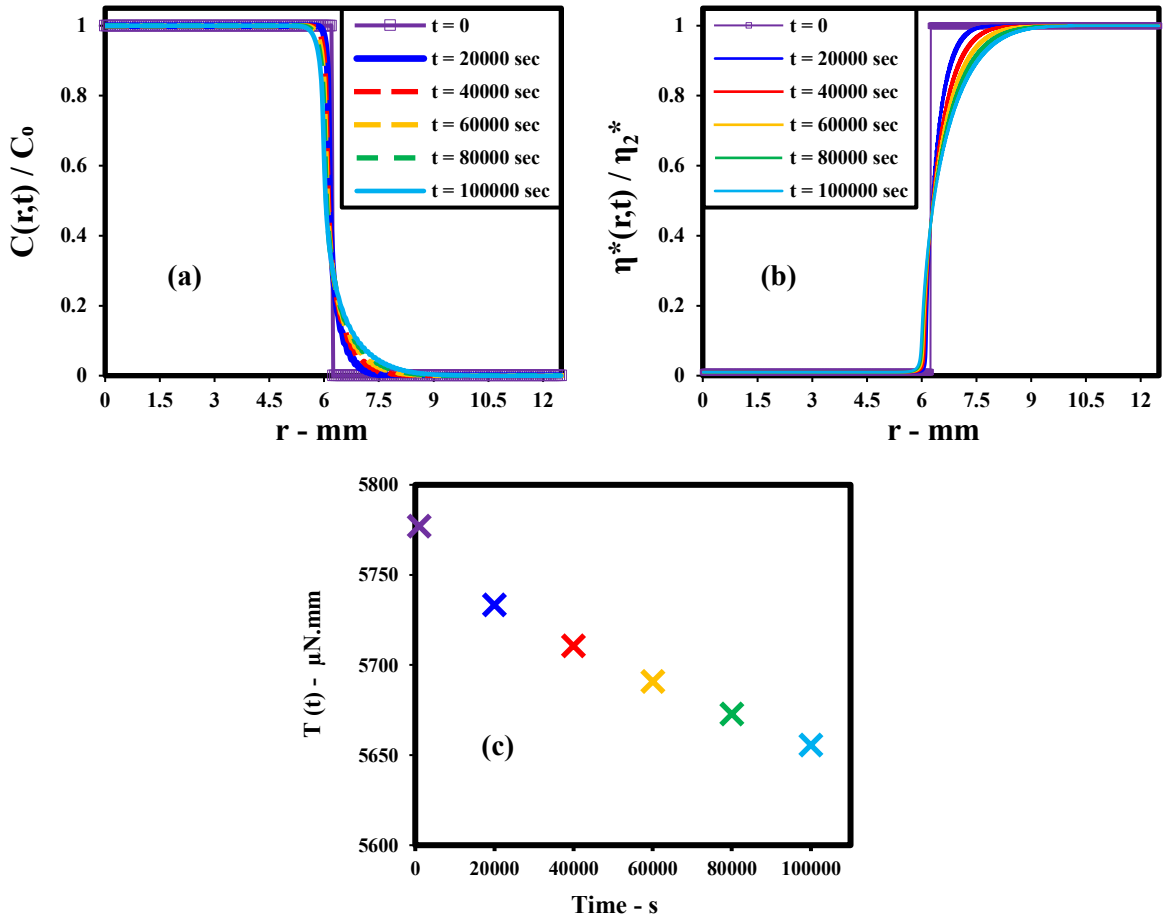

Figure 4.4. Simulated non-Fickian data with R = 4, χ_{AB} = 1, η_1^*=500 Pa.s and η_2^*=50 000 Pa.s, Δt = 20 000s, Δr = 0.05 mm, and k = 2. (a) Concentration profile (Eq. 12); (b) Viscosity profile (Eq. 14); (c) Torque Profile (Eq. 16).

Experimental techniques to study diffusion are often limited to a particular choice of system [66] and experimental conditions [67]. Some of these techniques may be restricted to solvent-polymer [71] or polymer-polymer [66] systems, and are likely to be constrained by a narrow range of experimental temperatures. Diffusion data at elevated temperatures are often extrapolated from limited data at low temperatures, which can result in orders of magnitudes of errors. Our experimental technique [65] to measure diffusion is versatile, and is based on rheological measurements under SAOS flow. Such measurements present an advantage over other experimental techniques, they are reliable and repeatable for a wide range of diffusion systems and experimental conditions. Various aspects of diffusion and interdiffusion may be experimentally studied, and data from a wide range of solvent-polymer and polymer-polymer systems can be obtained, and at various experimental temperatures and frequencies. Our numerical procedure can then be applied to a wide range of experimental data, and is thus useful in determining diffusion properties for a variety of diffusion systems and experimental conditions.

4.4. NUMERICAL RESULTS

4.4.1. The Flattest Slope Method

The graphs in Figure 4.5. are plots of (λ, x^{λ}) and (λ, e_r^{λ}), for the Fickian case (Figure 4.5(a)) and the non-Fickian case (Figure 4.5(b)). Both are the result of solving Eq. 5 for a wide range of λ values, and the solution norm x^{λ} and relative errors e_r^{λ} are recorded at each iteration. We show on the same plot, the average relative error (λ, $| x_i^{\lambda} - x_i^{exact} |$) as a percent of x^{exact}. We observe that in both problems, the range of λ shown as solid black points on the (λ, x^{λ}) curve, coincides with the range where relative errors are smallest on the (λ, e_r^{λ}) curve. This observation is made by comparing regularized and exact solutions, and confirms the robustness of the flattest slope method in determining the optimal λ range, without a priori knowledge of the exact solution [75]. This region represents the optimal λ range where the most accurate viscosity profiles can be retrieved from the torque data. From Figure 4.5, the optimal range for λ is 0.001 - 0.002 for both Fickian

and non-Fickian cases. The performance of our approach is next discussed, and in all cases regularized and exact solutions are a close match.

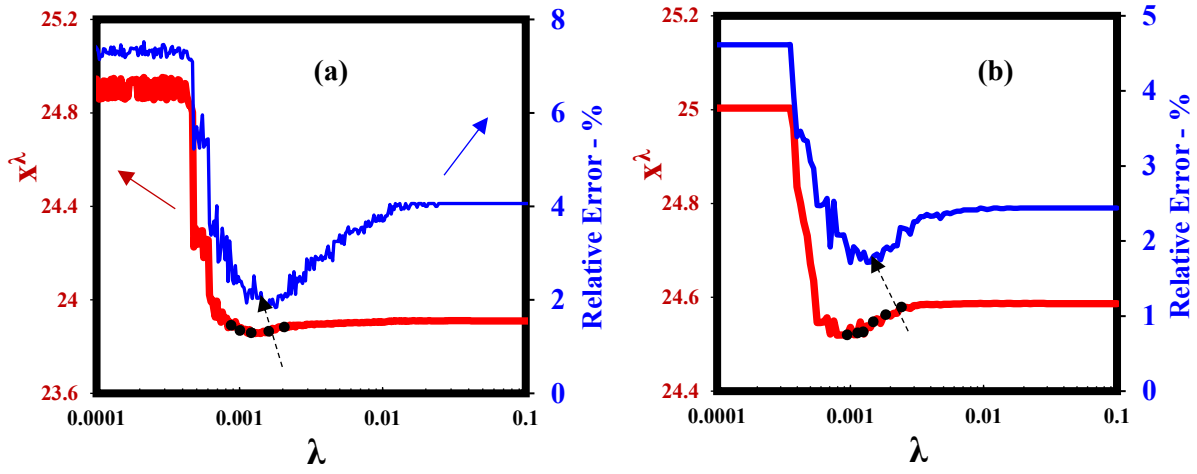

Figure 4.5. Plot of (λ, x^{λ}) and (λ, e_r^{λ}): (a) Fickian case with $D = 3.1 \cdot 10^{-4}$ mm² / s, A = 0.037 and B = 0.24. (b) Non-Fickian case with R = 4, $\chi_{AB} = 1$, η_1^*=500 Pa.s and η_2^*=50 000 Pa.s. Black solid points represent the trust region with the range of optimal λ values lying towards the right insensitive region.

4.4.2. The Regularized Solutions

Given torque-time data, the numerical solution of this inverse problem represents the local radial viscosity profiles as a function of time, which best match simulated torque data. The flattest slope method and regularized solutions [75] are applied using MATLAB [89] and its optimization toolbox [87, 90]. Constrained minimization as previously explained is applied using the Sequential Quadratic Programming algorithm, with an optimality tolerance of 10^{-9}. The number of spatial points per time step is 125, with 6 time steps for both Fickian and non-Fickian (a total of 750 unknown variables). Regularized solutions obtained within the optimal region for λ are smoothed using a smoothing parameter α, which is directly related to the slope of the torque dT/dt. The lower and upper bounds of regularized solutions are 0 and 100% (no diffusant), and complex viscosity profiles are expected to decrease from an initial Heaviside step condition [78].

Table 4.1 gives radial errors per time step (relative errors with respect to x^{exact}) for this optimal range of λ and for both diffusion cases, as well as the overall residual error for

the 6 time steps explored in each case. Table 4.1 confirms that our numerical procedure allows for an accurate determination of radial complex viscosity profiles across a thin polymeric ring, undergoing diffusion (or interdiffusion) under SAOS flow with constant flow parameters.

Table 4.1. Radial relative errors for the optimal range of regularization parameter λ. An overall error of less than 1.5% is observed for both Fickian and non-Fickian cases.

Time - s	**Fickian Case**	**Time - s**	**Non-Fickian Case**
0	0%	0	0%
1000	0.80%	20 000	0.50%
2000	0.90%	40 000	0.75%
3000	1.50%	60 000	0.79%
4000	2.50%	80 000	0.76%
5000	1.80%	100 000	0.91%
Average	**1.25%**	**Average**	**0.61%**

Figures 4.6 and 4.7 show the robustness of our procedure in effectively recovering radial viscosity profiles from torque data. Viscosity profiles can be used to determine the interface spread rate as a function of time [91], which ultimately contains the information on the diffusion type and coefficient [80, 83]. In all cases reported, radial viscosity profiles recovered from the regularization method are a very close match with the exact solution indicating the effectiveness of Tikonov regularization combined with the flattest slope method [75] and the smoothing procedure.

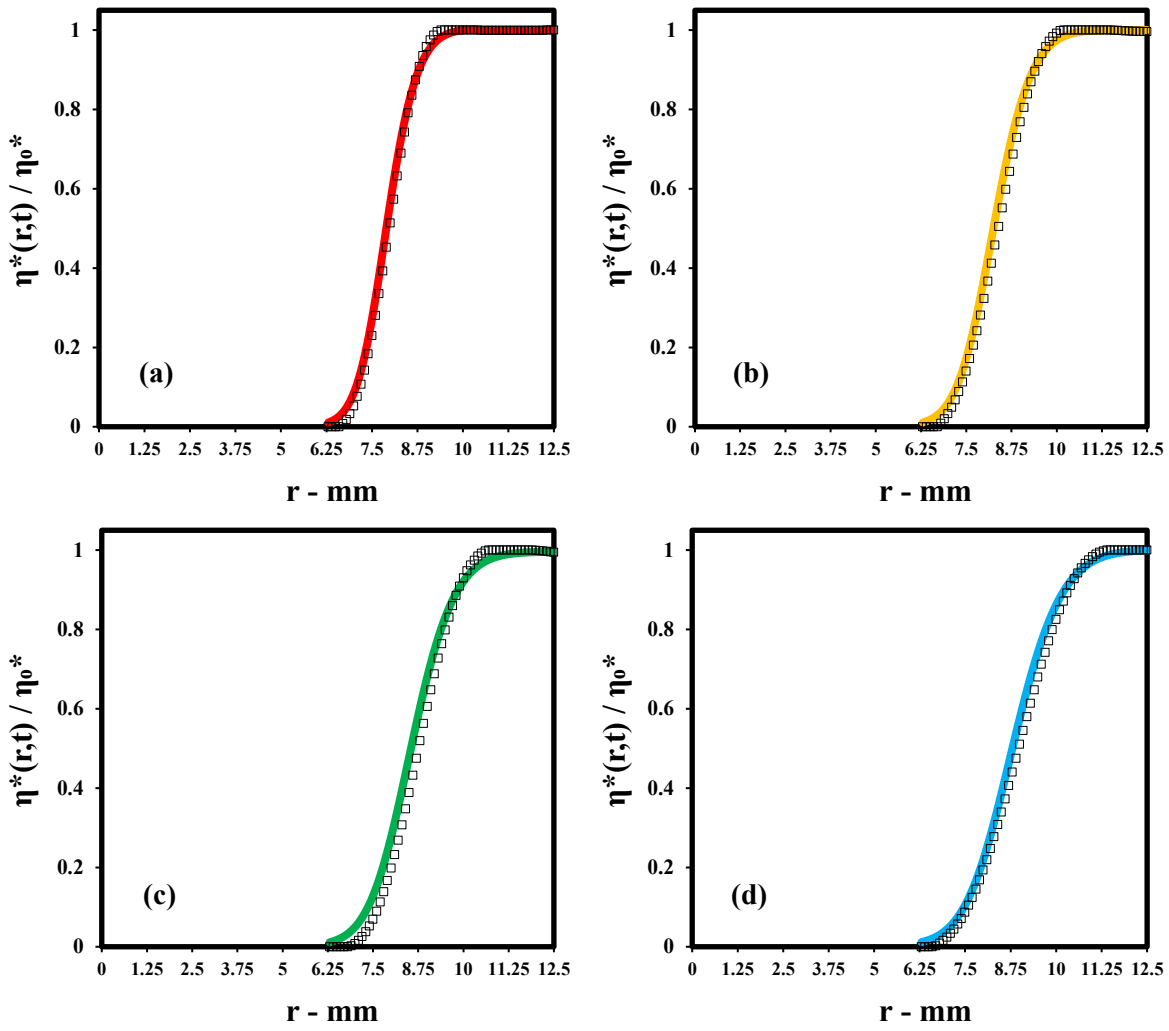

Figure 4.6. Simulated data and regularized viscosity profiles for Fickian diffusion. (a) Concentration profile (Discrete points are the regularized solutions and the continuous curve is the exact solution). (a) t = 2000s; (b) t = 3000s; (c) t = 4000s; (d) t = 5000s. Diffusion parameters: $D = 3.1 \cdot 10^{-4}$ mm² / s, A = 0.037 and B = 0.24, with Δr = 0.05mm and k = 2.

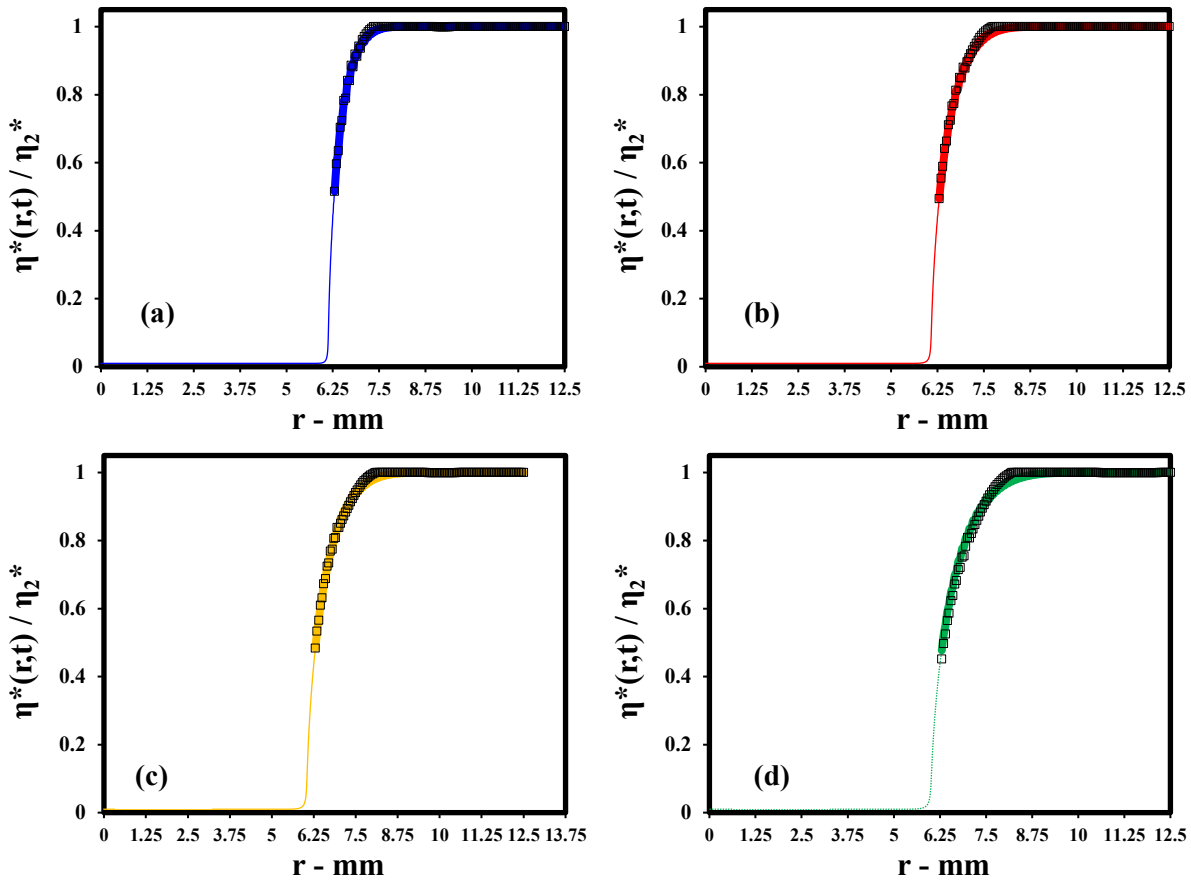

Figure 4.7. Simulated data and regularized viscosity profiles for non-Fickian diffusion. Discrete points are the regularized data and the continuous curve is the exact solution. (a) t = 20 000s; (b) t = 40 000s; (c) t = 60 000s; (d) t = 80 000s. Diffusion parameters: R = 4, χ_{AB} = 1, η_1^*=500 Pa.s and η_2^*=50 000 Pa.s, with Δr = 0.05mm, and k = 2.

4.5. RESULTS AND DISCUSSION

4.5.1. The Interface Width

We define the interface width, W(t), as the distance separating the pure polymer region from the pure diffusant region [79, 83, 89]. The diffusion type can be characterized using the time dependency of the interface width [80], and an estimate of the diffusion type and coefficient for each case can then be obtained. Figure 4.8 shows the normalized interface width as a function of time, obtained from the regularized viscosity profiles, for both the Fickian and non-Fickian cases. The interface width increases slower for the non-Fickian case than for the Fickian process. In the case of non-Fickian diffusion, Figure 4.8 shows

that the interface width increases faster at short time and levels off at sufficiently long times. In both cases, W(t) is well represented by a power model, $W(t)/(b-a) = D_0 \cdot t^n$. Fitted values of n are 0.5092 and 0.3162 and the values of D_0 are 0.0116 $1/s^{0.509}$ and 0.00148 $1/s^{0.316}$ for the Fickian and non-Fickian case respectively.

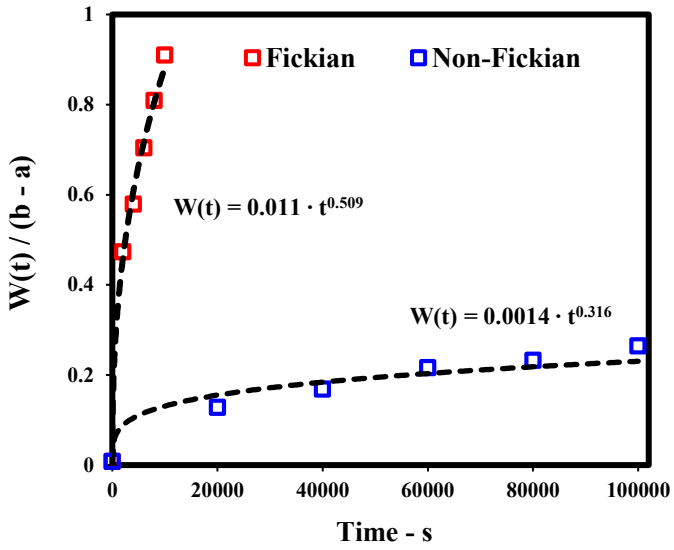

Figure 4.8. Normalized interface width obtained from regularized viscosity profiles of Fickian and non-Fickian diffusion. Points are values determined from the regularized viscosity profiles. Dashed lines are power law fits. Fickian parameters: D = 3.1 · 10^{-4} mm^2 / s, A = 0.037 and B = 0.24, with Δr = 0.05mm and k = 2.Non-Fickian parameters: R = 4, χ_{AB} = 1, η_1^*=500 Pa.s and η_2^*=50 000 Pa.s, with Δr = 0.05mm, and k = 2.

4.5.2. The Diffusion Coefficient:

For some miscible polymer-polymer systems and many solvent-polymer systems, the interface width increases with time according to the free or Fickian diffusion exponent as $W(t) \propto t^{0.5}$. Partially miscible systems do not follow Fickian transport [79], and an interface zone of finite width separates them at equilibrium [80]. The interface width, W(t) characterizes well the entire transport process [79, 80, 83, 89], and is most sensitive to the local structure of the interface, the temperature, and the molecular weight ratio R. W(t) provides a characterization of asymmetric non-Fickian polymer-polymer interdiffusion (R >>1), as well as for the symmetric Fickian case (R = 1) and solvent-

polymer Fickian diffusion cases. From the power law fit to the W(t) data in Figure 4.8, the diffusion coefficient D can then be estimated using Eq. (18):

$$\mathbf{W(t) \cong D \cdot t^n \cong \frac{D_0}{2\pi \cdot (b-a)^2} \cdot t^n} \quad \textbf{(18)}$$

Similar approaches to the calculation of diffusion coefficients have been extensively used in the literature [82, 78, 92]. Values of D are determined from regularized solutions, and the resulting interface width using the approach explained above. Values of D are listed in Table 4.2 and are compared with D_{exact}. A very small difference is observed and the diffusion coefficient is in agreement with the exact value, for each of the three cases studies (two Fickian and one non-Fickian).

Table 4.2. Comparison of exact diffusion coefficients and coefficients from the interface width of regularized solutions. The relative error is less than 5% for both Fickian and non-Fickian coefficients.

	Fickian	**Non-Fickian**	**Fickian (S.I)**
D_0 $(1/s^n)$	0.0116	0.00148	0.2827
D (mm^2/s)	$2.95 \cdot 10^{-4}$	$3.77 \cdot 10^{-5}$	$1.15 \cdot 10^{-3}$
D_{exact} (mm^2/s)	$3.1 \cdot 10^{-4}$	$3.65 \cdot 10^{-5}$	$1.10 \cdot 10^{-3}$

4.5.3. Applicability to Experimental Data:

Previously [65] we have studied the diffusion of 1, 2, 4-trichlorobenzene (TCB) in a commercial grade of polystyrene (M_W = 350 kg/mol, M_W / M_N = 2). SAOS measurements were done at 190°C under nitrogen atmosphere, using an Anton-Paar MCR500 rheometer, equipped with parallel plate geometry (25mm diameter). As considered in our simulated experiments, we used polymer specimens in the shape of flat rings, with the solvent in the center hole. The diffusion of TCB through molten polystyrene was studied under SAOS at constant strain amplitude and angular frequency.

The experimental data from ref. 1, with k = 2 and $\omega = 1s^{-1}$ is repeated in Figure 4.9. The effect of diffusion is more pronounced in the early stages of the experiment, and in

this case, the diffusion of TCB well above the polymer's glass transition temperature is Fickian. Using Eq. 11, a least-squared-error forward fitting of Eq. 16 described previously [65] was applied to the experimental torque data. A gradient-based iterative search method [76] was used, with the diffusion coefficient as single adjustable parameter. The diffusion coefficient determined from this forward-fitting procedure is $3.312 \pm 0.015\ 10^{-4}$ mm²/s.

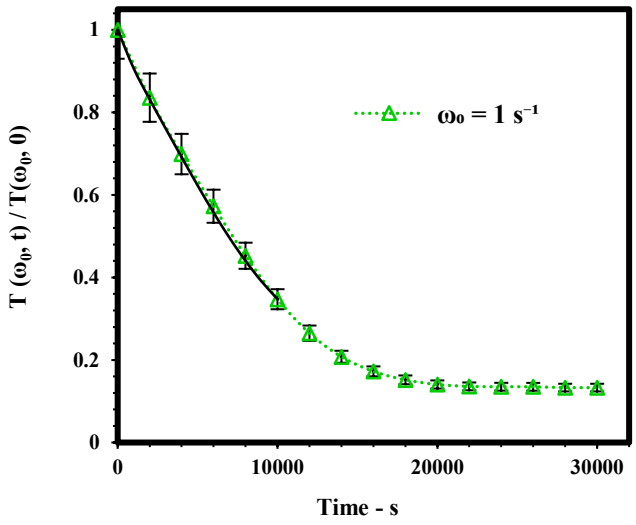

Figure 4.9. Experimental diffusion measurements at 190°C. Normalized torque as a function of time for k = 2, and $\omega_0 = 1s^{-1}$. Error bars are the standard deviation of 6 measurements. Full lines are the fits using Eq. (11) and Eq. (12), with D = 3.312 ± 0.015 (10^{-4} mm² / s), A = 0.037 and B = 0.24.

Next we apply the inverse method developed in this work to our experimental torque data in Figure 4.9. Figure 4.10 shows a plot of (λ, x^{λ}) and (λ, e_r^{λ}) determined from the experimental data. Here, the relative error (λ, e_r^{λ}), is evaluated using the forward fitting results (using Eq. (11) and Eq. (12), with D = 3.312 ± 0.015 (10^{-4} mm² / s), A = 0.037 and B = 0.24) as a percent of x^{Theo} (λ, $| x_i^{\lambda} - x_i^{Theo} |$). We observe again, that the optimal range or value of λ coincides with the range where relative errors are smallest. Figure 4.10 confirms that our numerical procedure can be successfully applied to experimental data for a polymer ring during solvent diffusion under SAOS, without prior knowledge of exact profiles. The overall error observed in Figure 4.10 within the optimal range of λ values, is between 0.8% and 1.5%.

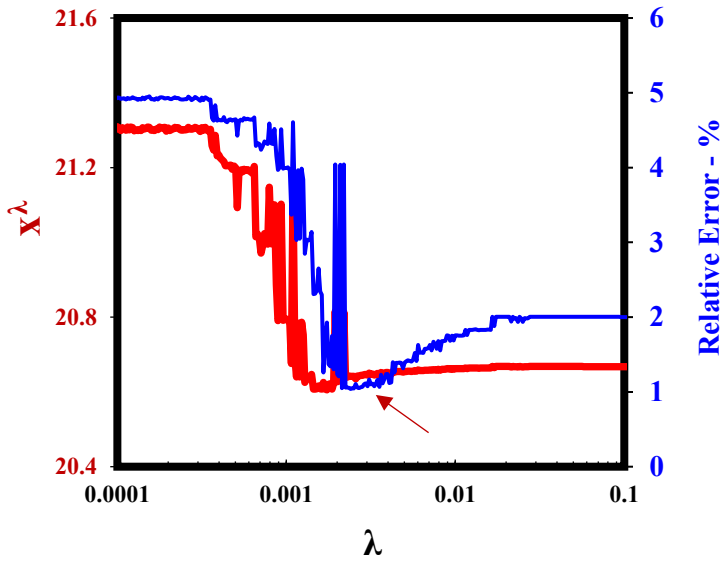

Figure 4.10. Plot of (λ, x^λ) and (λ, e_r^λ) for the experimental torque data at 190°C, for TCB diffusion in molten polystyrene, with $k = 2$ and $\omega_0 = 1 s^{-1}$.

The value of D is determined from regularized solutions using the plot of W(t) in Figure 4.11 and the power model Eq. 18. Discrete points in Figure 4.11 are determined from the regularized solution, and dashed lines are the power model fit that yields the exponent n and pre-exponent D_0. Values of n and D_0 are 0.5086 and 0.01205 respectively, confirming the Fickian nature of the diffusion and yielding an estimate of the diffusion coefficient of $D = 3.183 \cdot 10^{-4}$ mm² / s. This produces a very small difference relative to the diffusion coefficient [63] obtained from the forward analytical approach ($D = 3.312 \pm 0.015\ 10^{-4}$ mm² / s). The robustness of our approach has thus been demonstrated on experimentally measured torque data, as well as virtual experiments with simulated data sets from Fickian and Non-Fickian torque profiles.

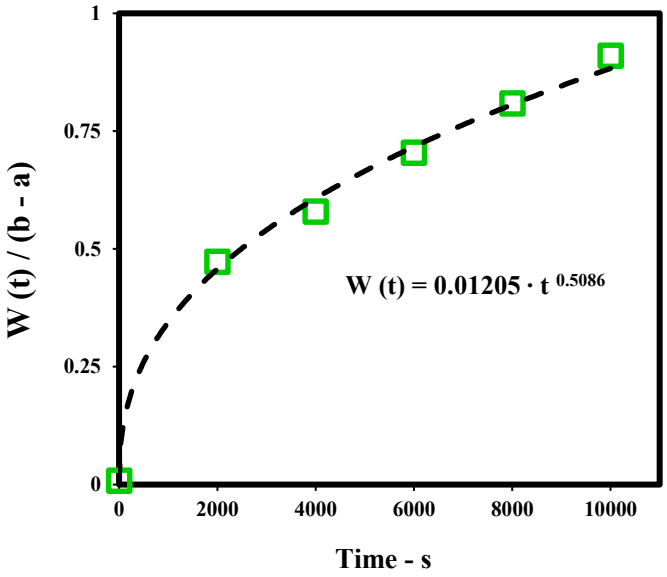

Figure 4.11. Normalized interface width obtained from regularized solutions of experimental diffusion of TCB in PS for k = 2 and $\omega_0 = 1s^{-1}$, at 190°C. The dashed line is the power law fit.

4.6. CONCLUSIONS

A numerical technique for recovering radial viscosity profiles from SAOS torque data is developed. This inverse problem is solved using Tikhonov regularization, which depends on making a good choice of the regularization parameter λ. The flattest slope method is used to locate the optimal value by detecting regions of the solution that are sensitive and insensitive to the choice of λ. We then determine the diffusion coefficient and type from the interface width of recovered profiles, using the linear viscoelastic constitutive equation and a general power law dependency of the diffusion process on time. In all cases studied, we found that the interface width and radial viscosities from regularized solutions are a close match to those of the exact or theoretical solutions, provided λ is rigorously chosen. Additionally, the interface width provides an estimate of the diffusion type and coefficient that are consistent with the exact or theoretical values within 5%. Our results indicate that this numerical technique is effective in determining the diffusion type and coefficient from torque data in SAOS, and provides significant insight into the dynamics of diffusion in molten polymers.

CHAPTER 5

Effect of Temperature on Solvent Diffusion in Molten Polystyrene Under Small Amplitude Oscillatory Shear

ABSTRACT

Diffusion of 1, 2, 4-trichlorobenzene through molten polystyrene is studied under small amplitude oscillatory shear (SAOS) at various temperatures. The torque (or the sum of circumferential stresses) is measured during radial diffusion of the solvent from the center of the sample into a polymeric ring, at constant temperature and frequency. The radial concentration profile can be inferred from experiments by monitoring the torque as a function of time. It is necessary to first determine the concentration-viscosity relationship. This relationship is obtained experimentally from the frequency response of solvent concentrated polymer solutions. The free volume model is then applied to describe the effect of solvent concentration on the polymer complex viscosity. We have previously confirmed that our rheological technique can be used to measure radial diffusion in molten polymers, and obtain a good estimate of the diffusion coefficient. We also found that small amplitude oscillatory shear significantly accelerates the diffusion process. This study investigates this accelerated diffusion kinetics due to SAOS flow as a function of temperature, and confirms that the diffusion rate is increased by oscillatory motion. Temperature has a significant impact on the magnitude of this effect, and the combined temperature-oscillation effect on diffusion is characterized.

5.1. INTRODUCTION

The transport of solvents through molten polymer is a determining factor in several industrial polymer processes [93, 94]. Current challenges in this field include establishing a relationship between diffusion dynamics and polymer structure [95]. In particular, diffusion of solvents in molten polymers remains difficult to measure experimentally [96] although it is relevant in several processing operations [93, 94, 97]. Diffusion coefficients at elevated temperatures are often extrapolated from limited data obtained at low temperatures, which results in orders of magnitudes of errors. Polymer-solvent diffusion data over a wide temperature range is rare, and limited experimental data at elevated temperatures have been published [98, 99], despite its importance in industrial applications.

The free volume theory [100] serves as a method for describing polymer–solvent systems, it is commonly used to correlate the effect of solvent concentration on viscoelastic behavior, and it has been shown to produce good predictions for melt, rubbery and glassy polymer-solvent systems [100] as well as being convenient for use in understanding diffusion [101]. Due to thermal fluctuations, free volume is continuously being redistributed, causing fluctuations in the local density, and allowing for the diffusion of solvent molecules. Fujita and Kishimoto [100] derived an equation analogous to the WLF [24] and Arrhenius equations [101], to determine the concentration-viscosity relationship. In this paper, we use the Fujita-Kishimoto model to describe the viscosity-concentration relationship, and the WLF [24] and Arrhenius models [101] to develop the viscosity-temperature relationship. The combined effects of solvent concentration and temperature must also be determined, using superposition at various temperatures and concentrations.

The effect of temperature on the viscoelasticity of polymer melts is commonly described using the WLF [24] approach rather than the Arrhenius approach, when the temperature is close to the glass transition [101]. The WLF [24] approach also remains applicable to a large number of materials, and is derived directly from the assumption that the free volume is a linearly increasing function of temperature [101]. A comparison

between the two models is not always experimentally possible, and in some cases only slight differences may be observed [101].

Polymers can exhibit pseudo-Fickian, Fickian, anomalous, and case II diffusion, and the type of diffusion behavior observed is strongly dependent on the experimental temperature [102]. In the case of solvent diffusing in a polymer well above its glass transition temperature, the polymer's relaxation rate is fast compared to the solvent, and the behavior is predominantly Fickian [98, 102].

It is of special interest [96, 103] to study the effect of SAOS and frequency on solvent-polymer diffusion, and to determine the diffusion coefficient over a wide temperature range. We have previously shown [96] that small amplitude oscillatory shear accelerates the diffusion of trichlorobenzene in polystyrene at 190°C. Polymer chains assume an equilibrium configuration under SAOS [104], and our goal is to explain how did SAOS alter the diffusion process, and what are the physical factors that lead to a faster diffusion [103, 105]. The diffusion coefficient of solvents in polymers strongly depend on temperature [106], and the primary focus is to determine the diffusion coefficient, and the extent to which SAOS accelerates diffusion when the temperature is varied. The focus is on detecting changes in the diffusion coefficient due to SAOS, and on examining this effect at various temperatures.

We provide a validated method for rheological studies of diffusion in molten polymers, focusing on the characterization of solvent diffusion [96]. This method combines experimental torque measurements in SAOS, a Fickian diffusion model [102], the free volume theory [100] and the theory of linear viscoelasticity [102]. We also provide a numerical method based on Tikhonov regularization [107, 108] for estimating the diffusion coefficient from the measured torque during diffusion, with reasonable accuracy.

5.2. EXPERIMENTAL METHODS

5.2.1. Materials and Sample Preparation

A commercial grade polystyrene (M_w = 350 kg/mol, M_w / M_n = 2) was purchased from Sigma - Aldrich **(**product 441147). The solvent, 1, 2, 4-trichlorobenzene (Acros Organics product 296104) was used as diffusant because of its high boiling point (214ºC). Polymer disks (1.2mm thick and 25mm diameter) for free volume measurements, flat rings (1.2mm thick with an outer diameter of 25mm and an inner diameter of 6.25 or 12.5mm) for diffusion measurements, and square specimens for sorption tests (45 x 45mm x 1.2mm) are all prepared by compression molding [96].

5.2.2. The Sorption Method

Several techniques are commonly used to determine diffusion coefficients in polymer–solvent systems [109, 110]. In this work, diffusion is studied using rheological measurements, as well as direct sorption measurements. Direct sorption involves weighing the uptake of the solvent using a high accuracy electronic balance [111]; this technique has been the source of the great majority of solvent-polymer diffusion data [112, 113]. The polymer is immersed in a solvent bath at a constant temperature, the change in mass of the polymer sample is measured with time and Fick's second law is applied to determine the diffusion coefficient [112]. The use of one dimensional Fick's second law in sorption measurements requires a thin sample, and a temperature below the solvent boiling point to avoid evaporation [112, 113].

A rectangular PS sheet of thickness 2L is immersed in a solvent bath, which diffuses through the faces between -L < x < L. The gain in weight of the PS sample is measured as a function of time, and the amount of solvent which has diffused at time t is given by Eq. (1), where M_∞ is the equilibrium solubility, which may be practically impossible to measure due to polymer dissolution.

$$\frac{M(t)}{M_\infty} = 1 - \frac{8}{\pi^2}\sum_{n=0}^{\infty}\left\{\frac{1}{(2n+1)^2}\right\}\cdot e^{\left[-\frac{Dt}{4L^2}\right]\cdot\pi^2\cdot(2n+1)^2} \quad (1)$$

Values of D for temperatures ranging from 130°C to 190°C are determined from fitting eq. (1) to the experimental sorption data, with the diffusion coefficient as single fitting parameter. Eq. (1) well describes the sorption process, provided the film does not dissolve. For our system at temperatures above 190°C, dissolution may be a limiting factor in the accuracy of this method.

5.2.3. The Rheological Method

Key rheological studies [96, 103, 105] show that SAOS accelerates diffusion, which defines new research directions in diffusion studies using rheological tools. Such measurements are sensitive to changes in composition [104], and we have previously shown that they can be used to capture the diffusion process in molten polymers [96]. SAOS measurements can also explain, why subjecting polymer melts to an oscillatory flow impacts their diffusion mechanism. Relatively few papers have been published on this topic [103, 105]. The focus is on the experimental characterization of diffusion using a parallel disk rheometer in SAOS, which measures the response of a circular sample in terms of torque. This response for a pure polymer is time-independent and the measured torque amplitude is constant. Our rheological technique [96] to measure diffusion experimentally, involves SAOS measurements carried out on a concentric binary specimen as shown in Figure 5.1 (the solvent in the center and the polymer in the outer ring). In this case, the measured torque is time-dependent and reflects the diffusion process.

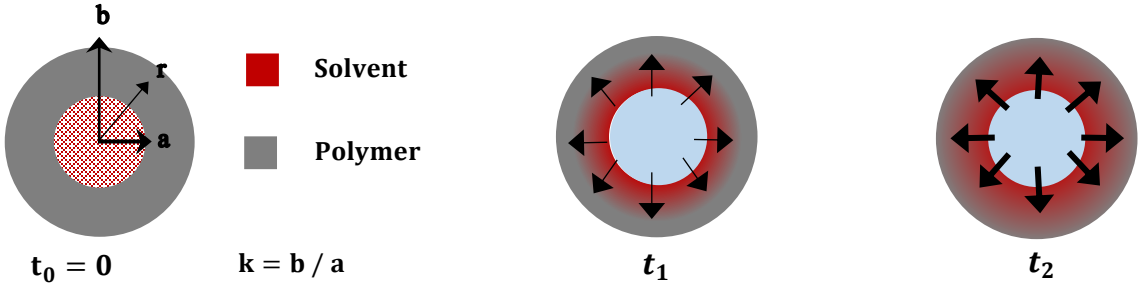

Figure 5.1. Schematic of the binary sample geometry considered in SAOS diffusion measurements. The solvent is dispensed at the center of a polymer ring.

Concentration is uniform in homogeneous solvent-polymer solutions, and the measured torque at constant frequency retains a constant value as a function of time [104]. When carried out on the binary solvent-polymer sample composed of a concentric PS ring with the solvent at the center (as shown in Figure 5.1), torque measurements become dependent on the concentration gradient and profile [96]. In this case, the torque measured at a constant frequency is a function of time and reflects the radial diffusion of the solvent (Eq. 2):

$$\mathbf{T(t) = \beta \cdot \int_a^b [|\, \eta^*(r,t)| \cdot r^3]\, dr = f(t)} \quad \textbf{(2)}$$

$$\boldsymbol{\beta} = \frac{\mathbf{2\pi\omega_0\theta_0}}{\mathbf{H}} \quad \textbf{(3)}$$

In Eq. 2, T (t) is the time-dependent torque, η*(r, t) is the concentration-dependent complex viscosity, b is the outer radius, and a is the inner radius that refers to the radial position of the diffusion interface. In Eq. 3, H is the gap size, θ_0 is the angular displacement, and ω_0 is the oscillation frequency.

5.3. DATA INTERPRETATION TECHNIQUES

5.3.1. Numerical Approach: Tikhonov Regularization

A numerical method [108, 114] based on Tikhonov regularization [115] can be applied, to recover radial viscosity profiles from the measured torque during diffusion under SAOS [116], and to estimate the diffusion coefficient with good accuracy. This inverse problem [115] can be solved using Tikhonov regularization [116], and the flattest slope method [108] is used to locate the optimal value of the regularization parameter λ. We show [114] that radial viscosities recovered from the numerical and theoretical approach are a close match, provided λ is rigorously chosen. Tikhonov regularization finds a weighted least squares solution using the regularization parameter λ and the regularized torque T_i^R (Eq. 4).

$$\mathbf{Min}\ \left|\sum_{i=0}^{t}\left\{T_i^M - T_i^C - T_i^R\right\}\right|^2 \quad \textbf{(4)}$$

The superscript M in Eq. 4 is used to denote the experimentally measured torque, and the superscript C is used to distinguish the computed torque T_i^C from its experimentally measured counterpart. In discretized form, T_i^C is given by Eq.5, and T_i^R by Eq. 6:

$$\mathbf{T_i^C = \beta \cdot \sum_{j=a}^{b} \eta^*(r_j, t_i) \cdot r_j^3 \cdot \alpha_j \cdot \Delta r} \quad \textbf{(5)}$$

$$\mathbf{T_i^R = \lambda \cdot \sum_{j=a}^{b} \eta^*(r_j, t_i)} \quad \textbf{(6)}$$

In Eq. 5, α_j are radial integration coefficients, which depend on the choice of discretization method, and $\eta^*(r_j, t_i)$ is the set of unknown complex viscosity profiles to be recovered from T_i^M.

5.3.2. Theoretical Approach: Free Volume Theory

The free volume theory [100] accounts for the contribution of solvent to the increase in free volume, and describes the effect of solvent concentration on the complex viscosity of a molten polymer. In combination with eq. (2), the free volume theory allows us to define a relationship between concentration, and measured torque eq. (7).

$$\mathbf{\frac{T(t)}{T(0)} = \frac{4}{R^4} \cdot \int_a^b \left[e^{-\frac{1}{A + B \cdot \frac{1}{C(r,t)}}} \right] \cdot r^3 \cdot dr} \quad \textbf{(7)}$$

where A, B are the free volume parameters, which are determined from a separate experiment. The complex viscosity of homogeneous solvent polymer solutions at different concentrations are obtained experimentally, from which concentration shift factors (a_C and b_C) are determined. The free volume theory is applied to these results, and is used to identify the free volume parameters A and B. A Fickian profile [102] determined by solving the diffusion equation with the appropriate boundary and initial conditions [94], is used for concentration (Eq.8):

$$\mathbf{\frac{C_{(r,t)}}{C_0} = \frac{1}{2Dt} \cdot e^{-\frac{r^2}{4Dt}} \cdot \int_0^a e^{-\frac{\acute{r}^2}{4Dt}} \cdot I_0\left(\frac{r\acute{r}}{2Dt}\right) \cdot \acute{r} d\acute{r}} \quad \textbf{(8)}$$

where D is the diffusion coefficient, and I_0 is the modified Bessel function of 1st kind and of order 0.

PS rings contain a small volume of solvent relative to the sample volume. In other words, the concentration tends to zero at the outer rim at all times [102]. This boundary condition is such as no concentration changes reach the outer rim during the time of the experiment. In some instances, small concentration changes do reach the outer rim [96], and this boundary condition fails, which limits the accuracy of the analytical solution at long times. Our results confirm that both the numerical and theoretical approach are effective in determining the diffusion coefficient from torque data at various temperatures, which provides insight into the observed effect of SAOS on diffusion [96].

To clarify this effect, continuous and intermittent experiments are performed [96] at temperatures from 130°C to 210°C. In continuous experiments shown in Figure 5.2, the sample is subjected to oscillations during the entire diffusion test. In intermittent experiments, oscillations are applied for short cycles intermittently with long rest periods, where no flow is applied. We have previously shown [96] that SAOS accelerates diffusion of TCB in molten PS at 190°C and that longer rest periods decrease this acceleration effect. The focus is thus on examining the effect of SAOS and frequency at various temperatures.

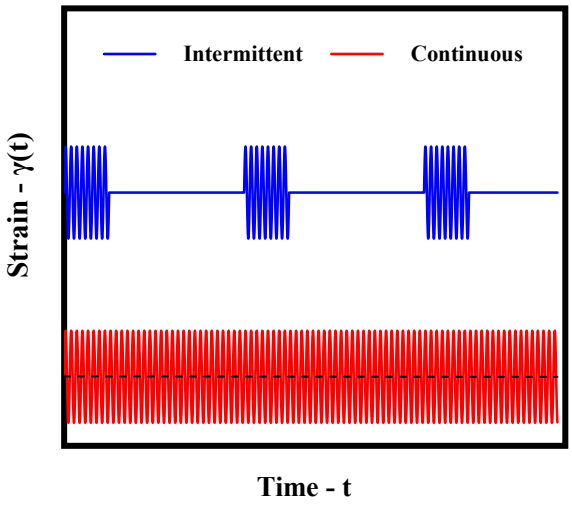

Figure 5.2. Schematic illustration of strain histories in intermittent-type oscillation experiments compared with continuous-type oscillation experiments. Intermittent oscillations are applied for 100s followed by rest stages of 1000s and 10000s.

5.4. EXPERIMENTAL RESULTS

5.4.1. Sorption Measurements:

Sorption measurements [110] directly follow mass changes with time, they are commonly used [112] and yield valuable information about the diffusion process and its temperature dependence, without having to carry out difficult measurements [113]. Figure 5.3. shows the normalized mass uptake of 1,2,4-TCB diffusing in molten PS as a function of time, for temperatures ranging from 130°C to 190°C, and the values of D determined from the best fit of Eq. (1) to the data in Figure 5.3. Two factors limit the accuracy of this approach in determining the diffusion coefficient: the dissolution of PS at high temperatures (190°C and 210°C), and the determination of the equilibrium solubility M_∞.

The sorption method may capture the diffusion mechanism to reasonable extent, but diffusion coefficients can be determined with better accuracy from a number of other methods [99, 110], including the rheological approach [96, 103, 105]. Results in Figure 5.3 are then used to validate diffusion coefficients obtained from rheological measurements.

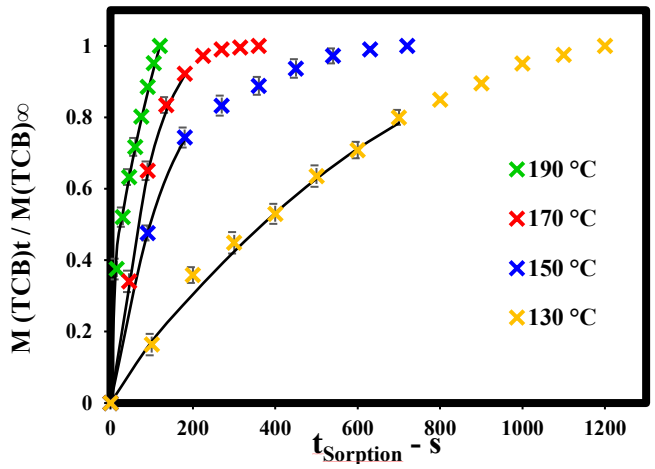

T (°C)	D (10^{-5} mm²/s
130	0.057
150	0.420
170	3.624
190	15.57
210	(31.68)*

Figure 5.3. Mass uptake measurements at 130°C, 150°C, 170°C, 190°C. Sorption plots for the TCB|PS system. Error bars represent an average of 6 experiments, and the curve represents Eq. (1) with the diffusion coefficient as single fitting parameter.

* Extrapolation from data at lower temperatures for 210 °C, using the Arrhenius model and Figure 5.

The values of the diffusion coefficient are expected to have a strong temperature dependence, which can be expressed through an Arrhenius model (Eq. 9):

$$\mathbf{D(T) = D_0 \cdot e^{\left[-\frac{E_A}{RT}\right]}} \quad \textbf{(9)}$$

where D_0 is the diffusion coefficient at an infinitely high temperature, E_A is the activation energy (kJ/mol), R is the universal gas constant (8.31 10^{-3} kJ/mol.K) and T is the temperature (K). In the Arrhenius plot (Figure 5.4), the activation energy E_A and the pre-exponent D_0 can be calculated from the slope and intercept.

Figure 5.4 shows the Arrhenius plot (ln (D) vs. 1/T) for the sorption data from the diffusion of 1,2,4-TCB in molten PS. The diffusion activation energy from the Arrhenius fit to sorption measurements is $E_A \approx 127$ kJ/mol.

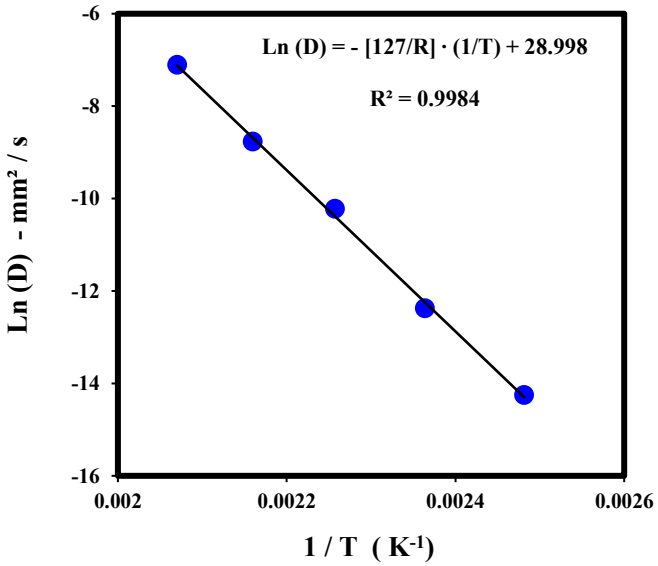

Figure 5.4. Effect of temperature on the diffusion coefficient from Sorption Measurements. Arrhenius plot of ln (D) vs. 1/T for TCB diffusion in PS, with $E_A \approx 127$ kJ/mol.

5.4.2. Rheological Measurements:

Characterization of Homogeneous Systems:

Free volume parameters (A and B) in Eq. 7 are determined first from the linear viscoelastic frequency response of neat PS and homogeneous solvent-polymer solutions at different concentrations. In Figure A5.1 in the Appendices, the storage and loss moduli for neat PS are plotted against frequency for the five temperatures studied. The relaxation spectrum H (λ) and relaxation times λ are calculated from this oscillatory data for each temperature, using a nonlinear Tikhonov regularization method and a software developed by the Freiburg Materials Research Center [117]. Figure 5.5 shows the weighted relaxation spectra, λ·H(λ), normalized and plotted against relaxation times λ.

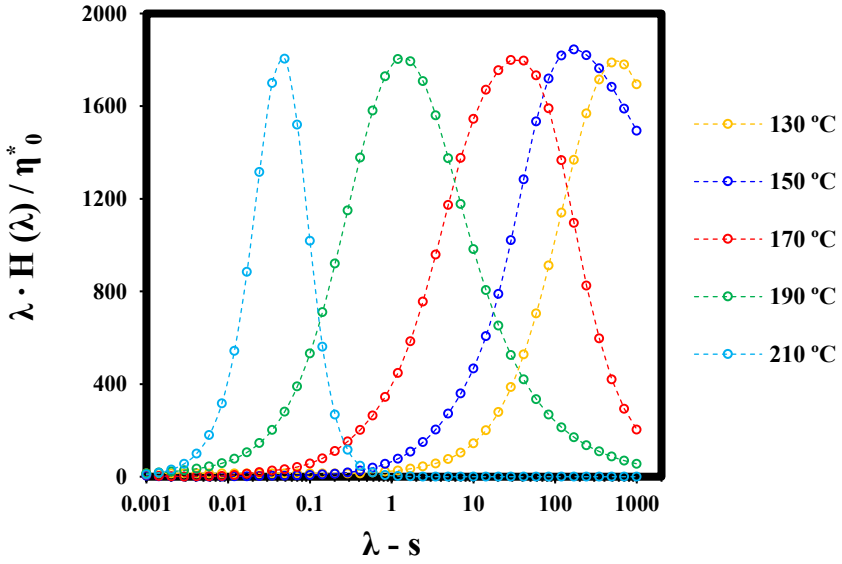

Figure 5.5. Normalized LVE relaxation spectra of neat PS with a strain amplitude γ_0 = 4% at 130°C, 150°C, 170°C, 190°C, and 210°C.

In Figure A5.2 (a)-(e) in the Appendices, the complex viscosity of homogeneous solvent-polymer solutions at several concentrations are shown, from which the concentration shift factors (a_C and b_C) are determined rigorously [96] and at each temperature. In practice, shift factors are determined sequentially, first the concentration effect and second the temperature effect. Combined we shift the complex viscosity curve vertically by ($[a_T \cdot b_T] \cdot [a_C \cdot b_C]$) and horizontally by ($[a_T \cdot a_C]$.

Figure 5.6(a) shows a master curve for each temperature using frequency-concentration superposition, and Figure 5.6(b) shows a single master curve using frequency-temperature superposition as well as frequency-concentration superposition.

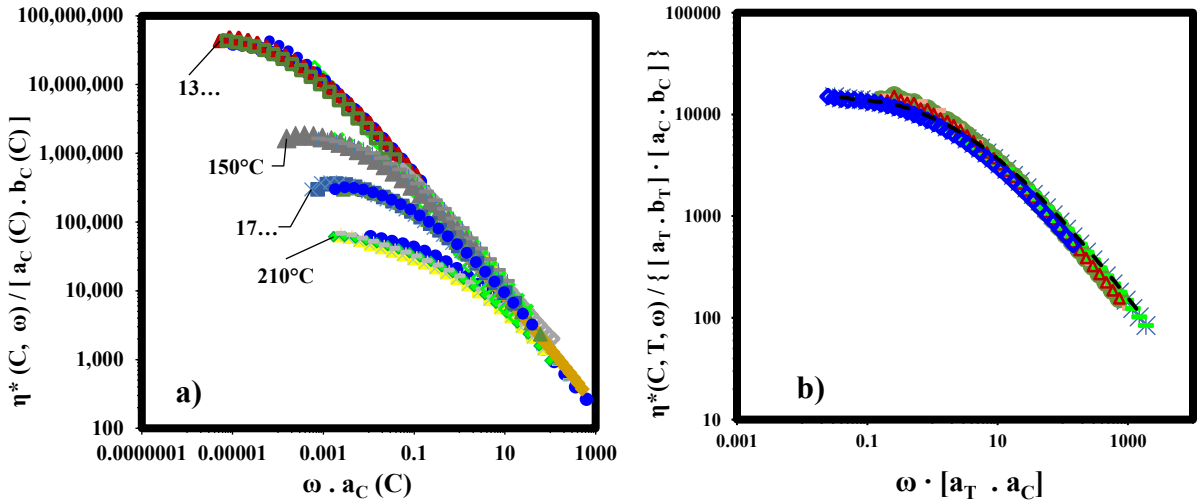

Figure 5.6. Experimental Data is obtained for samples from homogeneous solutions with 60wt% to 93.75wt% polymer. (a) Frequency-concentration master curves at 130°C, 150°C, 170°C, 190°C and 210°C; (b) Combined concentration-temperature master curve.

The concentration modulus shift factor, b_C, is verified using a constant density relation [96], whereas the temperature modulus shift factor, b_T, is expected to slightly and monotonically [105] diverge from unity. The temperature modulus shift factor [118] is determined from the crossover modulus G_x using Eq. 10.

$$\mathbf{b(T)} = \frac{\mathbf{G_x(T)}}{\mathbf{G_x(T_0 = 210\ ^\circ C)}} \qquad \mathbf{(10)}$$

The time scale shift factors (a_C and a_T) are determined using the ratio of the zero shear viscosities (Eq. 11) and the previously determined modulus shift factors [96].

Next we fit the Fujita-Kishimoto [100] free volume equation (Eq. 11). The free volume parameters A and B reflect the fractional free volume and the solvent contribution [100]. According to Eq. 11, a plot of 1 / ln [(a_C (C) . b_C (C)] versus [1 / C] should fall on a straight line with slope -B and intercept -A.

$$\mathbf{a_C(C) \cdot b_C(C) = \frac{\eta^*(\omega,\ C)}{\eta^*(\omega,\ 0)} = e^{-\frac{1}{[A]+[B]\cdot\frac{1}{C}}}} \qquad \mathbf{(11)}$$

As shown in Figure 5.7, it is clear that the free volume model, describes well the effect of solvent concentration on the complex viscosity of PS - TCB solutions in the concentration range of interest. The free volume parameters (A and B) in eq. 7 are shown as well in the table in Figure 5.7. The set of experiments on binary samples (as shown in Figure 5.1) is presented next.

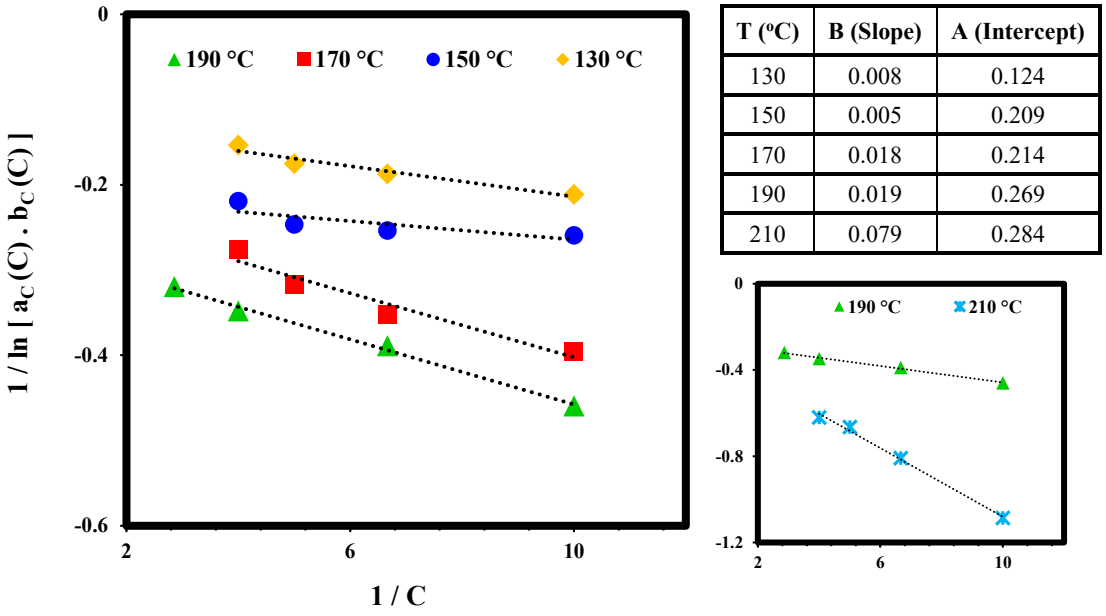

T (ºC)	B (Slope)	A (Intercept)
130	0.008	0.124
150	0.005	0.209
170	0.018	0.214
190	0.019	0.269
210	0.079	0.284

Figure 5.7. Free volume theory at 130°C, 150°C, 170°C, 190°C, and 210°C. Free volume parameters are determined from the line fit, for samples with 60wt% to 93.75wt% polymer.

Physical flow and diffusion are both transport processes, and the flow activation energy is thus comparable to the diffusion activation energy [105]. The effect of temperature on flow properties can be described by either the Arrhenius equation (Eq. 12) or the WLF [24] equation (Eq. 13).

$$\mathbf{\ln a_T(T) = \ln\left[\frac{\eta^*_0(T)}{\eta^*_0(T_0)}\right] = \frac{E_A}{R}\cdot\left[\frac{1}{T}-\frac{1}{T_0}\right]} \qquad \mathbf{(12)}$$

$$\mathbf{\ln a_T(T) = \ln\left[\frac{\eta^*_0(T)}{\eta^*_0(T_0)}\right] = \left[\frac{-C_1\cdot(T-T_0)}{C_2+(T-T_0)}\right]} \qquad \mathbf{(13)}$$

Here, E_A is the activation energy, C_1 is related to the fractional free volume at T_0 =210°C, and C_2 to the thermal expansion coefficient.

In Figure 5.8, the Arrhenius and WLF [24] equations are applied to the temperature shift factor a_T, and in Table 5.1 a summary of fitting parameters for WLF [24] and Arrhenius is shown. Both models fit similarly well although the correlation coefficient is slightly better for the WLF [24] equation. The flow activation energy from the Arrhenius fit to SAOS measurements for the homogeneous systems (E_A≈154 kJ/mol), is consistent with the diffusion activation energy (E_A≈127 kJ/mol) shown in Figure 5.4 (sorption measurements).

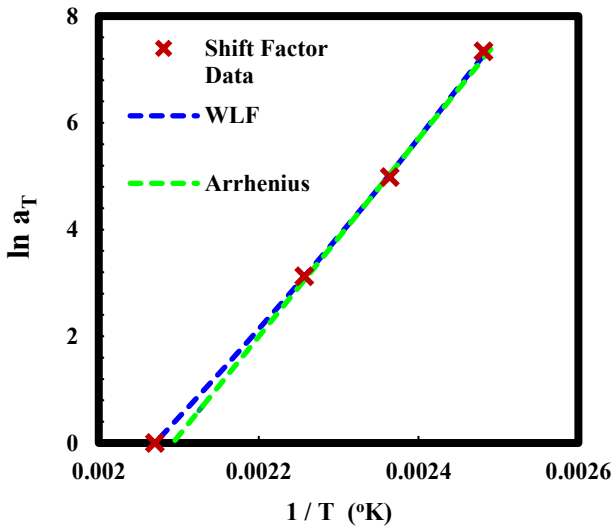

Figure 5.8. Fitting of Arrhenius and WLF [24] equations to experimental temperature shift factor data applied with T_0 = 210°C.

Table 5.1. Fitting parameters for Temperature Superposition: WLF [24] and Arrhenius models

Parameter	WLF	Parameter	Arrhenius
C1 [1/°C]	22	E [kJ/mol]	154 ± 1
C2 [°C]	323	R^2 [%]	98.6
R^2 [%]	99.96		

Diffusion Measurements using SAOS:

The solvent is initially at the center of a PS ring and diffuses outwards, which results in a decreasing torque over time. The torque measured during diffusion is normalized using the torque at time t = 0. Figure 5.9 shows plots of the normalized torque, $T(\omega_0, t) / T(\omega_0, t_0)$, as a function of time at 130°C, 150°C, 170°C, 190°C and 210°C, for k = 2 and $\omega_0 = 0.1\ s^{-1}$. In Figure 5.9, the experimental diffusion time is dependent on the temperature, and varies from 20 hours (≈72 000s) at 130°C, to 3 hours (≈10 800s) at 210°C. Figure 5.10 shows plots of the normalized torque during a time sweep at four different frequencies ω_0, at 130°C (Figure 5.10(a)) and 210°C (Figure 5.10(b)). In this figure we can see that except for the case of $\omega_0 = 100\ s^{-1}$, diffusion appears to be unaffected by frequency. We believe that something other than simple diffusion is occurring at $100\ s^{-1}$ (for example a secondary flow) and are therefore excluding this curve from all subsequent analyses. Similar plots for the other temperatures are presented in the supporting information. With the free volume parameters A and B previously determined, Eq. 7 can be used to fit experimental data with the diffusion coefficient as the only fitting parameter. The normalized data in Figure 5.10 are then used to determine the diffusion coefficient as a function of temperature and frequency.

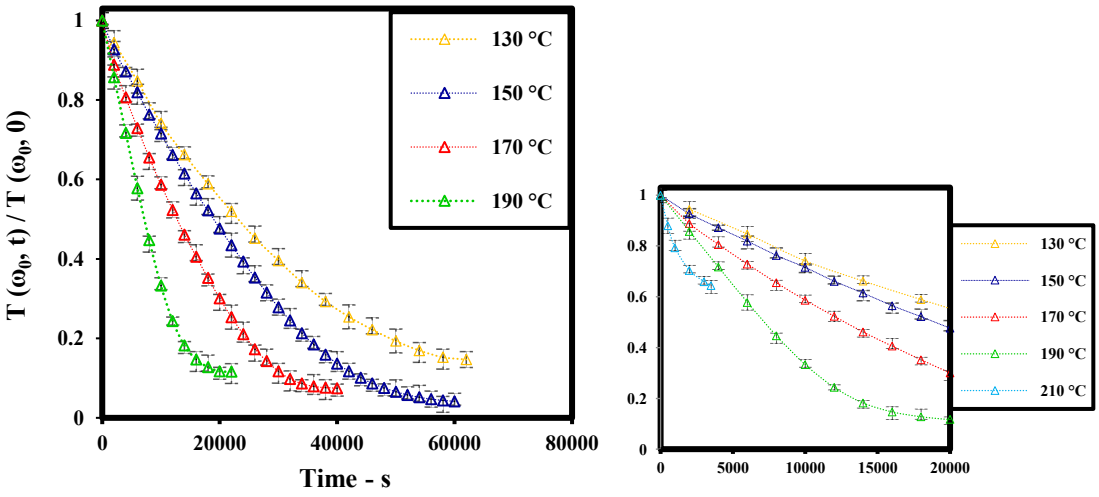

Figure 5.9. Normalized Torque as a function of time at 130°C, 150°C, 170°C, 190°C and 210°C, for k = 2 , $\omega_0 = 0.1\ s^{-1}$. Error bars represent an average of 6 experiments.

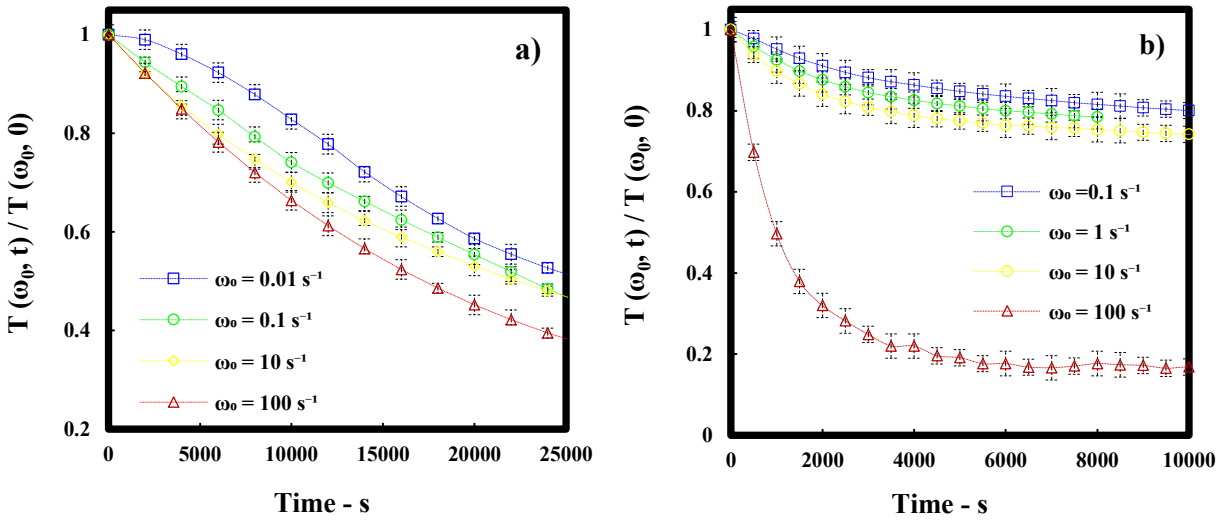

Figure 5.10. Normalized Torque as a function of time, for k = 2 and for 4 frequency decades from $0.01s^{-1}$ to $100s^{-1}$ for (a) 130°C; (b) 210°C. Error bars represent an average of 6 experiments.

The effect of SAOS on the diffusion rate, is studied experimentally by comparing diffusion in continuous and in intermittent SAOS tests. The sample during continuous SAOS tests is subjected to oscillatory flow during the entire test time. In intermittent SAOS tests (as shown in Figure 5.2), oscillations are applied for 100 s followed by long rest stages (1000 s and 10000 s) where no flow is applied. We have previously shown [96] that SAOS accelerates diffusion of TCB in molten PS at 190°C using the same approach. In Figure 5.11 (a)-(d), the normalized torque at 130°C is shown for samples continuously and intermittently sheared. A characteristic dynamics is observed at this lowest temperature (130°C) where the polymer initially imparts significant resistance to the solvent diffusion, and there is an apparent induction time, which precedes solvent diffusion into the nearly glassy polymer [119]. These anomalous dynamics lie between Fickian diffusion well above $T_g \approx 100°C$, and glassy diffusion below T_g, and can clearly be observed in Figure 5.11(a).

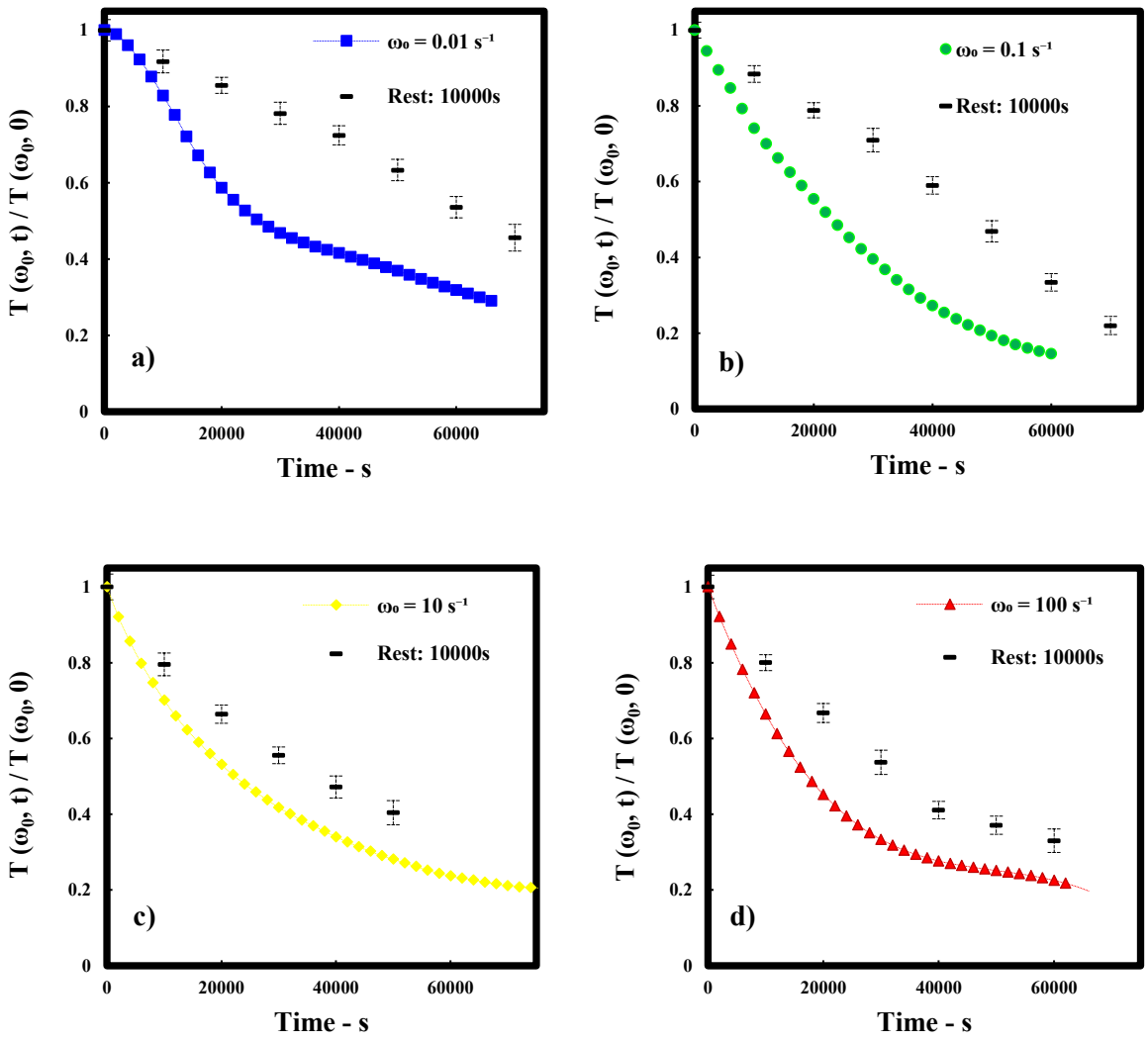

Figure 5.11. Normalized Torque at 130°C, for samples continuously sheared, compared with samples undergoing periods of intermittent oscillations and long rest periods, for k = 2, at 130°C and ω_0 = (a) 0.01 s^{-1}; (b) 0.1 s^{-1}; (c) 10 s^{-1}; (d) 100 s^{-1}.

In Figure 5.12 (a)-(c), the normalized torque (continuous and intermittent SAOS) at 210°C is shown. Similar data can be found in the Appendices for 150°C (Fig. A5.5), and for 170°C (Fig. A5.6). This study provides insight into the effect of SAOS on solvent diffusion in molten polystyrene at different temperatures. Samples continuously sheared exhibit the steepest decrease in measured torque, compared with samples undergoing only short intermittent oscillation cycles and very long rest periods. This observation is consistent for all temperatures studied, and confirms that the diffusion rate is increased by SAOS.

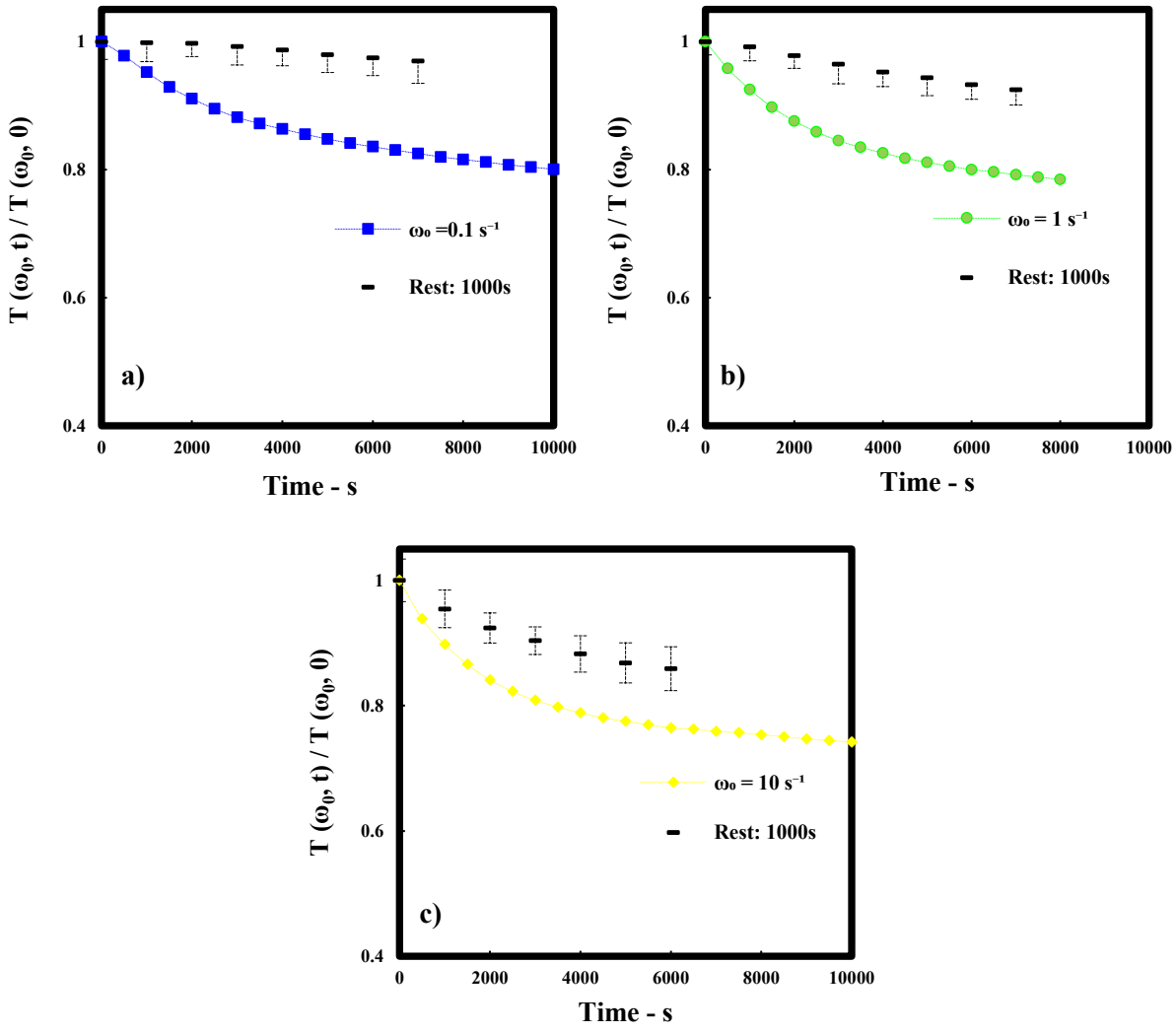

Figure 5.12. Normalized Torque at 210°C, for samples continuously sheared, compared with samples undergoing periods of intermittent oscillations and long rest periods, for k = 2, at 210°C and ω_0 = (a) 0.01 s^{-1}; (b) 0.1 s^{-1}; (c) 10 s^{-1}.

5.5. RESULTS AND DISCUSSION

5.5.1. Effect of SAOS:

In Figures 5.11-5.12, we see that continuous shearing accelerates diffusion, relative to the case of intermittent oscillations. From these data, we conclude that intermittent SAOS measurements can be used to measure a diffusion coefficient for this TCB|PS system close to the quiescent value over a broad frequency and temperature. Additionally, using the continuous oscillation tests, we can explore the effect of SAOS on diffusion. From results in Figures 5.11-5.12, we can make the following observation: relative to diffusion under intermittent SAOS, diffusion under continuous SAOS is always faster, regardless of frequency and temperature. This occurs even though the flow is oscillatory and there is no net transport of material in one direction [104].

5.5.2. Effect of Frequency and Temperature:

A least-squared-error forward fitting of Eq. (7)-(8) is applied to the experimental SAOS torque data, using the linear viscoelastic constitutive equation, the free volume theory, and a Fickian concentration profile. In this case, diffusion coefficients are determined using a gradient-based search method with the diffusion coefficient as single fitting parameter [96].

The inversion technique in Eq. (4)-(6) is also applied using Tikhonov regularization to recover radial viscosity profiles [114] from SAOS torque data. We then determine the diffusion coefficient and type from the interface width of recovered profiles, using a power law dependency of the interface width on time [114]. Diffusion coefficients obtained for samples continuously sheared from (a) the interface width of regularized solutions using the numerical approach and from (b) a forward fitting of Eq. (7)-(8) using the theoretical approach, are shown in Table 5.1. Calculated diffusion coefficients from both numerical and analytical approaches, also show good agreement with our data from sorption experiments.

We use rheological diffusion measurements in SAOS and apply both a theoretical and a numerical approach, to compare diffusion coefficients for various experimental

conditions. Diffusion coefficients determined from the continuous SAOS experiments shown in Table 5.1 and plotted in Figure 5.13 are independent of oscillation frequency for all temperatures studied. We see a small change in D at $\omega_0 = 100s^{-1}$ although it is unclear whether this observation is physically meaningful. The diffusion exponent, n, reflects the characteristic anomalous dynamics observed at 130 °C, as well as the Fickian dynamics for all other temperatures. We can see in Table 5.2 for $\omega = 0.1\ s^{-1}$ at 130 °C, that the diffusion exponent n increases by about 20% from the expected exponent of 0.5 for Fickian diffusion. The relative error is computed with respect to $D_{Fickian}$, and also increases to 3% at 130 °C. Anomalous effects at 130 °C are related to the influence of temperature on polymer structure, and result in a decreased solubility and mobility. As shown in Figure 5.13, diffusion is enhanced by the presence of an oscillatory flow, which allows polymer chains to push the solvent along. When SAOS is removed, diffusion occurs while the sample is kept at rest for almost the entire test, a slower diffusion is observed and a higher diffusion activation energy is required. For diffusion to occur, the system has to have sufficient energy to overcome the activation barrier energy.

Table 5.2. Comparison of the diffusion coefficient for samples continuously sheared, obtained from (a) the numerical interface width of regularized solutions and (b) by fitting D using a Fickian profile.

	130 °C			**170 °C**			**190 °C**		
ω (s^{-1})	**0.1**	**1**	**10**	**0.1**	**1**	**10**	**0.1**	**1**	**10**
n	0.62	0.58	0.55	0.52	0.49	0.51	0.51	0.49	0.51
$D_{Numerical}$ 10^{-5} (mm^2/s)	0.897	0.967	1.021	2.237	2.449	2.428	9.899	10.08	10.07
$D_{Fickian}$ 10^{-5} (mm^2/s)	0.934	1.009	1.057	2.261	2.465	2.4654	9.927	10.033	9.978
E_r %	3.96	4.16	3.41	1.06	0.65	1.52	0.28	0.47	0.92

Figure 5.13 confirms that oscillation effectively reduces the energy barrier, with the lowest activation energy occurring under continuous oscillation followed by intermittent oscillation with a higher activation energy and quiescent diffusion with the highest of all. Diffusion coefficients are a function of temperature and are clearly affected by SAOS. The temperature dependence of the diffusion coefficient in Figure 5.13 is further evidence for the change in the diffusion mechanism due to SAOS. A characteristic approach to glassy dynamics is observed at the lowest temperature (130 °C), and the magnitude of the diffusion acceleration due to SAOS increases at this temperature. This increase becomes smaller at higher temperatures, which suggests that diffusion is accelerated due to SAOS by a relatively lower amount at higher temperatures. It is thus possible to infer the diffusion coefficients from SAOS measurements, and extrapolate to static sorption conditions. The slopes for diffusion during SAOS in Figure 5.13, or the activation energies required, can be readily used to predict diffusion properties in static sorption conditions.

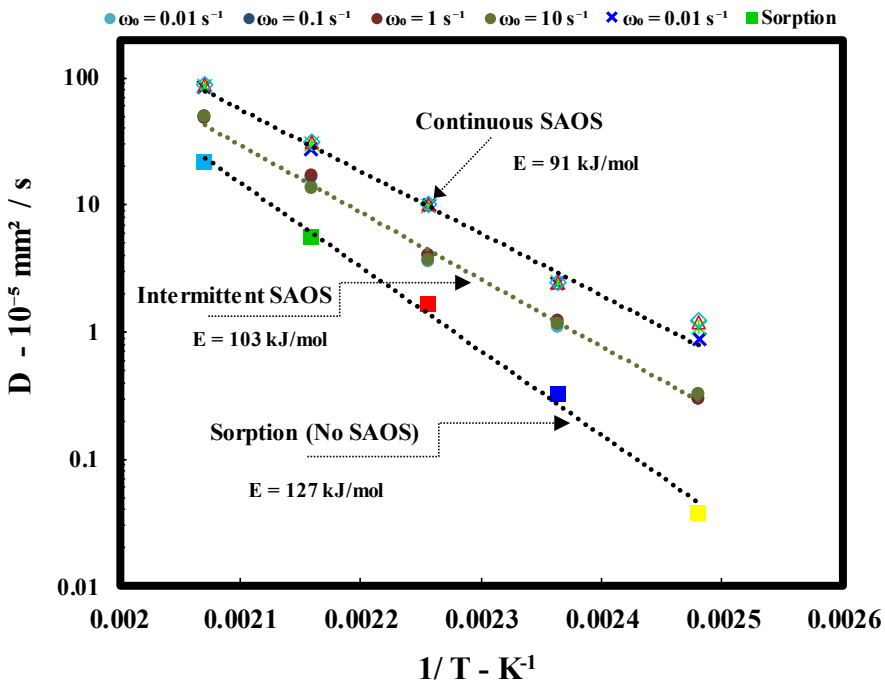

Figure 5.13. Effect of SAOS and frequency on the diffusion coefficient determined by fitting the Fickian profile under continuous oscillation, intermittent oscillation and from static sorption measurements.

5.6. CONCLUSION

Our rheological technique is used to determine the temperature dependence of the diffusion coefficient of 1,2,4-TCB diffusing in molten PS using SAOS measurements. A Fickian model and the free volume theory as well as a numerical regularization technique are applied to experimental data to determine the diffusion coefficient. Accelerated diffusion dynamics due to SAOS is observed experimentally at all temperatures. Temperature has a significant impact on the magnitude of this effect. At constant temperature, the diffusion coefficient is independent of the oscillation frequency, and at temperatures closer to the glass transition temperature, applying SAOS further accelerates the diffusion. A characteristic glassy type diffusion dynamics is observed at the lowest temperature (130 °C). We observe the highest activation energy for diffusion (127 kJ/mol) under quiescent conditions, with a lower activation energy (103 kJ/mol) under intermittent oscillation and the lowest activation energy (91 kJ/mol) under continuous oscillation.

CHAPTER 6

Interdiffusion Dynamics at The Interface Between Two Polystyrenes With Different Molecular Weight Probed by a Rheological Tool

ABSTRACT:

Interdiffusion at 190°C between two polystyrenes is studied under small amplitude oscillatory shear (SAOS) at various frequencies. Our rheological technique exploits differences in molecular weights and thus in viscosity to investigate interdiffusion dynamics. Interdiffusion between identical polymers, with identical chemical structures, are expected to form ideal solutions. However, several experimental observations indirectly question this ideal-solution assumption. We measure the torque during radial interdiffusion in a concentric binary sample, with a lower molecular weight polystyrene at the center and an outer ring with a higher molecular weight, at constant temperature and frequency. The radial concentration profile can be inferred from experiments by monitoring the torque as a function of time. We have previously confirmed that our rheological technique can be used to measure radial diffusion in molten polymers, and obtain a good estimate of the diffusion coefficient. We have also shown that our numerical approach based on Tikhonov regularization can be used to invert torque curves from time dependent SAOS experiments in which diffusion occurs to determine the diffusion coefficient. This study investigates interdiffusion kinetics due to SAOS flow as a function of frequency, and confirms that the interdiffusion rate is significantly increased by oscillatory motion at higher frequencies. We have inferred the time dependence of the interface between two polystyrenes and have found that the width of the interface increases with time considerably faster at higher frequencies.

6.1. INTRODUCTION

Polymer/Polymer interdiffusion have been studied using two similar polystyrenes with similar physical properties, but the literature on this topic remains limited [120-123]. Experimental observations for binary protonated and deuterated polystyrene and polybutadiene melts have indirectly questioned the ideal-solution assumption, which is expected to form during interdiffusion between identical polymers, with identical chemical structures [121]. They found that the interface width and mass uptake follow a power law quite different from the Fickian relation, and that at long times the interface is characterized by a non-Fickian equilibrium composition, with a power law with an exponent significantly lower than 0.5 for free diffusion [122, 124]. Interdiffusion across the interface of a binary polymeric assembly determines its mechanical and interface properties, and has attracted significant attention because of its designable structure. Interdiffusion determines the final properties of the interface, and may be used to modify the final structure. Interdiffusion applications include composites, welding, adhesion, and coating. Understanding this process may be a key factor in improving polymer products and polymer processing operations in industry. Polymeric interdiffusion is thus a problem of considerable interest for basic knowledge and industrial applications, and from theoretical and experimental standpoints.

We study interdiffusion between chemically identical polystyrenes but with different molecular weights under SAOS at 190°C. It is of special interest to study the effect of SAOS and frequency on polymer-polymer interdiffusion [127]. Our rheological method may essentially be used to measure and control the interdiffusion rate. Experimental torque-time curves produced by this rheological method [128] are used to characterize the interdiffusion behavior, over a broad frequency range. We have previously shown that SAOS accelerates solvent diffusion in polystyrene over wide ranges of temperature. One objective is to determine if this observation extends to polymer-polymer interdiffusion. The main objective is to determine the diffusion coefficient from time-dependent rheological measurements of interdiffusion in a binary polymeric sample.

6.2. THEORETICAL CONSIDERATIONS

During interdiffusion, polymer chains experience structural changes. Mixing depends on interactions between polymer chains, but Fick's laws do not account for these interactions, and are only valid when diffusing molecules are sufficiently small [129]. Non-Fickian diffusion is best explained in terms of chemical thermodynamics [130, 131], in which the chemical potential gradient of each component in the system is the driving force. The Flory-Huggins and mean field theories describe the thermodynamics of polymer melts, and the competition between entropy and enthalpy of mixing (See Eq. 1). The Flory-Huggins model and the Gibbs free energy are almost always used to describe the evolution of an initial sharp interface separating two polymers [124-127].

Mixing of two identical (chemically and physically) polymers is expected to be spontaneous, and the Gibbs free energy Eq.1, is always negative. For two chemically identical polymers that differ in molecular weight and for two dissimilar polymers, the Gibbs free energy determines the degree of miscibility (Eq. 2).

$$f[\phi_A(r,t)] = \Delta G = \Delta H - T\Delta S \quad (1)$$

$$\Delta G = [\chi_{AB} \cdot \phi_A \cdot (1-\phi_A)] + \left[\frac{\phi_A}{N_A}\ln(\phi_A) + \frac{1-\phi_A}{N_B}\ln(\phi_A)\right] \quad (2)$$

In Eq. 1, G is Gibbs free energy, H enthalpy, T temperature and S entropy. In Eq. 2, χ is the Flory-Huggins interaction parameter, ϕ_A is the composition of component A, and N_A (and N_B) is the molecular weight of component A.

The chemical potential in a closed system reflects the change in the Gibbs free energy (See Eq. 3). For systems with two different polymers of unequal molecular weights, chains move with unequal fluxes from higher chemical potential to lower chemical potential regions [124-127]. For systems with two identical polymers having equal molecular weights, the flux in both directions is the same, and chains move from a high concentration to a low concentration region (Eq. 4).

$$F = \int \left\{ f[\phi_A(r,t)] + \frac{\kappa}{4}[\nabla\phi_A(r,t)]^2 \right\} dV \quad (3)$$

$$\frac{\partial \phi_A}{\partial t} = -\nabla \cdot (J_A) \qquad J_A = -D \cdot \nabla \mu \qquad , \qquad \mu = \frac{\partial F}{\partial \phi} \tag{4}$$

In Eq. 3, f is the Gibbs free energy (See Eq. 1), and κ is a control parameter for the interface formation. In Eq. 4, J_A is the flux of component A, μ is the chemical potential, and D is the diffusion coefficient.

For the latter case, diffusion is of Fickian type and the initial sharp interface quickly spreads out according to the free-diffusion exponent [133, 134]. For the former case, the two polymers do not interdiffuse freely, and an interfacial zone separates them at equilibrium [133]. In this case, the interdiffusion exponent is considerably smaller than the Fickian type exponent, the two polymers partially mix and the initial sharp interface slowly broadens. Composition profiles are such that the thickness of the interface increases with time slower than that of a symmetric Fickian-type diffusion. Thus, interdiffusion strongly depends on molecular weight, and interaction between polymers. A diffusion model based on the Flory-Huggins theory has been applied to a binary polystyrene system [124] of similar chemical structure with different molecular weights (Eq. 5). The composition profile predicted agrees very well with experimental results obtained by Klein and co-workers using an ion-beam technique.

$$\frac{\partial \psi_A}{\partial t} = \frac{\partial}{\partial x}\left\{\left(\frac{2}{1+R+(R-1)\psi_A}\right) \cdot \left[\left\langle 1 + \frac{1}{R} - \chi_{AB} + \left(\frac{1}{R} - 1\right) \cdot \psi_A + \chi_{AB} \cdot {\psi_A}^2 \right\rangle \cdot \frac{\partial \psi_A}{\partial x} - \frac{\partial^3 \psi_A}{\partial x^3}\right]\right\} \tag{5}$$

Here, ψ is the concentration, and R is the ratio of molecular weights (N_B/N_A). The factor in front of the first concentration gradient term describes a diffusion coefficient, and the second term involving the third concentration gradient accounts for interactions and moderates the interface formation.

The interaction between two polymers and the change in free energy associated with their mixing is modeled in two steps: compression or expansion of each component, and mixing of the components at constant volume. The size and molecular weights of chain molecules is an important model parameter as well, which affects the combinatorial enthalpy and entropy of mixing.

6.3. RHEOLOGICAL MEASUREMENTS

6.3.1. Materials

A commercial grade polystyrene (M_w = 350 kg/mol, M_w / M_n = 2) was purchased from Sigma - Aldrich **(**product 441147). Three research grades polystyrenes were purchased from polymer source, and their properties are listed in Table 6.1. Two high molecular weight polystyrenes ($M_w \approx$ 350 kg/mol), one polydispersed of commercial grade and one monodispersed of research grade, used as test material for the outer ring and are denoted with subscript 1,A and 1,B. Two low molecular weight polystyrenes, one exceeding the critical molecular weight for entanglement, are used as test material for the inner disk and are denoted with subscript 2,A and 2,B.

Table 6.1. Polymers' molecular characteristics

Materials	**Supplier**	$\mathbf{M_w}$ $(\mathbf{kg/mol})$	$\mathbf{M_w/M_n}$
$\mathbf{PS_{1,A}}$	PolymerSource	345	1.07
$\mathbf{PS_{1,B}}$	SigmaAldrich	350	2
$\mathbf{PS_{2,A}}$	PolymerSource	4.5	1.06
$\mathbf{PS_{2,B}}$	PolymerSource	43.5	1.03

6.3.2. Experimental Method

The experimental characterization of interdiffusion using a parallel disk rheometer in SAOS, is carried out on a concentric binary specimen as shown in Figure 6.1 (Polymer A in the center and polymer B in the outer ring). In this case, the measured torque is time-dependent as in Eq. 6:

$$T(\omega_0, t) = \left[\frac{2\pi\omega_0\theta_0}{H}\right] \int_a^b [|\eta^*(\omega_0, C)| \cdot r^3]dr = f(t) \quad (6)$$

Here T (ω_0, t) is the time-dependent torque amplitude, a is the inner radius, b is the outer radius, and $\eta^*(\omega_0, C)$ is the concentration-dependent complex viscosity.

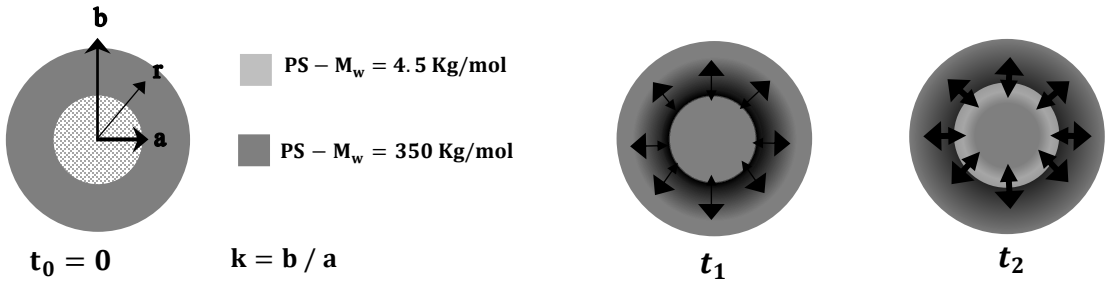

Figure 6.1. Schematic of the binary sample geometry considered in SAOS interdiffusion measurements. The center disk is a low molecular weight polystyrene and the outer ring is a high molecular weight polystyrene.

6.3.3. Numerical Method

A numerical method based on Tikhonov regularization [135, 138] can be applied, to recover radial viscosity profiles from the measured torque during interdiffusion under SAOS, and to estimate the diffusion coefficient. This inverse problem can be solved using the flattest slope [136] method to locate the optimal value of the regularization parameter λ. Tikhonov regularization finds a weighted least squares solution using the regularization parameter λ and the regularized torque T_i^R (Eq. 7).

$$\text{Min } \left|\sum_{i=0}^{t}\left\{T_i^M - T_i^C - T_i^R\right\}\right|^2 \tag{7}$$

The superscript M in Eq. 4 is used to denote the experimentally measured torque, and the superscript C is used to distinguish the computed torque T_i^C from its experimentally measured counterpart. In discretized form, T_i^C is given by Eq.8, and T_i^R by Eq. 9:

$$T_i^C = \beta \cdot \sum_{j=a}^{b} \eta^*(r_j, t_i) \cdot r_j^3 \cdot \alpha_j \cdot \Delta r \tag{8}$$

$$T_i^R = \lambda \cdot \sum_{j=a}^{b} \eta^*(r_j, t_i) \tag{9}$$

In Eq. 5, α_j are radial integration coefficients, which depend on the choice of discretization method, and $\eta^*(r_j, t_i)$ is the set of unknown complex viscosity profiles to be recovered from T_i^M.

6.3.4. Analytical Method

We use rheological interdiffusion measurements under SAOS and apply both an analytical and a numerical approach, to determine the concentration profile and the diffusion coefficient under various experimental conditions, and for a wide range of oscillation frequencies.

The interdiffusion model based on the mean-field theory and a free energy mixing function is used to describe the composition profile (Eq. 5), and a non-linear mixing rule [142] in Eq. 10 is used to describe the effect of composition on the complex viscosity, where η_1^* and η_2^* are the pure polymers viscosities.

$$|\eta^*(r,\ t)| = \left\{\psi_A(r,\ t) \cdot |\eta_A^*|^{(1/3.4)} + [1 - \psi_A(r,\ t)] \cdot |\eta_B^*|^{(1/3.4)}\right\}^{3.4} \quad (10)$$

A relationship between composition (Eq. 5), complex viscosity (Eq. 10), and measured torque (Eq. 6), can essentially be obtained from the mixing rule by substituting Eq. 5 for composition and Eq. 10 for complex viscosity, in the SAOS flow integral (Eq. 6) for torque.

The radial composition profile and the interface width can be inferred from experiments by monitoring the torque as a function of time. This approach can be applied to experimental torque-time curves during radial interdiffusion in a concentric binary sample to determine a diffusion coefficient as well. A least-squared-error fitting of Eq. 6 is applied to experimental torque data, and a gradient-based iterative search method is used with a single adjustable coefficient. Tikhonov regularization, with an appropriate choice of regularization parameter, can also be used to reconstruct the solution of a one-dimensional diffusion problem in the radial direction and recover viscosity and interface width profiles.

6.3.5. Effect of SAOS & Frequency

To clarify the effect of SAOS and oscillation frequency [139, 140], continuous and intermittent experiments are performed, as shown in Figure 6.2. In continuous experiments in Figure 6.2, the binary PS-PS sample is subjected to oscillations at constant frequency during the entire diffusion test [128]. In intermittent experiments, oscillations are only applied for short cycles intermittently with long rest periods, where no flow is applied. The focus is on examining the effect of SAOS and frequency on interdiffusion interdiffusion dynamics at the Interface between two polystyrenes with different molecular weight.

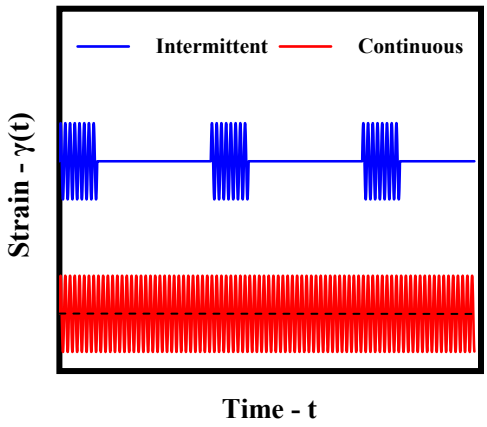

Figure 6.2. Schematic illustration of strain histories in intermittent-type oscillation experiments compared with continuous-type oscillation experiments. Intermittent oscillations are applied for 100s followed by rest stages of 1000s and 10000s.

We have previously shown [128] that continuous shearing accelerates diffusion, relative to the case of intermittent oscillations for solvent-polymer system. We have also shown that intermittent SAOS measurements can be used to measure a diffusion coefficient for this TCB|PS system close to the quiescent value over a broad frequency range. We have made the following observation: relative to diffusion under intermittent SAOS, diffusion under continuous SAOS is always faster, even though the flow is oscillatory and there is no net transport of material in one direction.

6.4. EXPERIMENTAL RESULTS

6.4.1. Characterization of Neat Polystyrenes

Neat polymer pellets are first dried in a vacuum oven, and are then prepared by compression molding, using a 1.2mm thick mold with 25mm diameter cavities. Dried pellets are confined in the mold's cavities between thin Mylar films, to avoid contamination and obtain a smooth surface. Circular disks 1.2mm thick and 25mm in diameter are produced under identical molding conditions that reduce sample-to-sample variability. For strains with sufficiently small amplitude, deformation occurs within the linear viscoelastic limit, and rheological properties become independent of the size of the deformation. A strain sweep is performed first, to determine the critical strain below which material functions become independent of the strain amplitude. A strain sweep at 190°C, and ω=10 rad/s, is used to identify this region, and the critical strain amplitude for the LVE region is determined in Figure 6.3. Then, a frequency sweep in the LVE region at 190°C, with ω ϵ [0.001-100] 1/s is used to determine LVE properties of neat polymers. Storage/Loss Moduli as a function of frequency are shown in Figure 6.3.

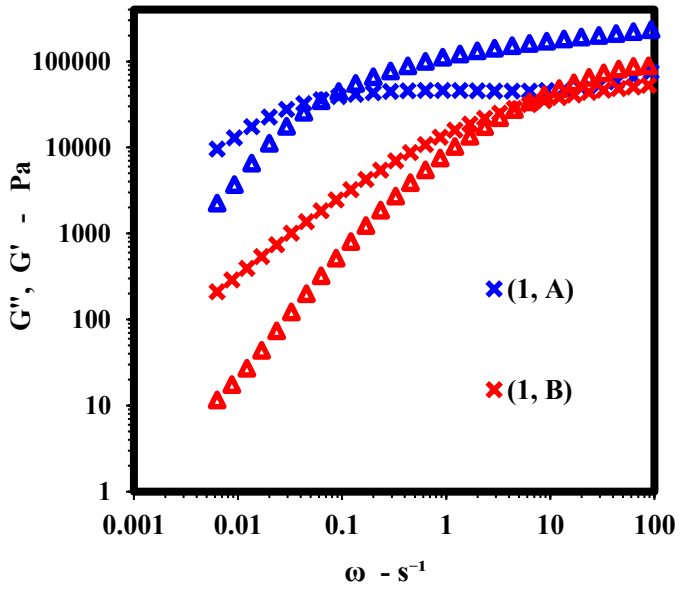

Figure 6.3. Storage and loss modulus data with a typical cross-over frequency for neat polystyrene samples (1,A) and (1, B) at 190°C. Curves are averages of three experiments.

6.4.2. Interdiffusion Measurements using SAOS

The binary sample in Figure 6.1 is produced by pressing together a smooth disk and a flat ring each composed of a polystyrene with a different molecular weight (See Table 6.1). Interdiffusion is studied at 190°C using a rotational rheometer under small amplitude oscillatory shear (SAOS), and the diffusion coefficient is determined at each frequency. The main objectives are to measure polymeric interdiffusion experimentally, to assess the effect of SAOS and frequency, and to determine the diffusion coefficient in a molten binary polystyrene system from SAOS measurements.

Under SAOS, polymer chains are in quasi-equilibrium, and the torque remains constant with time for neat polystyrene, in the LVE region at constant frequency, strain amplitude and temperature. The torque obtained from concentric binary samples in Figure 6.1, is time and composition dependent and reflects the interdiffusion dynamics. The inner polystyrene is of lower molecular weight and diffuses deeper in the radial direction than the outer polystyrene ring, which overall results in a decreasing torque over time. Although these measurements lie in the LVE region, there are indications that SAOS may still affect interdiffusion. For (1, A-B; 2, A) systems in Table 6.1, Figure 6.4 shows plots of the torque, $T(\omega_0, t)$, as a function of time at 190°C, for a sample geometry k = 2, and at different frequencies ω_0.

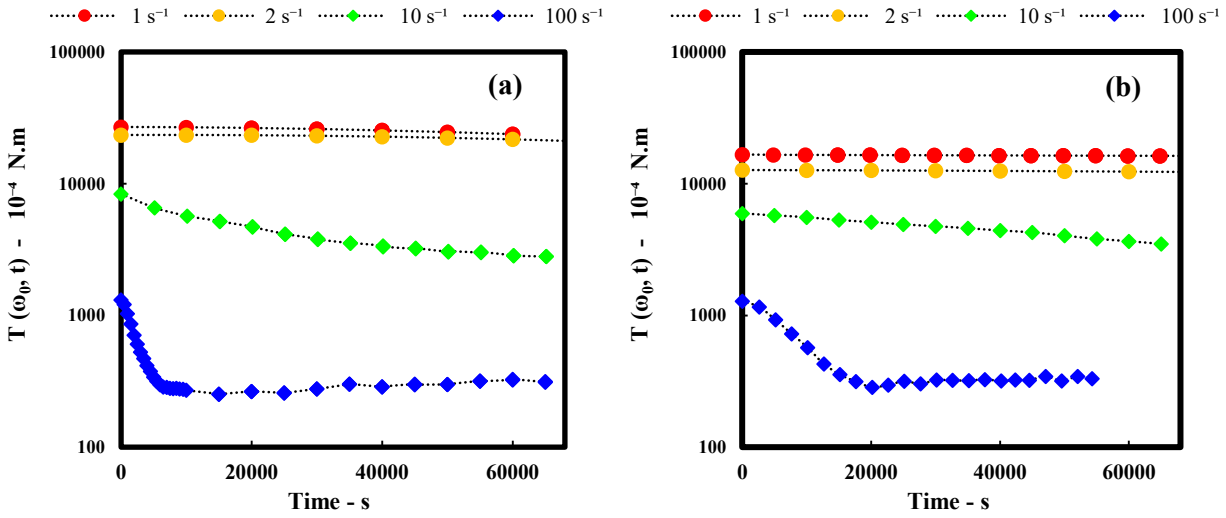

Figure 6.4. Interdiffusion measurements at 190°C for 4 frequencies: torque T (ω_0, t) as a function of frequency for samples with inner disk $PS_{2,\ A}$ and outer ring (a) $PS_{1,\ A}$; (b) $PS_{1,\ B}$. Curves are averages of three experiments.

At higher frequencies for $\omega_0 \geq 10\ s^{-1}$, interdiffusion is more pronounced and the system reaches a state where the torque becomes independent of time, significantly faster than for $\omega_0 \leq 2\ s^{-1}$. The key feature of this plot for $\omega_0 = 100\ s^{-1}$ (and $\omega_0 = 10\ s^{-1}$), is the time required for the torque to become constant to ±2%. This time, 4hours (~ 15 000s) for $\omega_0 = 100\ s^{-1}$, is characteristic of the interdiffusion time scale and of the interface behavior between two identical polystyrenes with large differences in molecular weights.

In Figure 6.5, the measured torque is normalized by the torque at time t = 0, as T (ω_0, t) / T (ω_0, 0). The initial torque T (ω_0, 0) reflects the response of the system before interdiffusion, and before the broadening of the initial sharp interface. The normalized data in Figure 6.5 is useful to understand interdiffusion dynamics at different frequencies and for different molecular weights, and to determine the diffusion coefficient for these systems as a function of frequency. In this figure we can see that interdiffusion is very much affected by increasing frequency. From Figure 6.5 we can see that increasing the frequency significantly accelerates the interdiffusion process. Interdiffusion appears to be unaffected by frequencies lower than $2s^{-1}$.

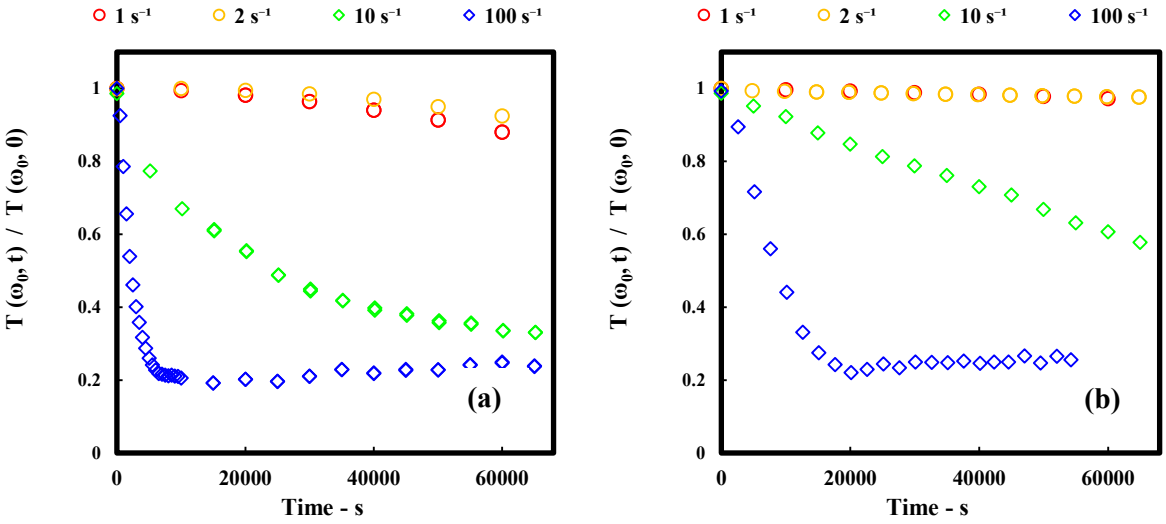

Figure 6.5. Normalized Torque from experimental interdiffusion measurements at 190°C: T (ω_0, t) as a function of frequency for samples with inner disk $PS_{2,\ A}$ and outer ring (a) $PS_{1,\ A}$; (b) $PS_{1,\ B}$.

To explore the effect of SAOS on the interdiffusion rate, we study interdiffusion under intermittent oscillations, as shown in Figure 6.2. In Figure 6.6, samples continuously sheared produce a steep decrease in measured torque, compared with samples undergoing only short intermittent oscillation and long rest periods. Intermittent measurements, including at high frequencies, show a relatively constant torque, which indicates a significantly slower interdiffusion and broadening of the initial sharp interface. The effect of SAOS on the diffusion rate is studied experimentally by comparing diffusion in continuous and in intermittent SAOS tests. In Figure 6.6, oscillations are applied for 100s in intermittent SAOS tests, followed by long rest stages, where no flow is applied: 5000s for ω_0 =100s^{-1} and 10000s for ω_0 =10s^{-1}. A characteristic dynamics is observed when SAOS is applied continuously; the torque decreases significantly, whereas there is little apparent interdiffusion when SAOS is applied intermittently. This dynamics can clearly be observed in Figure 6.6 and is consistent for all PS/PS systems studied. This observation confirms that the interdiffusion rate is drastically by SAOS, and provides insight into the effect of SAOS on interdiffusion in molten polystyrene with different molecular weights.

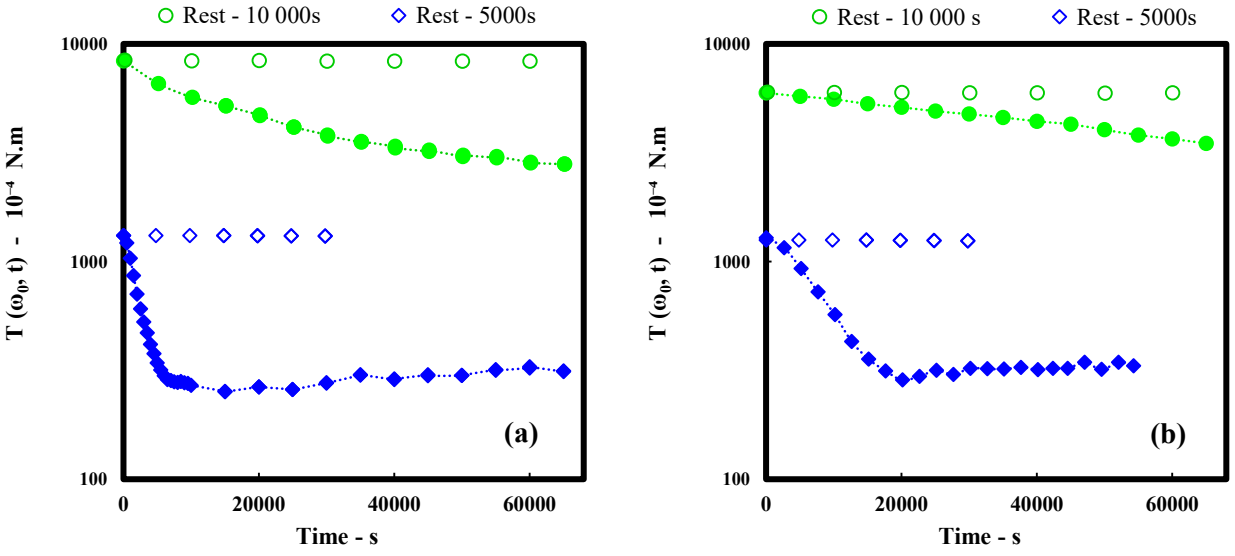

Figure 6.6. Interdiffusion measurements at 190°C for samples continuously sheared, compared with samples continuously sheared with long rest periods: T (ω_0, t) as a function of frequency for samples with inner disk $PS_{2,\,A}$ and outer ring (a) $PS_{1,\,A}$; (b) $PS_{1,\,B}$. (● ω_0 =10 s^{-1}; ♦ ω_0 =100 s^{-1}) Curves are averages of three experiments.

6.4.3. Effect of Polydispersity on Interdiffusion

In Figures 6.4(a) and 6.5(a), the outer ring is a monodispersed polystyrene (System 1, A; Table 6.1), and in Figures 6.4(b) and 6.5(b) the outer ring is a broad commercial grade polystyrene (System 1, B; Table 6.1), of about the same weight average molecular weight. Experimental torque-time curves produced by this rheological method is used to determine the effect of polydispersity [141], by comparing the response of the above two systems. Interdiffusion torque measurements for ω_0 =10 s^{-1} and ω_0 =100 s^{-1} are plotted in Figure 6.7(a) and 6.7(b). We see a significantly steeper slope for the monodispersed polystyrene, and this observation extends to lower frequencies. As shown in Figure 6.7, interdiffusion is faster when both system components, inner disk and outer ring, are mono-dispersed. When the outer ring is a broad distribution polystyrene, interdiffusion is slowed by the presence of physical chain length differences. Interdiffusion is clearly affected by polydispersity. The polydispersity dependence of interdiffusion can be seen in Figure 6.7, which is evidence for the change in interdiffusion rate due to polydispersity. A characteristic faster interdiffusion is observed for monodispersed polystyrene rings, and the steepness of the measured torque increases, compared to broad molecular weight distribution polystyrene rings.

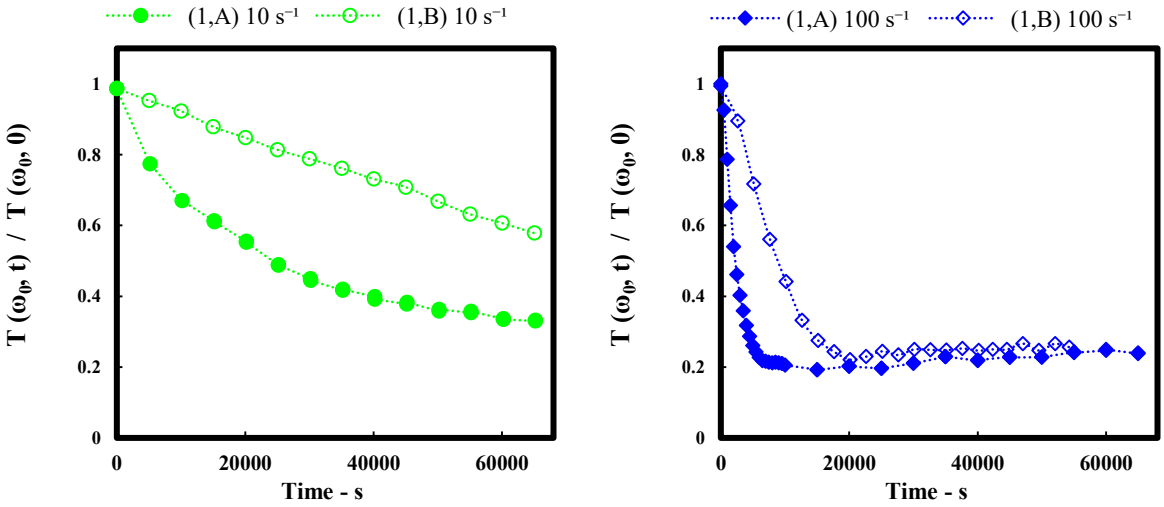

Figure 6.7. Normalized Torque from interdiffusion measurements at 190°C: T (ω_0, t) as a function of frequency (a) ω_0 =10 s^{-1}; (b) 100 s^{-1}, for samples with inner disk. (● ♦ $PS_{1,A}$; ○ ◊ $PS_{1,B}$).

6.5. CONCLUSION

We have introduced a new rheological technique to study interdiffusion in identical polystyrenes utilizing differences in viscosities. A closer view on the kinetics of interdiffusion and on the evolution of a sharp interface between two identical polystyrenes with different molecular weights is provided. We have performed experiments in SAOS and we have been able to observe a shift in diffusion behavior at higher frequencies, at and above $10s^{-1}$. There is strong evidence that higher frequencies induced faster chain migration and interface spread. In the near future, we will explore the role of entanglements and present a study on the effect of molecular weights above the critical entanglement molecular weight. We have shown that an equilibrium interface exists in low frequency interdiffusion, but not at higher frequencies, where interdiffusion is more likely to be of Fickian and form an ideal solution. In the presence of high frequency continuous SAOS, the interdiffusion model for binary polystyrene with similar (not same) chemical structure fails to describe the dynamics. Remarkably, high frequency interdiffusion results are well described by a symmetric Fickian composition profile, which illustrates the strong impact of SAOS at frequencies at or above $10s^{-1}$ on interdiffusion. This further shows the necessity of developing this field to give access to the full spectrum of knowledge, a portion of which we present here. The proposed rheological method is convenient and practical compared with energy spectrum techniques. This rheological technique opens a new path to a more in-depth study of interdiffusion dynamics.

CHAPTER 7

7.1. SUMMARY OF CONCLUSIONS

We have shown that SAOS accelerates diffusion of TCB in molten PS at 190°C. We have also introduced a new straightforward rheological technique to study solvent diffusion in molten polystyrene and interdiffusion in identical polystyrenes utilizing differences in viscosities. The free volume theory was applied to experimental data from homogeneous mixtures and compared to the neat polystyrene's response. The diffusion coefficient was determined as a function of frequency and temperature, and for intermittent and continuous oscillation conditions. The interface width was also determined, and its validity was verified using a refined Tikhonov regulation technique.

Diffusion coefficients for the TCB-PS solvent-polymer system as a function of frequency show a very slight dependence on oscillation frequency, but the presence of SAOS flow continuously resulted in larger diffusion coefficients compared with intermittent SAOS results. From our solvent diffusion results at low temperatures (130 °C) close to the glass transition for polystyrene, the diffusion coefficient was significantly higher when SAOS flow is applied continuously. As the temperature is increased above 170 °C, the accelerated kinetics due to oscillatory flow becomes less obvious. From our results, diffusion under continuous SAOS is always faster relative to diffusion under intermittent SAOS, regardless of frequency and temperature.

This occurs even though the flow is oscillatory and there is no net transport of material in one direction. For interdiffusion systems with two polystyrenes, applying SAOS accelerates interdiffusion by orders of magnitude, but only when high frequencies are used. We provide strong evidence that higher frequencies induce faster chain migration and interface spread. We have also shown that a sharp interface persists in low frequency interdiffusion, but not at higher frequencies, where interdiffusion is more likely to be of Fickian type and form an ideal solution. Remarkably, high frequency interdiffusion results, are well described by a symmetric Fickian composition profile, which illustrates the strong impact of SAOS at frequencies at or above $10s^{-1}$ on interdiffusion.

7.2. CONTRIBUTIONS

I. A rotational rheometry-based technique is developed to study diffusion through in molten polystyrene. This technique relies on equilibrium flow and LVE properties in SAOS, to measure the diffusion coefficient. We provide a validated rheological method based on viscosity differences between diffusant and host, to study solvent-polymer and polymer-polymer diffusion for a wide range of experimental conditions.

II. Inversion of torque-time SAOS data is applied using Tikhonov regularization and the flattest slope method to resolve the torque-viscosity integral. The flattest slope minimizes the residual error and the solution norm versus the regularization parameter and locates the optimal regularization parameter. Local viscosity profiles are recovered from SAOS torque data during diffusion, and the diffusion coefficient is determined for a wide range of diffusion systems.

III. Novel data on the diffusion of TCB in molten polystyrene and the interdiffusion of polystyrene are produced. We have also shown that the diffusion rate is increased by oscillatory motion and that this effect is increased at lower temperatures. We further show the necessity of developing the field of diffusion and interdiffusion to give access to the full spectrum of knowledge, a portion of which we presented here.

7.3. RECOMMENDATIONS FOR FUTURE WORK

Some suggestions for future work to expand this study are summarized in the following:

- Further experimental efforts in standardizing the molding of binary samples (ring and disk) using injection molding, which offers advantages over compression molding. It would be worth improving the experimental procedure, which would result in even more accurate diffusion results. The results of such improvements would help in increasing the resolution and accuracy in capturing diffusion processes.

- It would be interesting to examine the post-diffusion concentration profile from atomic force microscopes and nano-indenters. The results of such study could be used to confirm rheological measurements and the long-time diffusion behavior. The interconnectivity between our rheological measurements and the post-shearing nano-indentation results should be explored.

- Further investigation on the effect of shearing and the strain amplitude. Diffusion in the solvent-polymer system and interdiffusion in the polymer-polymer system may have a dependency on the strain amplitude. Further experiments with a wider range of systems, including interdiffusion between chemically dissimilar polymers, and diffusion in molten nano-filled polymers. Further investigation on the interdiffusion dynamics is recommended, since limited literature on the topic exists.

- Research is needed to understand the diffusion dynamics of complex systems. Theoretical frameworks on the topic of diffusion in complex polymeric systems exist, but have only been explored intermittently with very few approaches validated experimentally. It is also only recently that rheological analyses of diffusion have been carried out, with very limited literature.

REFERENCES

[1] M. Bousmina, H. Qiu, M. Grmela, "Diffusion at Polymer/Polymer Interfaces Probed by Rheological Tools," *Macromolecules*, vol. 31, pp. 8273-8280, 1998.

[2] T. Cherdhirankorn, V. Harmandaris, A. Juhari, P. Voudouris, G. Fytas, K. Kremer, K. Koynov, "Fluorescence Correlation Spectroscopy Study of Molecular Probe Diffusion in Polymer Melts," *Macromolecules*, vol. 42, pp. 4858–4866, 2009.

[3] S.R. Aragon, R. Pecora, "Fluorescence correlation spectroscopy as a probe of molecular dynamics," *The Journal of Chemical Physics,* vol. 64, pp. 1791-1803, 1976.

[4] V. Vukojevic, A. Pramanik, T. Yakovleva, R. Rigler, L. Terenius, G. Bakalkin, "Study of molecular events in cells by fluorescence correlation Spectroscopy," *CMLS - Cell. Mol. Life Sci.*, vol. 62, pp. 535–550, 2005.

[5] M. Antonietti, J. Coutandin, H. Sillescu, "Diffusion of Linear Polystyrene Molecules in Matrices of Different Molecular Weights," *Macromolecules*, vol. 19, pp. 793-798, 1986.

[6] P. Ramya, C. Ranganathaiah, J.F. Williams, "Experimental Determination of Interface Widths in Binary Polymer Blends from Free Volume Measurements," *Polymer*, vol. 53, 2012.

[7] U. Steiner, J. Klein, "Interfacial Structure in Polymer Mixtures below the Critical Point," *Phys. Rev. Lett*., vol. 63, p. 616, 1989.

[8] Bernardo, G., "Diffusivity of Alcohols in Amorphous Polystyrene," *Journal of Applied Polymer Science*, vol. 127, pp. 1803-1811, 2012.

[9] Bernardo G.; Veseley D., "Solubility of Carboxylic Acids in a Matrix of Uncross-linked Polystyrene," *European Polymer Journal*, vol. 43, pp. 4983-4994, 2007.

[10] J. M. Dealy, K. F. Wissbrun, "Melt Rheology and Its Role in Plastics Processing," *Van Nostrand Reinhold, New York, USA*, 1990.

[11] F. A. Morrison, "Understanding Rheology," *Oxford University Press, New York, USA*, 2001.

[12] Dealy J.M.; Park H.E., "Effects of Pressure and Supercritical Fluids on the Viscosity of Polyethylene," *Macromolecule*, vol. 39, pp. 5438-5452, 2006.

[13] M. Antonietti, J. Coutandin, H. Sillescu, "Diffusion of Linear Polystyrene Molecules in Matrices of Different Molecular Weights," *Macromolecules,* vol. 17, pp. 798-802, 1984.

[14] M. Antonietti, J. Coutandin, H. Sillescu, “Diffusion of Linear Polystyrene Molecules in Matrices of Different Molecular Weights,” *Macromolecules,* vol. 19, pp. 793-798, 1986.

[15] Areerat S., Funami E., Hayata Y., Ohshima M., “Measurement and Prediction of Diffusion Coefficients of Supercritical CO_2 in Molten Polymers,” *Polymer Engineering and Science*, vol. 44, p. 10, 2004.

[16] Qiu H., Bousmina M., “New technique allowing the quantification of diffusion at polymer/polymer interfaces using rheological analysis: Theoretical and experimental results,” *Journal of Rheology*, vol. 43, p. 551, 1999.

[17] Joubert C., Cassagnau P., Choplin L., Michel A., “Diffusion of plasticizer in elastomer probed by rheological analysis,” *Journal of Rheology*, vol. 46, p. 629, 2002.

[18] F. Xie, C. Zhou, “Effects of Small-Amplitude Oscillatory Shear on Polymeric Reaction,” *Polymer Composites*, vol. 29, 1, pp. 72-76, 2008.

[19] J.M Smith, M.M. Abbott, H.C. Van Ness, “Introduction to Chemical Engineering Thermodynamics,” *McGraw-Hill, New York City, New York, USA*, 5th Edition, 1996.

[20] L.H. Sperling, “Introduction to Physical Polymer Science,” *Wiley, New York, USA*, 4th Edition, 2004.

[21] P.J. Flory, "Thermodynamics of Polymer Solutions,” *Discuss. Faraday Soc., 15th Spiers Memorial Lecture*, vol. 49, p. 7, 1970.

[22] H. Fujita, A. Kishimoto, “Interpretation of Viscosity Data for Concentrated Polymer Solutions,” *Journal of Chemical Physics*, vol. 34, p. 2, 1961.

[23] A. Indrakanti, N. Ramesh, J.L. Duda, S.K. Kumar, “Modeling diffusion in miscible polymer blend films,” *Journal of Chemical Physics*, vol. 121, p. 1, 2004.

[24] L. Williams, F. Landel; J. Ferry, "The Temperature Dependence of Relaxation Mechanisms in Amorphous Polymers and Other Glass-forming Liquids". *J. Am. Chem. Soc*. **77** (14) 3701–3707.

[25] W.C. Kim, H. Pak, “Interdiffusion at Interfaces of Binary Polymer Mixtures with Different Molecular Weights,” *Bull. Korean Chem. Soc.*, vol. 20, p. 11, 1999.

[26] W.C. Kim, H. Pak, “Dynamics of Interdiffusion at Interface between Partially Miscible Polymers,” *Bull. Korean Chem. Soc.,* vol. 20, p. 12, 1999.

[27] W.C. Kim, C.J. Lee, H.G. Sim, H. Pak, “Interdiffusion at Interfaces of Polymers with Similar Physical Properties,” *Bull. Korean Chem. Soc*., vol. 21, p. 6, 2000.

[28] Mueller F., Krueger K.; Sadowski G., “Non-Fickian Diffusion of Toluene in Polystyrene in the Vicinity of the Glass-Transition Temperature,” *Macromolecules,* vol. 45, pp. 926-932, 2012.

[29] Anton Peterlin, “Type II Diffusion as a Particular Solution of the Conventional Diffusion Equation,” *Journal of Research of the National Bureau of Standards*, Vol. 81 A, pp. 243-250, 1977.

[30] Matthew G.H., Giulia L.F., Joao T.C., “A minimal model for solvent evaporation and absorption in thin films,” *Journal of Colloid and Interface Science*, vol. 488, pp. 61-71, 2017.

[31] Costeux S., Zhu L., “Low Density Thermoplastic Foams Nucleated by Nanoparticles,” *Polymer*, vol. 54, 2785-2795, 2013.

[32] Dealy J.M., Bousmina M., Qiu H., “Coupling between Flow and Diffusion at Polymer/Polymer Interface: Large Amplitude Oscillatory Shear Experiments,” *Rheologica Acta*, vol. 41, pp. 87-92, 2002.

[33] Schabel W., Siebel D., Scharfer P., “Determination of Concentration-Dependent Diffusion Coefficients in Polymer−Solvent Systems: Analysis of Concentration Profiles Measured by Raman Spectroscopy during Single Drying Experiments Excluding Boundary Conditions and Phase Equilibrium,” *Macromolecules*, vol. 48, pp. 8608-8614, 2015.

[34] Zhang H., Lamnawar K., Mazzouz A., “Rheological Modeling of the Mutual Diffusion and the Interphase Development for an Asymmetrical Bilayer Based on PMMA and PVDF Model Compatible Polymers,” *Macromolecules*, vol. 46, pp. 276-299, 2013.

[35] Asai M., Awata M., Koike Y., “Effects of Rotation of Benzene Rings on Diffusion of Solvents in Polymer Melts,” *Ind. Eng. Chem. Res.*, vol. 50, pp. 3280–3286, 2011.

[36] Shams S., Haghi E., Cakmak M., “Mass and heat diffusion in ternary polymer solutions: A classical irreversible thermodynamics approach,” *Polymer*, vol. 97, pp. 472-479, 2016.

[37] Bernardo, G., “Diffusivity of Alcohols in Amorphous Polystyrene,” *Journal of Applied Polymer Science*, vol. 127, pp. 1803-1811, 2012.

[38] Karimi M., Tashvigh A.A., Asadi F., Ashtiani F.Z., “Determination of concentration-dependent diffusion coefficient of seven solvents in polystyrene systems using FTIR-ATR technique: experimental and mathematical studies,” *RSC Adv.*, vol. 6, pp. 9013-9022, 2016.

[39] Miller-Chou B.A., Koenig J.L., “A review of polymer dissolution,” *Prog, Polym. Sci.*, vol. 28, pp. 1223-1270, 2003.

[40] Sillescu H., Antonietti M., Coutandin J., "Diffusion of Linear Polystyrene Molecules in Matrices of Different Molecular Weights," *Macromolecules*, vol. 19, pp. 793-798, 1986.

[41] Seiffert S., Oppermann W., "Diffusion of linear macromolecules and spherical particles in semidilute polymer solutions and polymer networks," *Polymer*, vol. 49, pp. 4115–4126, 2008.

[42] Finerman T.M., Crist B., "Self-diffusion of polydisperse linear polymers," *Journal of Non-Crystalline Solids*, vol. 131-133, pp. 620-623, 1991.

[43] Composto R.J., Lin C-C.., Parrish E., "Macromolecule and Particle Dynamics in Confined Media, Application of ion scattering techniques to characterize polymer surfaces and interfaces," *Materials Science & Engineering R*, vol. 38, p. 107, 2002.

[44] Lin C.C., Parrish E., Composto R.J., "Macromolecule and Particle Dynamics in Confined Media, Macromolecules," vol. 49, pp. 5755−5772, 2016.

[45] Bousmina M., Qiu H., Grmela M., "Diffusion at Polymer/Polymer Interfaces Probed by Rheological Tools," *Macromolecules,* vol. 31, pp. 8273-8280, 1998.

[46] Masaro L., Zhu X.X., "Physical models of diffusion for polymer solutions, gels and solids," *Prog. Polym. Sci.*, vol. 24, pp. 731-775, 1999.

[47] Bernardo G., Veseley D., "Solubility of Carboxylic Acids in a Matrix of Uncross-linked Polystyrene," *European Polymer Journal,* vol. 43, pp. 4983-4994, 2007.

[48] Pestryaev E. M., "Molecular Dynamics Study of Chain Reptation in a Gel," *Polymer Science,* vol. 55, pp. 336–352, 2013.

[49] Kathryn R., Shea R., Rae M. R-A, "DNA as a Model for Probing Polymer Entanglements: Circular Polymers and Non-Classical Dynamics," *Polymers*, vol. 8, p. 336, 2016.

[50] Fujita H., Kishimoto, A., "Interpretation of Viscosity Data for Concentrated Polymer Solutions," *Journal of Chemical Physics*, vol. 34, pp. 393-397, 1961.

[51] Morrison F.A, "Understanding Rheology," *Oxford University Press: New York*, 2001.

[52] Dealy J.M., Park H.E., "Effects of Pressure and Supercritical Fluids on the Viscosity of Polyethylene," *Macromolecule,* vol. 39, pp. 5438-5452, 2006.

[53] Park H.E., "Effects of Pressure and Dissolved Carbon Dioxide on the Rheological Properties of Molten Polymers," *Doctoral Thesis, McGill University, Montreal, CA*, 2005.

[54] Xie F., Zhou C., "Effects of Small-Amplitude Oscillatory Shear on Polymeric Reaction," *Polymer Composites*, vol. 29, 1, pp. 72-76, 2008.

[55] Dinga F., Giacomin A. J., Bird R. B., Kweona C-B, "Viscous dissipation with fluid inertia in oscillatory shear flow," *J. Non-Newtonian Fluid Mech*., 86, 359-374, 1999.

[56] Kim W.C., Lee C.J., Sim H.G., Pak H., "Interdiffusion at Interfaces of Polymers with Similar Physical Properties," *Bull. Korean Chem. Soc.*, vol. 21, p. 6, 2000.

[57] Kim W.C., Pak, H., "Dynamics of Interdiffusion at Interface between Partially Miscible Polymers," *Bull. Korean Chem. Soc.*, vol. 20, p. 12, 1999.

[58] Steiner U., Krausch G., Schatz G., Klein, J., "Dynamics of Mixing between Partially Miscible Polymers," *Phys. Rev. Lett.*, vol. 64, p. 10, 1990.

[59] Dealy J. M., "Melt Rheology and Its Role in Plastics Processing," *Van Nostrand Reinhold: New York*, 1990.

[60] J. Cranck, "The Mathematics of Diffusion", *Oxford Science Publications, Clarendon Press, Oxford, UK*, 1975.

[61] Yang L., Suo T., Niu Y., Wang Z., Yan D., Wang H., "Effects of phase behavior on mutual diffusion at polymer layers interface," *Polymer*, vol. 51, pp. 5276-5281, 2010.

[62] Ultracki L.A., Sammut P., "Molten Polystyrene Structures Above the Glass Transition, $T > T_g$," *Journal of Polymer Science - Part B*, *Polymer Physics*, vol. 49, pp. 1369-1380, 2011.

[63] NLREG, "Non-Linear Regularization, Version 1650," *Freiburg Materials Research Center* (Service Group Scientific Data Processing), 2006.

[64] Li J., Ding R., Yang Y., "Iterative parameter identification methods for nonlinear functions," *Applied Mathematical Modelling*, vol. 36, pp. 2739-2750, 2012.

[65] Nakhle W., Wood-Adams P., "Solvent diffusion in molten polystyrene under small amplitude oscillatory shear," *Polymer*, vol. 132, pp. 59-68, 2017.

[66] Bousmina M., Qiu H., Grmela M., "Diffusion at Polymer/Polymer Interfaces Probed by Rheological Tools," *Macromolecules,* vol. 31, pp. 8273-8280, 1998.

[67] Schabel W., Siebel D., Scharfer P., "Determination of Concentration-Dependent Diffusion Coefficients in Polymer−Solvent Systems: Analysis of Concentration Profiles Measured by Raman

Spectroscopy during Single Drying Experiments Excluding Boundary Conditions and Phase Equilibrium*," Macromolecules*, vol., 48, pp. 8608-8614, 2015.

[68] Matthew G.H., Giulia L.F., Joao T.C., Matar O., "A minimal model for solvent evaporation and absorption in thin films," *Journal of Colloid and Interface Science*, vol. 488, pp. 61-71, 2017.

[69] Costeux S., Zhu L., "Low Density Thermoplastic Foams Nucleated by Nanoparticles," *Polymer*, vol. 54, pp. 2785-2795, 2013.

[70] Hofmann B., Fleischer G., "Stability Rates for Linear Ill-Posed Problems with Convolution and Multiplication Operators," *Journal for Analysis and its Applications*, vol. 2, pp. 267-286, 1999.

[71] Cornelio A., Piccolomini L., Nagy G., "Constrained numerical optimization methods for blind deconvolution," *Numerical Algorithms*, vol. 65, pp. 23-42, 2014.

[72] Liu Y., Yang B., Cao D., Ma N., "State-of-the-art in distributed privacy preserving data mining," *ICCSN and IEEE 3rd International Conference*, pp 545-549, 2011.

[73] Leong Y. Y., Chandra D., Wijaya H., Khan A., "A general method for obtaining shear stress and normal stress functions from parallel disk rheometry data," *Rheol Acta*, vol. 44, pp. 270-277, 2005.

[74] Sun A., Painter S. L., Gordon W. W., "A constrained robust least squares approach for contaminant release history identification," *Water Resources Research*, vol. 42, 2006.

[75] Jakob K., Jarom D., Grant K., Rosemary A., "Non-negatively constrained least squares and parameter choice by the residual periodogram for the inversion of electrochemical impedance spectroscopy data," *Journal of Computational and Applied Mathematics*, vol. 278, pp. 52–74, 2015.

[76] Limin W., "A parameter choice method for the Tikhonov regularization," *Electronic Transactions on Numerical Analysis*, vol. 16, pp. 107–128, 2003.

[77] Li J., Ding R., Yang Y., "Iterative parameter identification methods for nonlinear functions," *Applied Mathematical Modelling*, vol. 36, pp. 2739-2750, 2012.

[78] Muralidhar K., Sarathy R., "Some Additional Insights on Applying Differential Privacy for Numerical Data," *Privacy in Statistical Databases*, vol. 6344, pp. 210-219, 2011.

[79] J. Cranck, "The Mathematics of Diffusion," *Oxford Science Publications, Clarendon Press, Oxford, UK*, 1975.

[80] Kim W.C., Pak, H., "Interdiffusion at Interfaces of Binary Polymer Mixtures with Different Molecular Weights," *Bull. Korean Chem. Soc.*, vol. 20, p. 11, 1999.

[81] Kim W.C., Pak, H., "Dynamics of Interdiffusion at Interface between Partially Miscible Polymers," *Bull. Korean Chem. Soc.*, vol. 20, p. 12, 1999.

[82] Steiner U., Krausch G., Schatz G., Klein, J., "Dynamics of Mixing between Partially Miscible Polymers," *Phys. Rev. Lett.*, vol. 64, p. 10, 1990.

[83] Masaro L., Zhu X.X., "Physical models of diffusion for polymer solutions, gels and solids," *Prog. Polym. Sci.*, vol. 24, pp. 731-775, 1999.

[84] Kim W.C., Lee C.J., Sim H.G., Pak H., "Interdiffusion at Interfaces of Polymers with Similar Physical Properties," *Bull. Korean Chem. Soc.*, vol. 21, p. 6, 2000.

[85] Fujita H., Kishimoto, A., "Interpretation of Viscosity Data for Concentrated Polymer Solutions," *Journal of Chemical Physics*, vol. 34, pp. 393-397, 1961.

[86] Dealy J.M., Park H.E., "Effects of Pressure and Supercritical Fluids on the Viscosity of Polyethylene," *Macromolecule*, vol. 39, pp. 5438-5452, 2006.

[87] Liu Y., Montgomery T. S., "Investigation of the nonlinear mixing rule for its adequacy in viscosity to molecular weight distribution transforms," *Journal of Rheology*, vol. 42, p. 267, 1998.

[88] Pestryaev E. M., "Molecular Dynamics Study of Chain Reptation in a Gel," *Polymer Science*, vol. 55, pp. 336-352, 2013.

[89] MATLAB 2017b, "the MathWorks," *Natick, MA, U.S.A*, 2017.

https://www.mathworks.com/products/optimization.html

[90] P. C. Hansen, "Regularization Tools: A Matlab package for analysis and solution of discrete ill-posed problems," *Numerical Algorithms*, vol. 6, pp. 1-35, 1994.

[91] Ramya, P., Ranganathaiah, C., Williams, J.F., "Experimental Determination of Interface Widths in Binary Polymer Blends from Free Volume Measurements," *Polymer*, vol. 53, pp. 4539-4546.

[92] Bernardo, G., "Diffusivity of Alcohols in Amorphous Polystyrene," *Journal of Applied Polymer Science*, vol. 127, pp. 1803-1811, 2012.

[93] Matthew G.H., Giulia L.F., Joao T.C., "A Minimal Model for Solvent Evaporation and Absorption in Thin Films," *Journal of Colloid and Interface Science*, vol. 488, pp. 61-71, 2017.

[94] Cella R., Mumbach G., Oliveira P., Marangoni C., Bolzan A., Bernard S., Machado R., "Polystyrene Recycling Processes by Dissolution in Ethyl Acetate," *J. App. Poly. Sci.*, 46208, 2018.

[95] Lin C.C., Parrish E., "Composto R.J., Macromolecule and Particle Dynamics in Confined Media," *Macromolecules*, vol. 49, pp. 5755-5772, 2016.

[96] Nakhle W., Wood-Adams P. M., "Solvent Diffusion in Molten Polystyrene under Small Amplitude Oscillatory Shear," *Polymer*, vol. 132, pp. 59-68, 2017.

[97] Costeux S., Zhu L., "Low Density Thermoplastic Foams Nucleated by Nanoparticles," *Polymer*, vol. 54, pp. 2785-2795, 2013.

[98] Mueller F., Krueger K., Sadowski G., "Non-Fickian Diffusion of Toluene in Polystyrene in the Vicinity of the Glass-Transition Temperature," *Macromolecules*, vol. 45, pp. 926-932, 2012.

[99] Asai M., Awata M., Koike Y., "Effects of Rotation of Benzene Rings on Diffusion of Solvents in Polymer Melts," *Ind. Eng. Chem. Res.*, vol. 50, pp. 3280–3286, 2011.

[100] Fujita H., Kishimoto A., "Interpretation of Viscosity Data for Concentrated Polymer Solutions," *Journal of Chemical Physics*, vol. 34, pp. 393-397, 1961.

[101] Lomellini P., "Williams-LandeI-Ferry versus Arrhenius Behaviour: Polystyrene Melt Viscoelasticity Revised," *Polymer*, vol. 33, p. 23, 1992.

[102] Cranck J., "The Mathematics of Diffusion", *Oxford Science Publications, Clarendon Press, Oxford, UK*, 1975.

[103] Xie F., Zhou C., "Effects of Small-Amplitude Oscillatory Shear on Polymeric Reaction," *Polymer Composites*, vol. 29, 1, pp. 72-76, 2008.

[104] Morrison F.A, "Understanding Rheology," *Oxford University Press: New York*, 2001.

[105] Dealy J.M., Park H.E., "Effects of Pressure and Supercritical Fluids on the Viscosity of Polyethylene," *Macromolecules*, vol. 39, pp. 5438-5452, 2006.

[106] Tung W., Clarke N., Composto R.J., "Temperature Dependence of Polymer Diffusion in MWCNT/PS Nanocomposites," *Macromolecules*, vol. 46, pp. 2317-2322, 2013.

[107] Leong Y. Y., Chandra D., Wijaya H., Khan A., "A General Method for Obtaining Shear Stress and Normal Stress Functions from Parallel Disk Rheometry Data," *Rheol Acta*, vol. 44, pp. 270-277, 2005.

[108] Limin W., "A Parameter Choice Method for the Tikhonov Regularization," *Electronic Transactions on Numerical Analysis*, vol. 16, pp. 107-128, 2003.

[109] Aragon S.R., R. Pecora, "Fluorescence Correlation Spectroscopy as A Probe of Molecular Dynamics," *The Journal of Chemical Physics*, vol. 64, pp. 1791-1803, 1976.

[110] Ramya P., Ranganathaiah C., Williams J.F., "Experimental Determination of Interface Widths in Binary Polymer Blends from Free Volume Measurements," *Polymer*, vol. 53, 2012.

[111] Areerat S., Funami E., Hayata Y., "Measurement and Prediction of Diffusion Coefficients of Supercritical CO_2 in Molten Polymers," *Polymer Engineering and Science*, vol. 44, p. 10, 2004.

[112] Bernardo G., "Diffusivity of Alcohols in Amorphous Polystyrene," *Journal of Applied Polymer Science*, vol. 127, pp. 1803-1811, 2012.

[113] Bernardo G., R. Choudhury, H. Beckham, "Diffusivity of Small Molecules in Polymers: Carboxylic Acids in Polystyrene," *Polymer*, vol. 53, pp. 976-983, 2012.

[114] Nakhle W., Wood-Adams P.M., "A General Method for Obtaining Diffusion Coefficients by Inversion of Measured Torque from Diffusion Experiments under Small Amplitude Oscillatory Shear," *Rheologica Acta*, (in press), 2018.

[115] Jakob K., Jarom D., Grant K., Rosemary A., "Non-Negatively Constrained Least Squares and Parameter Choice by The Residual Periodogram for The Inversion of Electrochemical Impedance Spectroscopy Data," *Journal of Computational and Applied Mathematics*, vol. 278, pp. 52-74, 2015.

[116] Cornelio A., Piccolomini L., Nagy G., "Constrained Numerical Optimization Methods for Blind Deconvolution," *Numerical Algorithms*, vol. 65, pp. 23-42, 2014.

[117] NLREG, "Non-Linear Regularization, Version 1650," *Freiburg Materials Research Center* (Service Group Scientific Data Processing), 2006.

[118] Wood-Adams P. M., Dealy J. M., "Effect of Molecular Structure on the Linear Viscoelastic Behavior of Polyethylene," *Macromolecules*, vol. 33, pp. 7489-7499, 2000.

[119] Masaro, L., Zhu, X.X., "Physical models of diffusion for polymer solutions, gels and solids," *Prog. Polym. Sci.*, vol. 24, pp. 731-775, 1999.

[120] U.K. Chaturvedi, U. Steiner, O. Zak, G. Krausch, J. Klein, "Interfacial Structure in Polymer Mixtures below the Critical Point," *A.P.S – Phys. Rev. Lett.*, vol. 63, p. 6, 1989.

[121] Ludwik Leibler, "Theory of Phase Equilibria in Mixtures of Copolymers and Homopolymers. 2. Interfaces near the Consolute Point," *Macromolecules*, vol. 15, pp. 1283-1290, 1989.

[122] F. S. Bates, G. D. Wignall and W. C. Koehler, "Critical Behavior of Binary Liquid Mixtures of Deuterated and Protonated Polymers," vol. 55, p. 22, 1985.

[123] U. Steiner, G. Krausch, G. Schatz, J. Klein, "Dynamics of Mixing between Partially Miscible Polymers," *A.P.S – Phys. Rev. Lett.*, vol. 64, p. 10, 1990.

[124] W.C. Kim, H. Pak, "Interdiffusion at Interfaces of Binary Polymer Mixtures with Different Molecular Weights," *Bull. Korean Chem. Soc.*, vol. 20, p. 11, 1999.

[125] W.C. Kim, H. Pak, "Dynamics of Interdiffusion at Interface between Partially Miscible Polymers," *Bull. Korean Chem. Soc.*, vol. 20, p. 12, 1999.

[126] W.C. Kim, C.J. Lee, H.G. Sim, H. Pak, "Interdiffusion at Interfaces of Polymers with Similar Physical Properties," *Bull. Korean Chem. Soc.*, vol. 21, p. 6, 2000.

[127] M. Bousmina, H. Qiu, M. Grmela, "Diffusion at Polymer/Polymer Interfaces Probed by Rheological Tools," *Macromolecules*, vol. 31, pp. 8273-8280, 1998.

[128] Nakhle W., Wood-Adams P. M., "Solvent Diffusion in Molten Polystyrene under Small Amplitude Oscillatory Shear," *Polymer*, vol. 132, pp. 59-68, 2017.

[129] P. Ramya, C. Ranganathaiah, J.F. Williams, "Experimental Determination of Interface Widths in Binary Polymer Blends from Free Volume Measurements," *Polymer*, p. 53, 2012.

[130] R.B. Bird, R.C. Armstrong, 0. Hassager, "Dynamics of Polymeric Liquids: Fluid Mechanics," *Wiley, New York, USA, Vol. 1, 2nd Edition*, 1987.

[131] J.M. Smith, M.M. Abbott, H.C. Van Ness, "Introduction to Chemical Engineering Thermodynamics," *McGraw-Hill, New York City, New York, USA, 5th Edition*, 1996.

[132] P.J. Flory, "Thermodynamics of Polymer Solutions", *Discuss. Faraday Soc., 15th Spiers Memorial Lecture*, vol. 49, p. 7, 1970.

[133] Nakhle W., Wood-Adams P.M., "A General Method for Obtaining Diffusion Coefficients by Inversion of Measured Torque from Diffusion Experiments under Small Amplitude Oscillatory Shear," *Rheologica Acta*, 2018.

[134] J. Cranck, "The Mathematics of Diffusion," *Oxford Science Publications, Clarendon Press, Oxford, UK*, 1975.

[135] A. Cornelio, E.L. Piccolomini, J.G. Nagy, "Constrained numerical optimization methods for blind Deconvolution," *Numerical Algorithms*, p. 42, 2014.

[136] L. Wu, "A Parameter Choice Method for the Tikhonov Regularization", *ETNA*, vol. 16, pp. 107-128, 2003.

[137] P. C. Hansen, “Regularization Tools: A Matlab package for analysis and solution of discrete ill-posed problems,” *Numerical Algorithms*, vol. 6, pp. 1-35, 1994.

[138] Leong Y. Y., Chandra D., Wijaya H., Khan A., “A general method for obtaining shear stress and normal stress functions from parallel disk rheometry data,” *Rheol Acta*, vol. 44, pp. 270-277, 2005.

[139] Dealy J.M., Park H.E., “Effects of Pressure and Supercritical Fluids on the Viscosity of Polyethylene,” *Macromolecules*, vol. 39, pp. 5438-5452, 2006.

[140] F. Xie, C. Zhou, “Effects of Small-Amplitude Oscillatory Shear on Polymeric Reaction”, *Polymer Composites*, vol. 29, 1, pp. 72-76, 2008.

[141] M. Antonietti, “Diffusion of Linear Polystyrene Molecules in Matrices of Different Molecular Weights,” *Macromolecules*, vol. 19, pp. 793-798, 1986.

[142] Liu Y., Montgomery T. S., “Investigation of the nonlinear mixing rule for its adequacy in viscosity to molecular weight distribution transforms,” *Journal of Rheology*, vol. 42, p. 267, 1998.

APPENDICES

Appendix-A2.1.: SAOS – Material Functions & Torque

Appendix A2.1.1: SAOS – Material Functions for Parallel-Disk Apparatus

$$\gamma_{21}(t) = \int_0^t \dot{\gamma}_{21}(t')dt' = \frac{\dot{\gamma}_0}{\omega}\sin\omega t = \gamma_0 \sin\omega t = \Re\left(-i\gamma_0 e^{i\omega t}\right)$$

$$-\tau_{21}(t) = \tau_0 \sin(\omega t + \delta) = \Re\left(i\tau_0 e^{i(\omega t+\delta)}\right) = \Re\left(i\tau_0 e^{i\delta} e^{i\omega t}\right)$$

$$G^*(\omega) \equiv -\frac{\tau_{21}(t)}{\gamma_{21}(t)} = \frac{\left(-i\tau_0 e^{i\delta} e^{i\omega t}\right)}{(-i\gamma_0 e^{i\omega t})} = \frac{\tau_0}{\gamma_0} e^{i\delta}$$

$$\eta^*(\omega) \equiv -\frac{\tau_{21}(t)}{\dot{\gamma}_{21}(t)} = \frac{\left(-i\tau_0 e^{i\delta} e^{i\omega t}\right)}{(\dot{\gamma}_0 e^{i\omega t})} = \frac{\tau_0}{\dot{\gamma}_0}(-ie^{i\delta})$$

$$G^*(\omega) \equiv \frac{\tau_0}{\gamma_0}(\cos\delta + i\sin\delta)$$

$$G'(\omega) = \frac{\tau_0}{\gamma_0}\cos\delta \quad , \quad G''(\omega) = \frac{\tau_0}{\gamma_0}\sin\delta$$

$$\eta^*(\omega) \equiv \frac{\tau_0}{\dot{\gamma}_0}(\sin\delta - i\cos\delta)$$

$$\boldsymbol{\eta'(\omega) = \frac{\tau_0}{\dot{\gamma}_0}\sin\delta = \frac{G''(\omega)}{\omega} \quad , \quad \eta''(\omega) = \frac{\tau_0}{\dot{\gamma}_0}\cos\delta = \frac{G'(\omega)}{\omega}}$$

Appendix A2.1.2: Relationship between Torque & Material Functions - Pure Polymer

$$T(t) = \ T_0 * \ \mathrm{Re}\left\{e^{i(\delta+\omega t)}\right\} = T_0 * \ \mathrm{Re}\left\{e^{i\delta} * \ e^{i\omega t}\right\} = \ T_0 * \ \mathrm{Re}\left\{(\cos\delta + i\sin\delta) * \ e^{i\omega t}\right\}$$

$$T(t) = \ 2\pi * \int_0^R [\tau(r,t) * r]\, rdr = \left[\frac{2\pi\omega\theta_0}{H}\right] * \left[\int_0^R [r^3]\, dr\right] * \ \mathrm{Re}\left\{i\,\eta^*(\omega)\, e^{i\omega t}\right\}$$

$$T(t) = \ \left[\frac{2\pi\omega\theta_0}{H}\right] * \left[\frac{R^4}{4}\right] * \ \mathrm{Re}\ \left\{\{i\,\eta'(\omega) + \ \eta''(\omega)\} * \ e^{i\omega t}\right\}$$

$$T_0 * \ \mathrm{Re}\left\{(\cos\delta + i\sin\delta) * \ e^{i\omega t}\right\} = \ \left[\frac{\pi\omega\theta_0 R^4}{2H}\right] * \ \mathrm{Re}\ \left\{\{i\,\eta'(\omega) + \ \eta''(\omega)\} * \ e^{i\omega t}\right\}$$

$$\eta'(\omega) = \frac{2HT_0\sin\delta}{\pi\omega\theta_0 R^4} \quad , \quad \eta''(\omega) = \frac{2HT_0\cos\delta}{\pi\omega\theta_0 R^4}$$

$$\boldsymbol{|\eta^*(\omega)| = \ \frac{2HT_0(\omega)}{\pi\omega\theta_0 R^4}}$$

Appendix A2.1.3: Relationship between Torque & Material Functions – Diffusion

$$T(t) = \ 2\pi * \int_0^R [\tau(r,t) * r]\, rdr = \left[\frac{2\pi\omega\theta_0}{H}\right] * \left[\int_0^R [\,\eta^*(C,\omega)\cdot r^3]\, dr\right] * \ \mathrm{Re}\left\{i\, e^{i\omega t}\right\}$$

$$\boldsymbol{T_0 * \ \mathrm{Re}\left\{(\cos\delta + i\sin\delta) * \ e^{i\omega t}\right\} = \ \left[\frac{2\pi\omega\theta_0}{H}\right] * \left[\int_0^R \left[\{\, i\,\eta'(C,\omega) + \ \eta''(C,\omega)\} r^3\right] dr\right] * \mathrm{Re}\left\{e^{i\omega t}\right\}}$$

$$T_0\sin\delta = \ \left[\frac{2\pi\omega\theta_0}{H}\right] * \left[\int_0^R [\,\eta'(C,\omega) * r^3]\, dr\right]$$

$$T_0\cos\delta = \ \left[\frac{2\pi\omega\theta_0}{H}\right] * \left[\int_0^R [\,\eta''(C,\omega) * r^3]\, dr\right]$$

$$\boldsymbol{T_0(C,\omega) = \ \left[\frac{2\pi\omega\theta_0}{H}\right] * \left[\int_0^R \left[|\,\eta^*(C,\omega)| * r^3\right] dr\right]}$$

Appendix-A2.2.: SAOS – Flow Kinematics

Appendix A2.2.1: Assumptions

Unidirectional Flow:

$$\vec{v} = \begin{pmatrix} 0 \\ v_\theta \\ 0 \end{pmatrix}$$

Axisymmetric Flow:

$$\frac{\delta}{\delta_\theta}( ) = 0$$

Incompressible Fluid

$$\rho = \text{cste}$$

Linear Velocity Gradient in z-direction:

$$\frac{\delta}{\delta_z} v_\theta(r,z,t) = f(r,t) \qquad \rightarrow \qquad v_\theta(r,z,t) = z * f(r,t) + g(r,t)$$

Appendix A2.2.2: Boundary Conditions

1. $z = 0 \rightarrow v_\theta(r,0,t) = 0 \rightarrow g(r,t) = 0$

2. $z = H \rightarrow v_\theta(r,H,t) = H * f(r,t) = r * \frac{d\theta(t)}{dt}$

$$\theta(t) = \theta_0 * \mathrm{Re}\{e^{i\omega t}\} \rightarrow \frac{d\theta(t)}{dt} = \omega * \theta_0 * \mathrm{Re}\{ie^{i\omega t}\}$$

$$v_\theta(r,H,t) = H * f(r,t) = r * \frac{d\theta(t)}{dt} = r * \omega * \theta_0 * \mathrm{Re}\{ie^{i\omega t}\}$$

$$f(r,t) = \frac{\omega * \theta_0}{H} * r * \mathrm{Re}\{ie^{i\omega t}\}$$

$$\mathbf{v_\theta(r,z,t) = \left[\frac{\omega * \theta_0}{H} \cdot r \cdot z\right] * \mathrm{Re}\{ie^{i\omega t}\} = v_0(r,z) * \mathrm{Re}\{ie^{i\omega t}\}}$$

Appendix A2.2.3: **Velocity Gradient**

$$\nabla\vec{v} = \begin{bmatrix} \frac{\delta v_r}{\delta r} & \frac{\delta v_\theta}{\delta r} & \frac{\delta v_z}{\delta r} \\ \frac{1}{r}\frac{\delta v_r}{\delta \theta} - \frac{v_\theta}{r} & \frac{1}{r}\frac{\delta v_\theta}{\delta \theta} + \frac{v_r}{r} & \frac{1}{r}\frac{\delta v_z}{\delta \theta} \\ \frac{\delta v_r}{\delta z} & \frac{\delta v_\theta}{\delta z} & \frac{\delta v_z}{\delta z} \end{bmatrix}$$

$$\nabla\vec{v} = \begin{bmatrix} 0 & \frac{\delta v_\theta}{\delta r} & 0 \\ -\frac{v_\theta}{r} & 0 & 0 \\ 0 & \frac{\delta v_\theta}{\delta z} & 0 \end{bmatrix} \quad , \quad \nabla\vec{v}^T = \begin{bmatrix} 0 & -\frac{v_\theta}{r} & 0 \\ \frac{\delta v_\theta}{\delta r} & 0 & \frac{\delta v_\theta}{\delta z} \\ 0 & 0 & 0 \end{bmatrix}$$

Appendix A2.2.4: **Shear Rate & Shear Stress - SAOS**

$$\underline{\underline{\dot{\gamma}}} = \nabla\vec{v} + \nabla\vec{v}^T$$

$$\underline{\underline{\dot{\gamma}}} = \begin{bmatrix} 0 & 0 & 0 \\ 0 & 0 & \frac{\delta v_\theta}{\delta z} \\ 0 & \frac{\delta v_\theta}{\delta z} & 0 \end{bmatrix}$$

$$\dot{\boldsymbol{\gamma}}(\mathbf{r},\mathbf{t}) = \frac{\boldsymbol{\delta v_\theta}}{\boldsymbol{\delta z}} = \left[\frac{\boldsymbol{\omega} * \boldsymbol{\theta_0}}{\mathbf{H}} * \mathbf{r}\right] * \mathbf{Re}\left\{\mathbf{i}\mathbf{e}^{\mathbf{i}\omega\mathbf{t}}\right\} = \dot{\boldsymbol{\gamma}}_{\mathbf{0}}(\mathbf{r}) * \mathbf{Re}\left\{\mathbf{i}\mathbf{e}^{\mathbf{i}\omega\mathbf{t}}\right\}$$

$$\boldsymbol{\tau}(\mathbf{r},\mathbf{t}) = \boldsymbol{\eta}^*(\boldsymbol{\omega}) * \dot{\boldsymbol{\gamma}}(\mathbf{r},\mathbf{t}) = \dot{\boldsymbol{\gamma}}_{\mathbf{0}}(\mathbf{r}) * \mathbf{Re}\left\{\mathbf{i}\,\boldsymbol{\eta}^*(\boldsymbol{\omega})\,\mathbf{e}^{\mathbf{i}\omega\mathbf{t}}\right\}$$

Appendix A2.2.5: **Equation of Motion – Incompressible Flow**

$$\boldsymbol{\rho} * \left[\frac{\boldsymbol{\partial}\vec{\mathbf{v}}}{\boldsymbol{\partial t}} + \vec{\mathbf{v}}.\boldsymbol{\nabla}\vec{\mathbf{v}}\right] = -\boldsymbol{\nabla}\,\underline{\underline{\boldsymbol{\tau}}} + \boldsymbol{\rho}\vec{\mathbf{g}}$$

Appendix-A2.3.: SAOS – Free Volume Theory

Appendix-A2.3.1.: Free Volume Theory - Diffusion

Total Free Volume = Free Volume in Pure Polymer + Free Volume Produced by Diffusing Substance

$$V_{Free} = V_{F1} + V_{F2}$$

$$\mathbf{a_C(C) \cdot b_C(C)} = \frac{\eta(C)}{\eta(C^*)} = \frac{e^{\frac{1}{V_{F2}}}}{e^{\frac{1}{V_{F2}^*}}} = e^{\left[\frac{1}{V_{F2}} - \frac{1}{V_{F2}^*}\right]}$$

$$V_{F2} = \alpha + \beta \cdot {V_{F2}}^*$$

$$\mathbf{a_C(C) \cdot b_C(C)} = \mathbf{e}^{-\frac{1}{\alpha + \left[\frac{\alpha^2}{\beta}\right]\frac{1}{C}}} = \mathbf{e}^{-\frac{1}{\frac{1}{A} + \left[\frac{B}{A}\right]\frac{1}{C}}}$$

- α: Fractional free volume
- β: Contribution of diffusant to the increase of free volume
- C: Normalized concentration in amount of diffusant/amount of host

Appendix-A2.3.2: Free Volume Theory – SAOS

$$\mathbf{\eta^*(C,\omega) = \eta^*(0,\omega) \cdot a_C(C) \cdot b_C(C) = \eta^*(0,\omega) \cdot e^{-\frac{1}{\frac{1}{A} + \left[\frac{B}{A}\right]\frac{1}{C}}}}$$

- $a_C(C)$ and $b_C(C)$: Horizontal and Vertical Concentration Shift Factor
- $\eta^*(0,\omega)$: Pure Polymer Complex Viscosity

Appendix-A2.3.3: Relationship between Torque & Complex Viscosity – Diffusion

$$T_0(C,\omega) = \left[\frac{2\pi\omega\theta_0}{H}\right] \cdot \left[\int_0^R [|\eta^*(C,\omega)| \cdot r^3]\, dr\right]$$

$$\mathbf{\frac{T_0(C,\omega)}{T_0(0,\omega)} = \frac{4}{R^4}\left[\int_0^R \left[e^{-\frac{1}{\frac{1}{A} + \left[\frac{B}{A}\right]\frac{1}{C}}}\right] \cdot r^3 \cdot dr\right]}$$

Appendix-A2.4.: Flory-Huggins – Solution Theory

Appendix-A2.4.1.: Gibbs Free Energy – Constant Temperature/Pressure

$$f[\phi_A(r,t)] = \Delta G = \Delta H - T\Delta S$$

$$\text{Free Energy} = \text{Interaction Energy} - \text{Mixing Energy}$$

$$\boldsymbol{\Delta G = [\chi_{AB} \cdot \phi_A \cdot (1 - \phi_A)] + \left[\frac{\phi_A}{N_A}\ln(\phi_A) + \frac{1 - \phi_A}{N_B}\ln(\phi_A)\right]}$$

Appendix-A2.4.2.: Closed Volume – Conservation of Energy

$$\boldsymbol{F = \int \left\{ f[\phi_A(r,t)] + \frac{\kappa}{4}[\nabla\phi_A(r,t)]^2 \right\} dV}$$

- $f[\phi_A(r,t)] = \Delta G =$ Energy due to Chemical Potential (mixing)
- $\frac{\kappa}{4}[\nabla\phi_A(r,t)]^2 =$ Energy due to Concentration Gradient

Appendix-A2.4.3.: Closed Volume – Conservation of Mass

$$\frac{\partial\phi_A}{\partial t} = -\nabla \cdot (J_A)$$

$$J_A = -D \cdot \nabla\mu \quad , \quad \mu = \frac{\partial F}{\partial \phi}$$

$$\frac{\partial\psi_A}{\partial t} = \frac{\partial}{\partial x}\left\{\left(\frac{2}{1 + R + (R-1)\psi_A}\right) \cdot \left[\left\langle 1 + \frac{1}{R} - \chi_{AB} + \left(\frac{1}{R} - 1\right) \cdot \psi_A + \chi_{AB} \cdot {\psi_A}^2 \right\rangle \cdot \frac{\partial\psi_A}{\partial x} - \frac{\partial^3\psi_A}{\partial x^3}\right]\right\}$$

$$\psi_A = 2 \cdot \left(\phi_A - \frac{1}{2}\right) \quad | \quad R = \frac{N_B}{N_A}$$

χ_{AB} : Flory – Huggins Interaction Parameter

Appendix-A3: The Role of Small Amplitude Oscillatory Shear in Solvent-Diffusion through Amorphous Polystyrene in the Melt State.

Wissam Nakhle and Paula Wood-Adams

Department of Mechanical & Industrial Engineering, Concordia University, Canada

Appendix-A3.1.: Figure A3.1.(a) shows the complex viscosity of homogeneous polymer solutions at several polymer concentrations ranging from 60wt% to 100wt% polymer. In Figure A3.1.(b), the complex viscosity is normalized by the shift factor product ($a_C \cdot b_C$) and the frequency is normalized by the horizontal shift factor a_C.

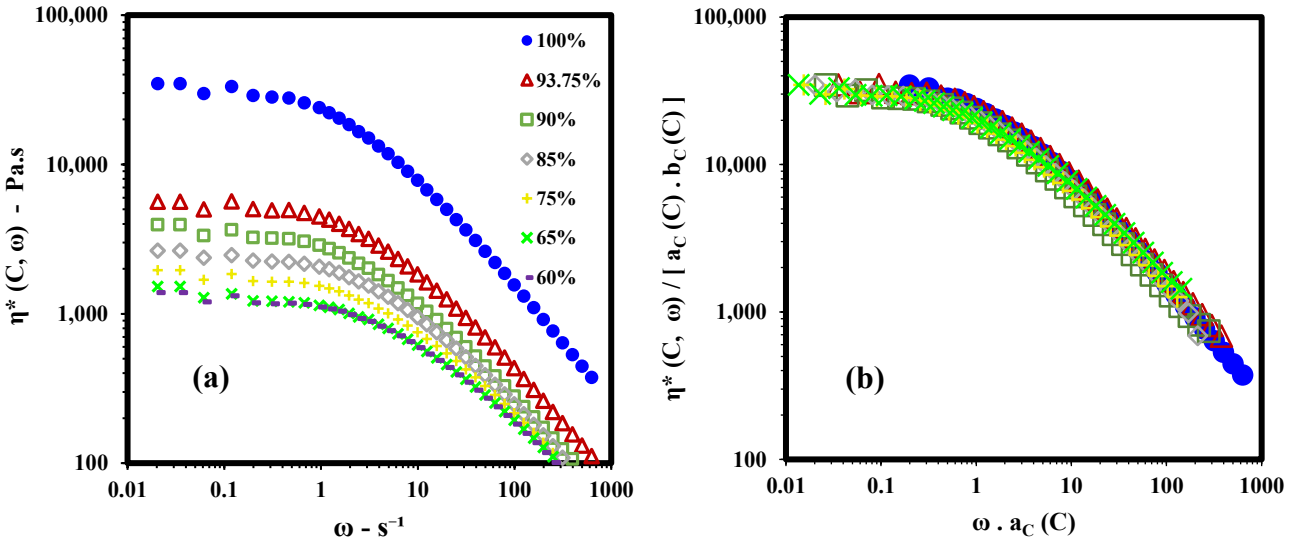

Fig. A3.1. Characterization of homogeneous solvent polymer mixtures with γ_0 = 4% at 190°C. (a) Complex viscosity η* (C, ω) as a function of frequency ω; (b) Master curve: shifted data using frequency-concentration superposition:

Appendix-A3.2.: In Figure A3.2, we can see that sorption data after 60s of immersion are somewhat affected by polymer dissolution and at an even longer times (after 120s) dissolution overcomes sorption and a weight loss is observed.

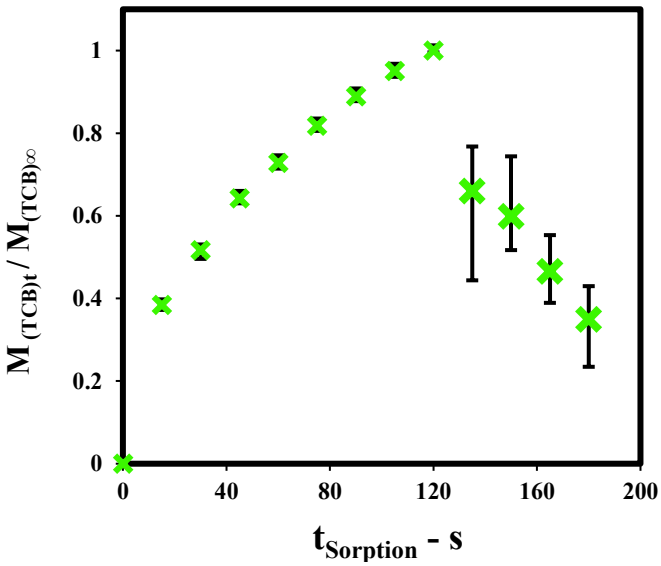

Fig. A3.2. Mass uptake measurements at 190°C

Appendix-A3.3.: As shown in Figure A3.3, samples continuously sheared produce a steeper decrease in measured torque, compared with samples undergoing long rest periods. Diffusion data presented in Figure A3.3 are obtained at 190°C for k = 2, and supports the conclusion that SAOS accelerates diffusion.

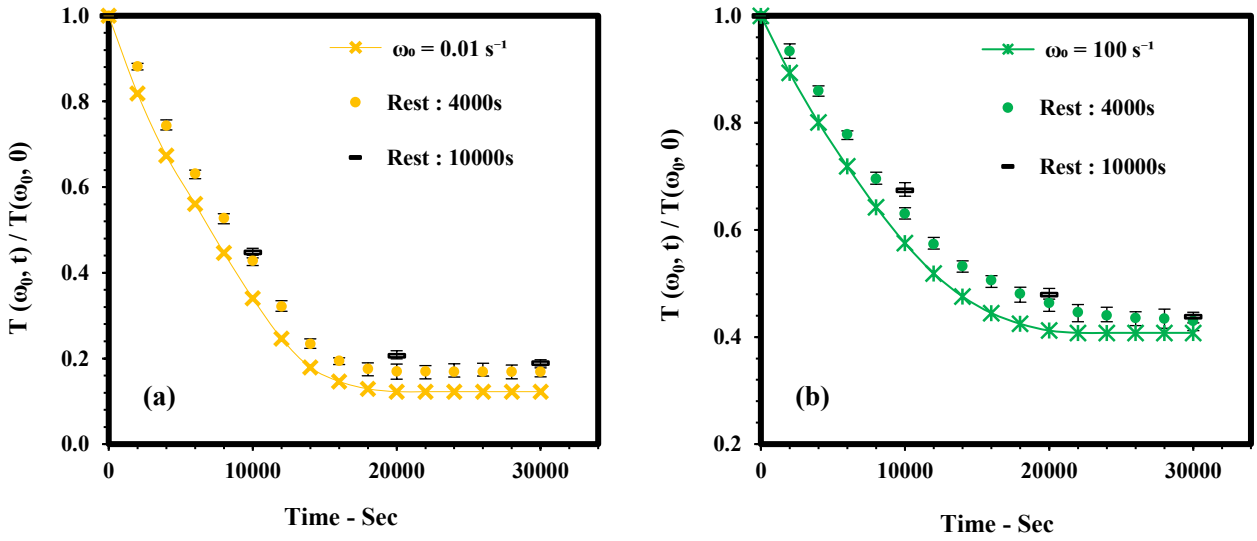

Fig. A3.3. Normalized Torque at 190°C, for samples continuously sheared, compared with samples undergoing periods of intermittent oscillations and long rest periods, for k = 2, at 190°C and ω_0 = (a) 0.01 s^{-1}; (b) 100 s^{-1}.

Appendix-A3.4.: Continuous SAOS data for k = 2 (for $1s^{-1}$ and $100s^{-1}$) and their fits are shown in Figure A3.4. The effect of frequency on diffusion can be deduced by comparing diffusion coefficients obtained at different frequencies.

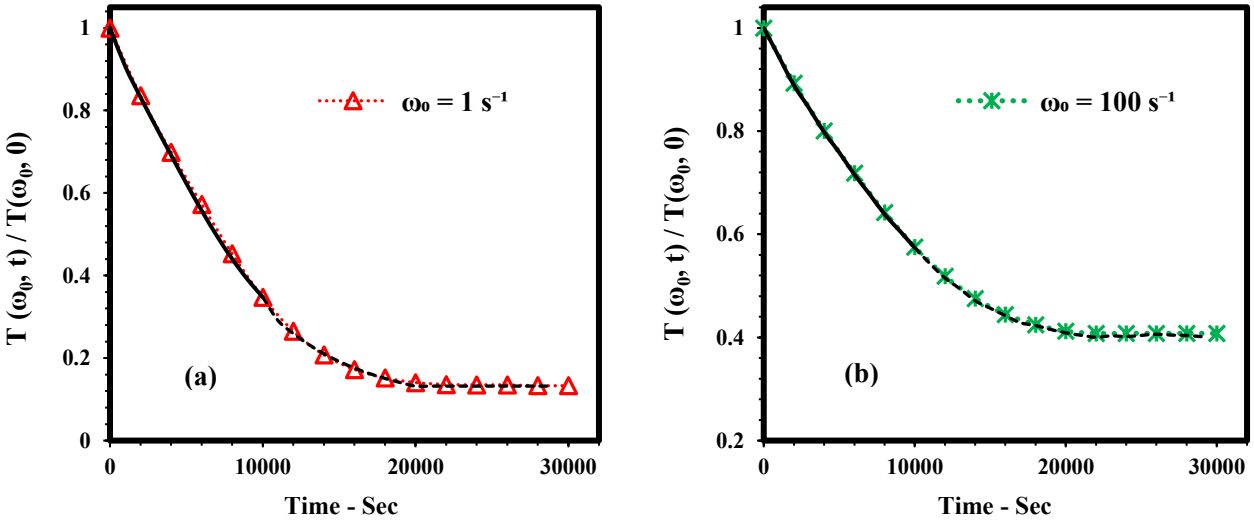

Fig. A3.4. Normalized torque during diffusion for k = 4, at 190°C. Full lines are the fits using eq. (4), (a) ω_0=$1s^{-1}$, D = 3.312 ± 0.015 (10^{-4} mm ² / sec); (b) 100 s^{-1}, D = 3.032 ± 0.005 (10^{-4} mm ² / sec).

Appendix-A4: general method for obtaining diffusion coefficients by inversion of measured torque from diffusion experiments under small amplitude oscillatory shear.

Wissam Nakhle and Paula Wood-Adams

Department of Mechanical & Industrial Engineering, Concordia University, Canada

Appendix-A4.1.: Figure A4.1. is a plot of (λ, x^{λ}) and (λ, e_r^{λ}), for a simulated Fickian case with D = $1.1 \cdot 10^{-3}$ mm² /s, and Δt = 100s. We observe again that the range of optimal λ on the (λ, x^{λ}) curve, coincides with the range where relative errors are smallest on the (λ, e_r^{λ}) curve. This trust region (0.01 - 0.02) is the optimal λ range where the most accurate viscosity profiles can be retrieved from the simulated torque data.

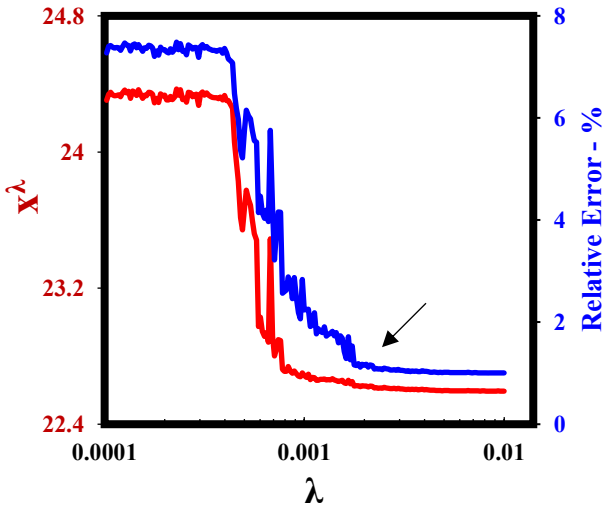

Fig. A4.1. Plot of (λ, x^{λ}) and (λ, e_r^{λ}) for a Fickian case with D = $1.1 \cdot 10^{-3}$ mm² /s, A = 0.027, B = 0.017 and Δt = 100s. The range of optimal λ values falls towards the right insensitive region.

Appendix-A4.2.: In Figure A4.2. we see radial viscosity profiles recovered from the regularization method, which are a very close match with the exact solution. Figure A4.2. confirms that our numerical procedure allows for an accurate determination of radial complex viscosity profiles during diffusion, for a wider range of diffusion rates or coefficients. Diffusion coefficients determined from the interface width are presented in Figure A4.3.

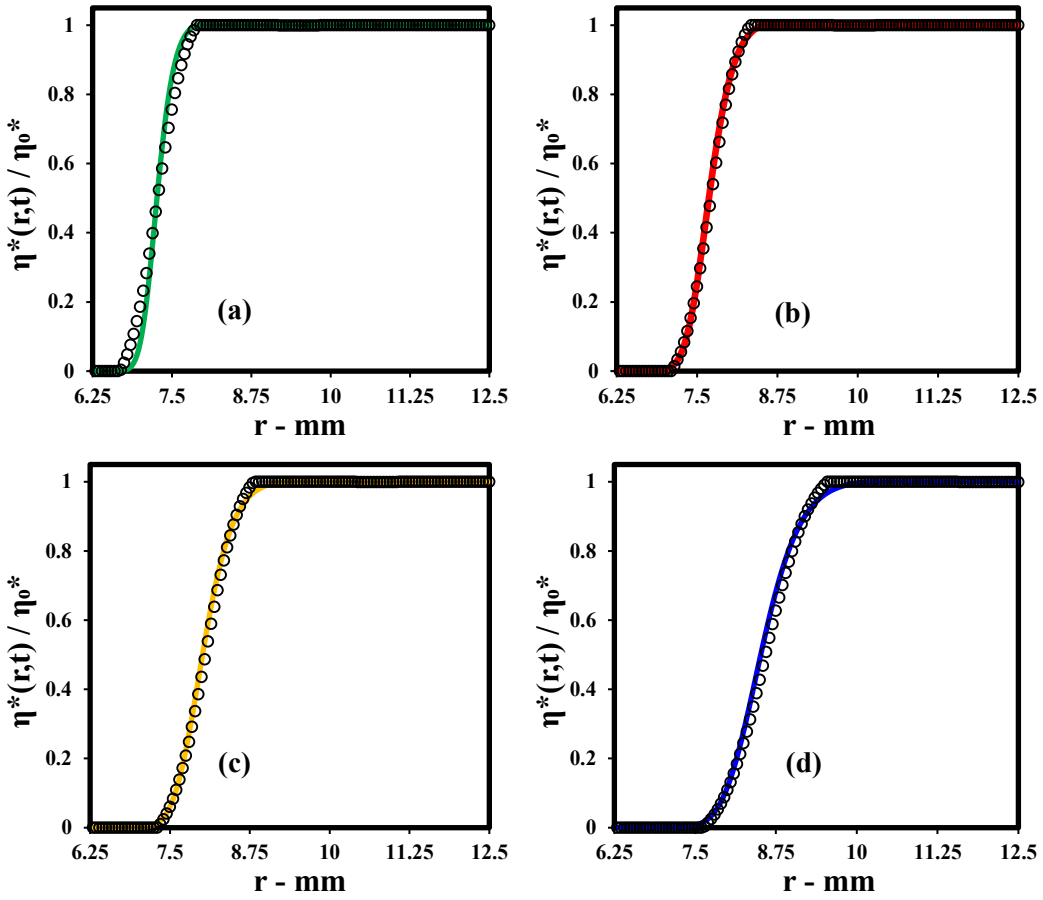

Fig. A4.2. Simulated and regularized viscosity profiles, for Fickian diffusion with D = 1.1 · 10^{-3} mm² /s, A = 0.027 and B = 0.017, and k = 2. (Discrete points are the regularized solutions and the continuous curve is the exact solution). (a) t = 200s; (b) t = 300s; (c) t = 400s; (d) t = 500s.

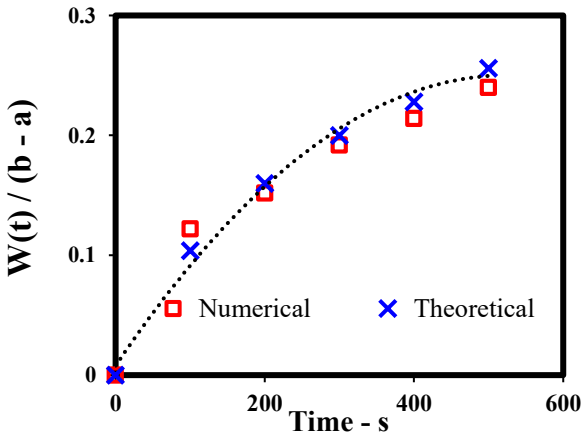

n = 0.5 ± 0.01	**Fickian**
D_0 $(1/s^{0.5})$	0.2827
D (mm^2/s)	$1.15 \cdot 10^{-3}$
D_{exact} (mm^2/s)	$1.10 \cdot 10^{-3}$

Fig. A4.3. Comparison of normalized interface width from numerical and exact viscosity profiles for the Fickian diffusion case in Figures A4.1-A4.2. Comparison of exact diffusion coefficients and coefficients from the interface width of regularized solutions.

Appendix-A5: Effect of Temperature on Solvent Diffusion in Molten Polystyrene under Small Amplitude Oscillatory Shear

Wissam Nakhle and Paula Wood-Adams

Department of Mechanical & Industrial Engineering, Concordia University, Canada

Appendix-A5.1.: Figure A5.1 shows storage and loss modulus data with a typical cross-over frequency, at the five temperatures studied. Figure A5.2 shows the complex viscosity of homogeneous polymer solutions at several polymer concentrations ranging from 60wt% to 100wt% polymer.

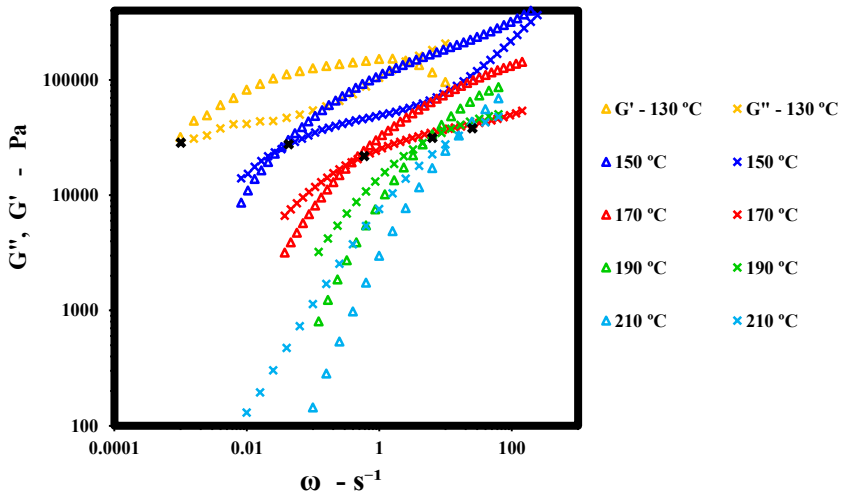

Fig. A5.1. A frequency sweep test with a shear amplitude γ = 4% at 130°C, 150°C, 170°C, 190°C, and 210°C. Storage modulus (G') and loss modulus (G") as a function of frequency for neat PS.

Appendix-A5.2.: Figure A5.2 shows complex viscosity of homogeneous solvent-polymer solutions from 60wt% to 100wt% at each temperature studied. From results in Figure A5.2, concentration shift factors (a_C and b_C) are determined at each of the five temperatures.

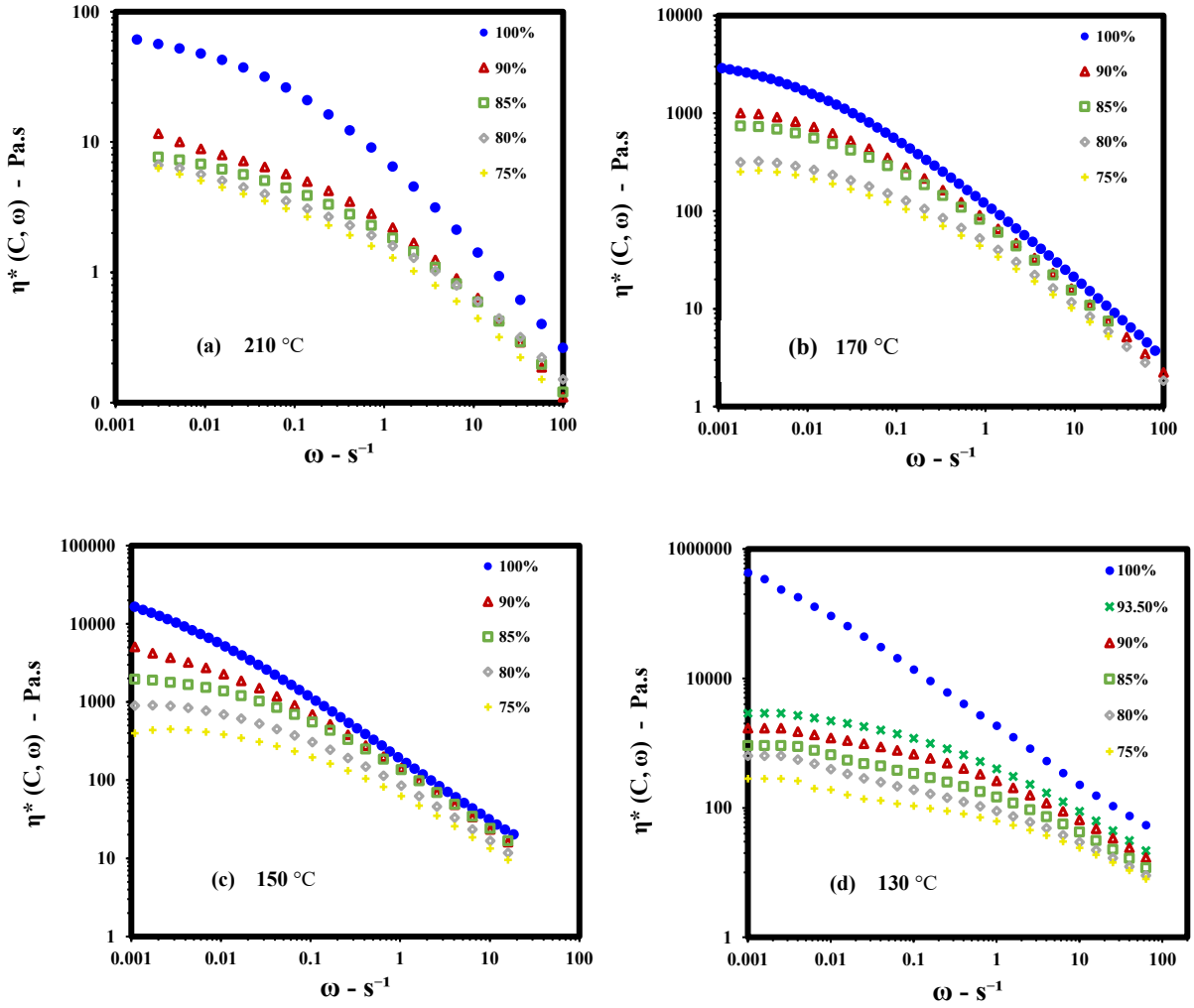

Fig. A5.2. Complex viscosity η* (C, ω) as a function of frequency ω of homogeneous solvent polymer mixtures with γ_0 = 4% at 130°C, 150°C, 170°C, and 210°C.

Carreau-Yasuda fit for η_0* (Pa.s) at different concentrations with $R^2 > 0.95$				
C	130°C	150°C	170°C	210°C
100%	5.32E+11	5.40E+09	3.83E+08	7.56E+07
90%	3.04E+09	4.15E+08	1.05E+08	3.88E+07
85%	3.24E+08	2.22E+08	7.51E+07	9.31E+06
80%	1.71E+08	9.67E+07	3.08E+07	6.10E+06
75%	1.15E+08	4.39E+07	2.44E+07	6.00E+06

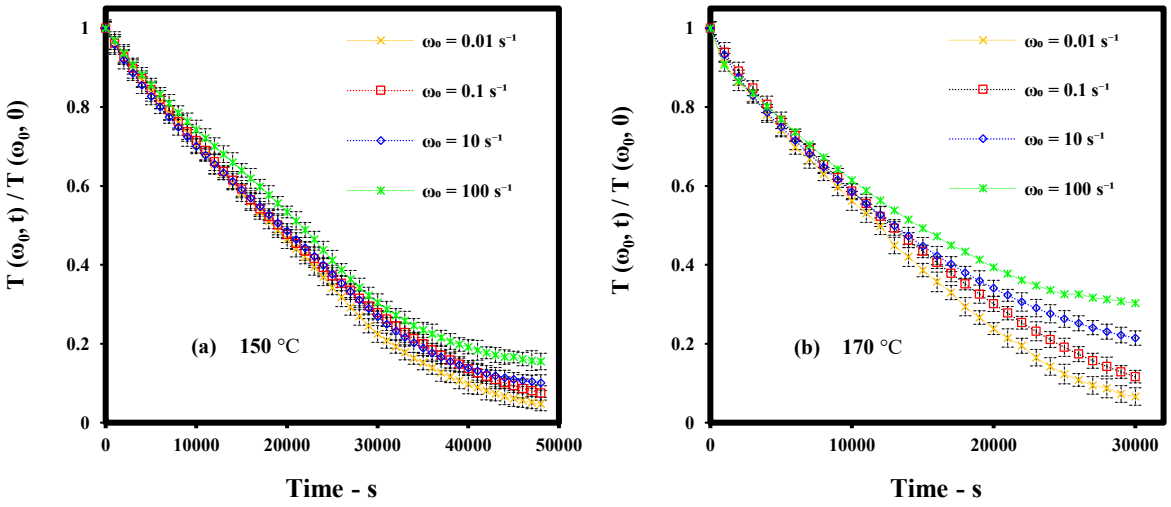

Fig. A5.3. Normalized Torque as a function of time, for k = 2 and for ω_0 from $0.01s^{-1}$ to $100s^{-1}$: torque T (ω_0, t) as a function of frequency for (a) 150°C; (b) 170°C. Error bars represent the standard deviation of 6 measurements.

Appendix-A5.3.: In intermittent SAOS tests shown in Figures A5.4-A5.5, oscillations are applied for 100s followed by long rest stages of 10000s where no flow is applied. In Figures A5.4-A5.5, the normalized torque at 150°C and 170°C is shown for samples intermittently sheared and are compared with the normalized torque from samples continuously sheared.

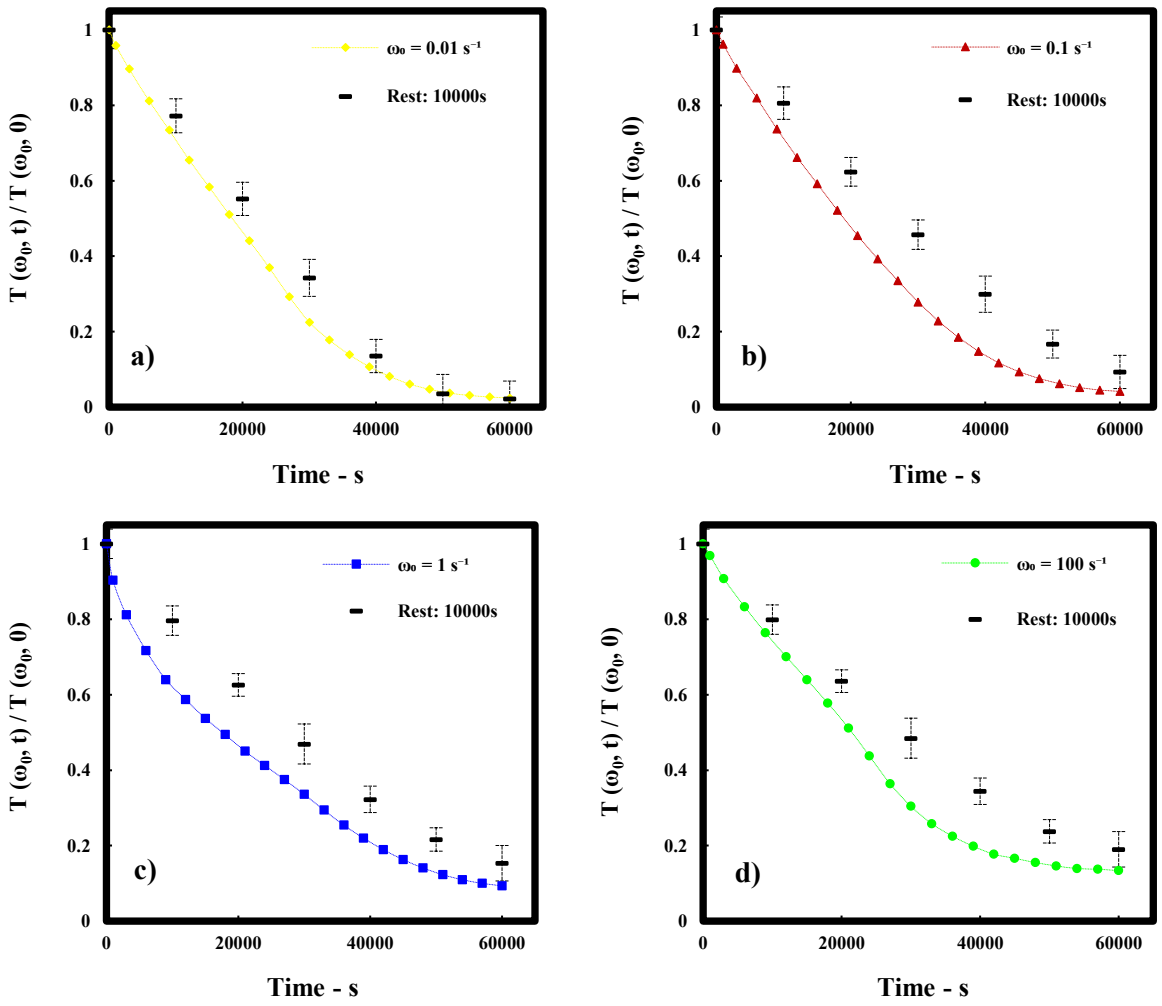

Fig. A5.4. Normalized Torque during diffusion in binary samples at 150°C. Samples continuously sheared, are compared with samples undergoing periods of intermittent oscillations, for k = 2, and ω_0 = (a) 0.01 s^{-1}; (b) 0.1 s^{-1}; (c) 1 s^{-1}; (d) 100 s^{-1}.

Appendix-A5.4.: In Figures A5.4-A5.5, we can see the effect of continuous shearing which also accelerates diffusion relative to the case of intermittent oscillation at 150°C and 170°C. We found that SAOS accelerates diffusion of TCB in molten PS at all five temperatures studied (130°C to 210°C), and that longer rest periods within the experiment decrease this effect. This effect also decreases at higher temperatures, which suggests that the accelerated diffusion due to SAOS is more effective at lower temperatures.

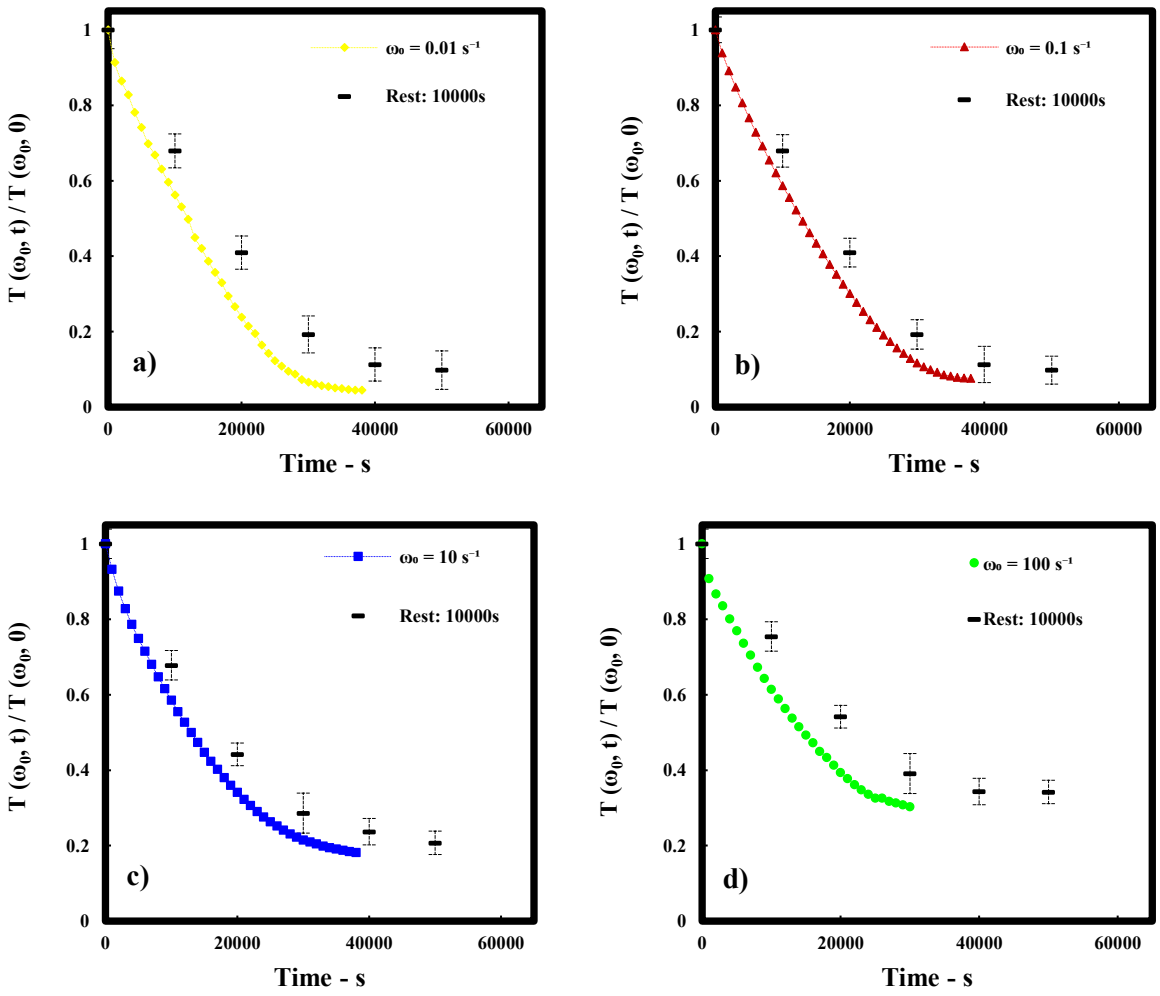

Fig. A5.5. Normalized Torque during diffusion in binary samples at 170°C. Samples continuously sheared, are compared with samples undergoing periods of intermittent oscillations, for k = 2, and ω_0 = (a) 0.01 s^{-1}; (b) 0.1 s^{-1}; (c) 10 s^{-1}; (d) 100 s^{-1}.